Power System Stability Analysis Using Wide Area Measurement System

A Thesis Submitted

to the College of Graduate Studies and Research

in

Partial Fulfillment of the Requirements

for the Degree of Master of Science

in the Department of Electrical and Computer Engineering
University of Saskatchewan

by

Bikash Shrestha

Saskatoon, Saskatchewan, Canada

Permission to Use

In presenting this thesis in partial fulfillment of the requirements for a Postgraduate degree from the University of Saskatchewan, it is agreed that the Libraries of this University may make it freely available for inspection. Permission for copying of this thesis in any manner, in whole or in part, for scholarly purposes may be granted by the professors who supervised this thesis work or, in their absence, by the Head of the Department of Electrical and Computer Engineering or the Dean of the College of Graduate Studies and Research at the University of Saskatchewan. Any copying, publication, or use of this thesis, or parts thereof, for financial gain without the written permission of the author is strictly prohibited. Proper recognition shall be given to the author and to the University of Saskatchewan in any scholarly use which may be made of any material in this thesis.

Request for permission to copy or to make any other use of material in this thesis in whole or in part should be addressed to:

Head of the Department of Electrical and Computer Engineering
57 Campus Drive
University of Saskatchewan
Saskatoon, Saskatchewan, Canada
S7N 5A9

Abstract

Advances in wide area measurement systems have transformed power system operation from simple visualization, state estimation, and post-mortem analysis tools to real-time protection and control at the systems level. Transient disturbances (such as lightning strikes) exist only for a fraction of a second but create transient stability issues and often trigger cascading type failures. The most common practice to prevent instabilities is with local generator out-of-step protection. Unfortunately, out-of-step protection operation of generators may not be fast enough, and an instability may take down nearby generators and the rest of the system by the time the local generator relay operates. Hence, it is important to assess power system stability over transmission lines as soon as the transient instability is detected instead of relying on purely localized out-of-step protection in generators.

This thesis proposes a synchrophasor-based out-of-step prediction methodology at the transmission line level using wide area measurements from optimal phasor measurement unit (PMU) locations in the interconnected system. Voltage and current measurements from wide area measurement systems (WAMS) are utilized to find the swing angles. The proposed scheme was used to predict the first swing out-of-step condition in a Western Systems Coordinating Council (WSCC) 9 bus power system. A coherency analysis was first performed in this multi-machine system to determine the two coherent groups of generators. The coherent generator groups were then represented with a two-machine equivalent system, and the synchrophasor-based out-of-step prediction algorithm then applied to the reduced equivalent system. The coherency among the group of generators was determined within 100 ms for the contingency scenarios tested. The proposed technique is able to predict the instability 141.66 to 408.33 ms before the system actually reaches out-of-step conditions.

The power swing trajectory is either a steady-state trajectory, monotonically increasing type (when the system becomes unstable), or oscillatory type (under stable conditions). Under large disturbance conditions, the swing could also become non-stationary. The mean and variance of the signal is not constant when it is monotonically increasing or non-stationary. An autoregressive integrated (ARI) approach was developed in this thesis, with differentia-

tion of two successive samples done to make the mean and variance constant and facilitate time series prediction of the swing curve.

Electromagnetic transient simulations with a real-time digital simulator (RTDS) were used to test the accuracy of the proposed algorithm with respect to predicting transient instability conditions. The studies show that the proposed method is computationally efficient and accurate for larger power systems. The proposed technique was also compared with a conventional two blinder technique and swing center voltage method. The proposed method was also implemented with actual PMU measurements from a relay (General Electric (GE) N60 relay). The testing was carried out with an interface between the N60 relay and the RTDS. The WSCC 9 bus system was modeled in the simulator and the analog time signals from the optimal location in the network communicated to the N60 relay. The synchrophasor data from the PMUs in the N60 were used to back-calculate the rotor angles of the generators in the system. Once the coherency was established, the swing curves for the coherent group of generators were found from time series prediction (ARI model). The test results with the actual PMUs match quite well with the results obtained from virtual PMU-based testing in the RTDS. The calculation times for the time series prediction are also very small.

This thesis also discusses a novel out-of-step detection technique that was investigated in the course of this work for an IEEE Power Systems Relaying Committee J-5 Working Group document using real-time measurements of generator accelerating power. Using the derivative or second derivative of a measurement variable significantly amplifies the noise term and has limited the actual application of some methods in the literature, such as local measurements of voltage or voltage deviations at generator terminals. Another problem with the voltage based methods is taking an average over a period: the intermediate values cancel out and, as a result, just the first and last sample values are used to find the speed. This effectively means that the sample values in between are not used. The first solution proposed to overcome this is a polynomial fitting of the points of the calculated derivative points (to calculate speed). The second solution is the integral of the accelerating power method (this eliminates taking a derivative altogether). This technique shows the direct relationship of electrical power deviation to rotor acceleration and the integral of accelerating power to

generator speed deviation. The accelerating power changes are straightforward to measure and the values obtained are more stable during transient conditions. A single machine infinite bus (SMIB) system was used for the purpose of verifying the proposed local measurement-based method.

Acknowledgments

I would like to thank all the people who have supported and motivated me on pursuing the masters' degree . First and foremost, I would like to extend my sincere gratitude to my supervisor Dr. Ramakrishna Gokaraju for the most precious and valuable opportunity to work in the Real-Time Power Systems Simulation Laboratory of University of Saskatchewan (U of S) and the guidance provided during the research. The creative ideas and thoughts shared generously and the invaluable insights and constructive criticisms throughout my M.Sc. program inspired me in my learning process tremendously. I am grateful for his immense contribution towards the betterment and successful completion of my research work and thesis. I would also like to thank Natural Sciences and Engineering Research Council (NSERC) of Canada and University of Saskatchewan for providing financial support throughout my study.

My sincere thanks to all the faculty at Department of Electrical and Computer Engineering who helped me to build understanding in different courses. I also owe a special thanks to Dr. Eli Pajuelo (former PhD student from the Power Systems Lab), for his conceptual contribution to "Power versus Integral of Accelerating Power Method" which was investigated during the course of this research work. I would like to thank, Mr. Ilia Voloh, Applications Engineering Manager and Dr. Mital Kanabar, Product R&D Manager from General Electric (GE) Digital Energy, Markham Canada for the discussions and valuable feedback they provided for the thesis work. The equipments provided by GE (N60 relays) are also greatly appreciated. I am also thankful to Eric Xu, Gregory Jackson from RTDS Technologies, Winnipeg, Canada for the training provided on IEC 61850 & GTNET-PMU Application and invaluable support and discussions while working with PMU models and interfacing the simulator with GE N60 relay.

I am very thankful to my fellow graduate students at the Power Lab, especially Mr. Shea Pederson, Mr. Indra Man Karmacharya, Mr. Binay K. Thakur, Mr. Xingxing Jin and Mr. Nripesh Ayer for a pleasant working atmosphere and their friendship. I am also grateful to Lab Support Engineers, staff and fellow students at the University for their direct and

indirect help during the research.

Last but not the least, I would like thank my wonderful parents, loving and caring brother and sister for always being a constant source of motivation and support through-out my educational journey. Their love and support has been critical for the successful completion of my degree.

—Bikash Shrestha

Dedicated

to my

family

Table of Contents

List of Tables

List of Figures

List of Symbols and Abbreviations

AM	Amplitude Modulation
CCA	Critical clearing angle
CCT	Critical clearing time
COA	Center of angle
CTs	Current transformers
CVT	Capacitive Voltage Transformer
DNP	Distributed Network Protocol
EAC	Equal area criteria
GOOSE	Genric Object Oriented Substation Events
GPC	GIGA Processor Card
GSE	Genric Substation Events
GSSE	Genric Substation State Events
GT I/O	Giga Transceiver Input/Output
GTAO	Gigabit Transceiver Analog Output
GTNET	Giga Transceiver Network Interface Card
GTSYNC	Giga Transceiver Synchronization Card
GTWIF	Gigabit Transceiver Workstation Interface Card
IEC	International Electrotechnical Commission

IED	Intelligent Electronic Device
IEEE	Institute of Electrical and Electronics Engineers
IRIG	Inter-Range Instrumentation Group
LRI	Left resistance element (inner)
LRO	Left resistance element (outer)
OECD	Organisation for Economic Co-operation and Development
OpenPDC	Open Phasor Data Concentrator
PMU	Phasor Measurement Unit
PPS	Pulse Per Second
PSBD	Power Swing Blocking Delay
PTs	Potential Transformers
RAM	Random access memory
ROM	Read only memory
RRI	Right resistance element (inner)
RRO	Right resistance element (outer)
SCADA	Supervisory Control and Data Acquisition
SCV	Swing Center Voltage
SONET	Synchronous Optical Networking
SV	Sampled Values
TCP	Transmission Control Protocol
UDP	User Datagram Protocol
WAMS	Wide Area Measurement Systems

Chapter 1

Introduction

1.1 Background

The overall production of electricity in 2009 reported by Organisation for Economic Co-operation and Development (OECD) was 20,053 TWh and the sources of electricity include 67% of fossil fuels, 16% of renewable energy (mainly hydroelectric, wind, solar and biomass), and 13% of nuclear power and 3% of other sources [1].

A power system is a complex dynamic system made up of interconnected power equipment. It mainly consists of generation, transmission, and distribution units. Generation and load are often located far apart and are interconnected through a transmission network maintaining the power demand and supply at equilibrium. An electric power system is therefore a network of electrical components designed to supply reliable, reasonably priced, and quality energy to consumers. The generation equipment generates electrical energy from other forms of energy, such as coal, hydro, nuclear, or fossil fuel, which are interconnected through networks of transmission lines (power grid). The transmission equipment transmits the bulk of the generated energy from one location to another at higher voltage levels. The distribution network finally distributes the energy to consumers at lower voltage levels.

During normal operating condition, generation of and demand for electrical power exist in balance in the system. However, the demand for electricity is usually unpredictable and shows a random nature. To accommodate these characteristics, a power system is equipped with power generation and flow control devices throughout the transmission and generation units (such as an excitation system, governor, regulating transformers, etc.) [2].

Such equipment helps to maintain the power system at its normal voltage and frequency, generate sufficient power to meet the load, and maintain optimum economy and security in the interconnected network as defined by the standards [3].

Steady-state operation of power system can be disturbed by faults, load changes, line trip- outs, etc., and cause system variables to deviate from normal values. The deviations due to small disturbances can be handled by control devices that bring them back to a normal condition. In cases of severe faults, the control devices may not be able to handle the changes, resulting in abnormal operation of the system. Protection system design must safeguard power systems from such abnormal conditions, which will be discussed in detail in Section 1.3. The response time of protection devices is generally faster than that of control devices. Protection functions act to open and close circuit breakers, thus changing the structure of the power system, whereas control functions act continuously to adjust system variables, such as the voltage, current, and power flow of the electrical network [3].

Power systems subjected to a wide range of large disturbances can lead to unstable system conditions. Power system faults, line switching, or loss of generation can cause sudden changes in electrical power, whereas mechanical power input to a generator tends to remain relatively constant. An imbalance between the input mechanical power and the output electrical power because of a disturbance causes generators in a region to run faster than the generators in another region. This results in angular separation between a given generator and the rest of the utility system, or between interconnected power systems of neighboring utilities, which continues to increase if the system cannot absorb the kinetic energy corresponding to the rotor speed differences. If the angular separation exceeds 180 degrees, the two regions lose synchronism. This condition in a power system is called an out-of-step condition. If such a loss of synchronism occurs, it is imperative that the generator or system areas operating asynchronously are immediately separated to avoid widespread outages and equipment damage. Out-of-step tripping was not widely used in power systems for many years. However, it is receiving more attention because of very large generating units connected to extra-high voltage and ultra-high voltage circuits. The lower inertias and the higher reactances of the generators reduce the stability limit of the system [4].The out-

of-step condition can cause unwanted relay operations at different network locations, which can aggravate the power system disturbance and cause major power outages or blackouts. Hence, predicting out-of-step conditions must occur in advance of system collapse due to cascading outage [3].

A number of major system blackouts have been occured in past decades. One of the recent major blackout took place in Turkey on 31st of March 2015. The blackout mainly affected the Turkish grid. The outage started with four 400 kV long transmission lines operating in the central section of the 400 kV East to West transmission corridor of Turkey. At first, the Osmanca Kursunlu line, carrying 1127 MW/1237 MVA, tripped on overload. This event initiated a loss of synchronism between the Eastern and Western subsystems of Turkey, with fast consequential tripping (in 1.9 seconds) of all of the parallel lines by the line distance protection relays. As a consequence, the Eastern and Western Turkish subsystems were separated. Further, the insufficient power supply reduced the Western subsystem frequency to below 47.5 Hz, causing several generators to trip in the subsystem. This caused the collapse of the Western subsystem approximately 11 minutes after the disturbance. The Eastern subsystem was left with a surplus of generation of approximately 4,700 MW, could not survive the disconnection of generators due to overfrequency, and collapsed within a few seconds [5].

The major North American outage/disturbance that is widely cited is the Northeast U.S. and Southeast of Canada disturbance of 14 August 2003, which caused the loss of 61.8 GW of generation in a matter of 1 to 2 hours and disconnection of approximately 50 million customers from supply. The outage started with the tripping of a generator in Ohio, caused by overloaded excitation, and several 345 kV lines. This caused a power swing in other lines and tripped many other lines and loads, which finally led to loss of synchronism among multiple regions in the Northeastern and Southeastern interconnected network. Similar disturbances happened in the Western USA on both 14 December 1994 and 2 July 1996, affecting millions of customers [6–8]. In such circumstances, several issues come into play for the system to collapse, and restoring the system quickly is another major challenge. Wide area measurements and proper operation of out-of-step relays on the order of seconds so that

there is a reasonable balance between generation and load within each island are some of the important considerations to prevent the scale of blackout and quickly bring the system back to normal operation.

Solution to widespread contingencies can be often difficult to achieve without information from all of the generation, transmission, and interconnected points in the network [9]. Local protection systems applied to protect equipment are not sufficient and, therefore, a wide area effective protection system design is necessary to handle such cases. Upon detection of a network instability condition, the wide area protection system permits selective tripping for clearly unstable cases so that the system is separated into islands, with a reasonable match between generation and load within each island [10]. The current practice is that the places where tripping is permitted are pre-determined based upon simulations performed during system planning studies [3]. However, a more appropriate procedure would be to determine both the nature of a swing in progress as well as desirable location points for separation in real time.

The main focus of this thesis is a wide area measurement system (WAMS) solution for finding network instability conditions in power systems. This involves developing and testing a scheme for out-of-step protection in a power system using the wide area measurements discussed above using a power systems simulator and a relay. Moreover, electromagnetic transient (EMT) type time domain simulations (i.e., RTDS) were used to determine the accurate behavior of a power system under faulted conditions, instead of the stability programming tools normally used. Such stability programs rely on phasor-type solutions and simplified models and do not provide an accurate representation of the behavior for out-of-step transient conditions. The EMT simulations described in this thesis use detailed transient models of the various power system components, and therefore give an accurate representation of the oscillations. They produce the responses of the components in a time domain that closely resembles actual component behaviors.

The following sections in this chapter explain the power system stability and protection in brief and the current research trends in the power industry in this area. The past and present practices in out-of-step relaying are discussed in the literature review section. The

contributions of this thesis and the thesis outline are also provided.

1.2 Power System Stability

The stability of a dynamic system is the ability of an electric power system to regain a state of operating equilibrium after it is subjected to a physical disturbance for a system operating at equilibrium condition initially. Power system stability equations involve nonlinear terms, higher order differential equations, and rapidly varying time varying quantities. The key factors that affect the stability can be classified into three major areas: rotor angle stability, frequency stability and voltage stability. Further classification of power system stability depends on the severity of the disturbance and the time duration to be considered for the stability studies. The rotor stability is typically a short term phenomena whereas the voltage and the frequency stability could be either a short term or long term phenomena. The classifications are shown using the following diagram, reported in the stability literature 1.1 [11].

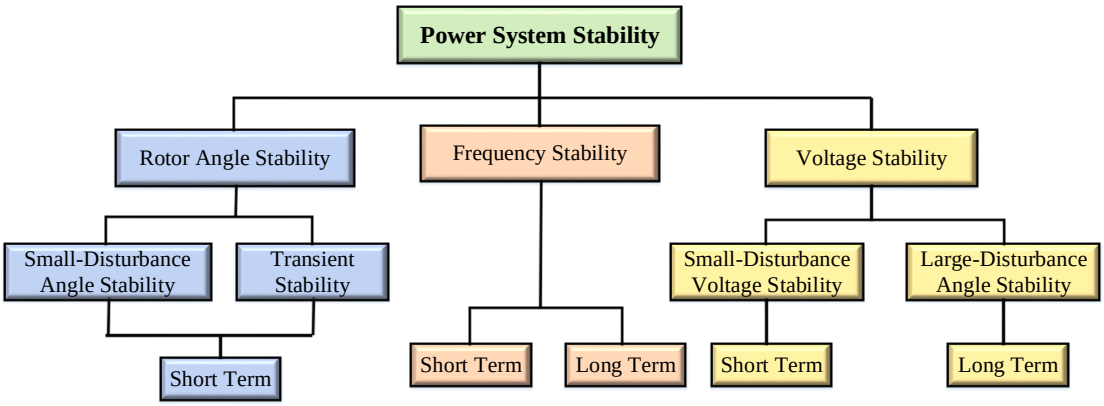

Figure 1.1: Classification of power system stability

Evaluation of stability depends upon the behaviour of the power system when subjected to a disturbance. The disturbance can either be small or large. The small disturbances are due to small perturbations on the system such as small continuous load changes from which a system is able to adjust itself. Severe disturbances are for example, short-circuit

on a transmission line, loss of tie line between two subsystems or loss of generation or huge load changes, which causes major variations in power transfer, machine rotor speed and bus voltages. The power output from a synchronous machine starts fluctuating, which causes the rotor of the machine to accelerate and decelerate with respect to the stator circuit. As a result, the synchronous generator starts oscillating with other synchronous machines in the system [12]. The stability of the system then is determined by the available synchronizing and damping torque in the system. If the oscillations damp out and settle to an equilibrium state in a finite time then it implies stable operation of the system. In case of the system not being able to dampen the oscillations, an unstable situation arises from which the system cannot return to a steady state and the generator or group of generators experience pole slipping [2]. This phenomenon is called an out-of-step condition in stability studies. It is also referred to as loss of synchronism or rotor angle instability. If the out-of-step condition is not detected ahead before its occurrence, it can create a cascading effect, such as unnecessary tripping of other major lines, generator tripping and so on. There have been multiple blackouts in the past decades due to out-of-step conditions as mentioned in reference [11] and reference [13]. Therefore, the design and implementation of accurate and fast out of step protection has become necessary.

1.3 Power System Protection

The modern day society has come to depend heavily upon continuous and reliable availability of electricity. Industries, telecommunication networks, transportation services like railways, banking sectors and dominantly the large number of domestic users rely highly on reliable sources of electricity. But the disturbances in power systems cannot be avoided no matter how robust the system design is, and they always put the system at risk. A proper protection system is therefore necessary for a secure and reliable power system operation [14].

1.3.1 Basic Protection

Power-systems protection is a part of power engineering that exclusively deals with the protection of power system components from faults during and after the fault inception. The prime objective of a protection scheme is to maintain the power system stable condition by separating the components that are under fault and leaving rest of the network still in operation [12]. The devices that are used to protect the power systems from faults are protection devices. These devices include instrument transformers (Current Transformers (CTs), Potential Transformers (PTs)), relays, breakers and communication devices which are the key equipments in power system protection. Instrument transformers are used as a metering device to scale down the high voltage and current signal and make it available to the relays. The protective relay detects abnormal power system conditions, and initiates corrective action as quickly as possible in order to return the power system to its normal state [14]. A relaying system is usually designed to protect only a certain portion of the power system. The communication system helps to establish a continuous communication between two or more relaying systems to ensure a coordinated operation of the whole protection system [7].

The protection scheme relay designed to protect a certain region should trip only those circuit breakers whose operation is required to isolate the fault in that region. However, there should be no region in a power system which is left unprotected. This requirement can be handled through the division of the power system into protective zones. In case a fault were to occur in a specific zone, necessary actions will be executed to isolate that zone from the entire system. Zone definitions account for generators, buses, transformers, transmission and distribution lines, and motors. An edge of a zone of protection is defined by the CTs through which the associated relay sees the system inside the zone of protection. Figure 1.2 gives an overview on how the protection zones are defined for different power system elements in the power system.

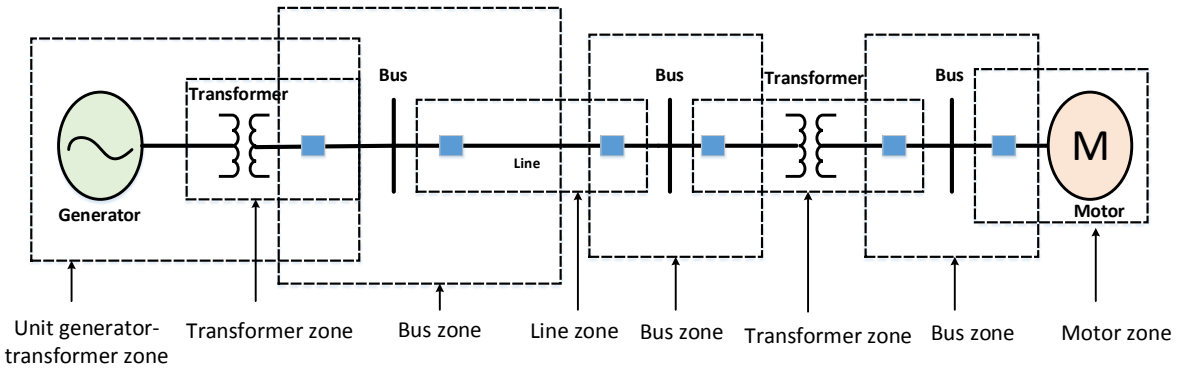

Figure 1.2: Typical relay primary protection zones in a power system with overlapping zones

1.3.2 Digital Protection

Initially substation protection, control, and metering functions were performed with electromechanical equipment. These equipment were gradually replaced by analog electronic equipment, most of which had similar single function approach of as electromechanical precursors. Both of these technologies required expensive cabling and auxiliary equipment to produce functioning systems. However, in recent days digital and numerical relays with multifunctional and communication capabilities are introduced. These relays have reduced the cabling and auxiliaries cost significantly. The functions performed by these products have become so broad that many users now prefer the term IED (Intelligent Electronic Device) [15]. A digital relay consists of an analog to digital (A/D) converter, microprocessor or microcontrollers, random access memory (RAM) , read only memory (ROM) and software programs to implement a protection logic. It provides low cost, fast performance, flexibility, wider range of settings and greater accuracy than mechanical relays. However, the limited computational power of the microprocessors used in digital relays results in longer operation time and also limits the number of protection functions that can be included in a relay. Numerical relays overcome such limitation by the use of specialized digital signal processors and dedicated microprocessors as computational hardware. Numerical relays are a one-box solution for power system protection and automation [14]. The GE N60 relay, manufactured by General Electric, Inc., is one example of a numerical relay which encompasses 9 protection functions, synchronism check, phase under/over voltage, under/over frequency, power

swing blocking, synchrophasor capabilities, etc. in a single unit [15]. It also supports high speed communications are required to meet the data transfer rates required by modern automatic control and monitoring systems between two IEDs, from transmission to reception as established by the IEC 61850 (International Electrotechnical Commission) standard.

1.3.3 Wide Area Based Protection

Local automatic actions are currently used to protect systems from the spread of fast-developing emergencies. However, protection systems in the power industry designed to address local problems are not able to consider the overall system, which may be affected by a disturbance. Due to the increased interconnections, modern power systems can benefit from system-wide protection schemes with modern relays and fast communication technologies. Computer-based relays with communication capabilities have made the solution promising and brought protection design practices to the next level. Wide area monitoring, protection, and control (WAMPAC) and synchronized phasor measurement technology (SPMT) are being explored and implemented in the power industry around the world [9]. WAMPAC uses phasor measurement units (PMUs) to gather data from various locations of power systems. The PMUs measure and transmit the data to a central control station where they are synchronized in time using a GPS clock. This allows accurate comparison of measurements from widely separated locations. The IEEE Power System Relaying Committee (PERC) has reported a scheme called the System Integrity Protection Scheme (SIPS) [13], which is proposed to protect the integrity of a power system or some portion thereof by incorporating various protection schemes in a package. The package includes Special Protection Schemes SPS), Remedial Action Schemes (RAS), and other additional schemes, such as those addressing underfrequency, undervoltage, and out-of-step conditions, and involves multiple detection and actuation units equipped with communication facilities. The SPS and RAS are event-based systems that are specially designed to directly detect selected disturbances potentially leading to instability using a binary signal and to perform a predetermined corrective action [13].

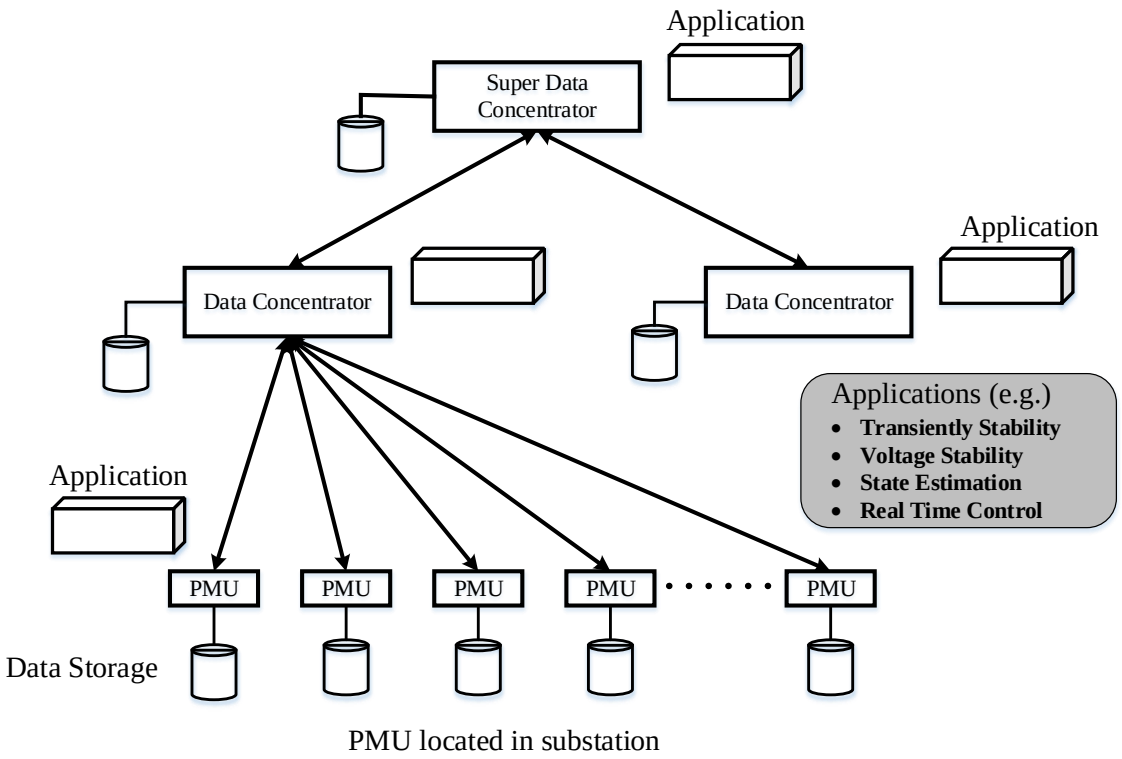

Figure 1.3: Wide area measurement system architecture

1.4 Literature Review

Several methods are proposed in the literature to predict out-of-step conditions in a power system. These methods can be segregated into two categories depending upon the location of measurement used for the application. The methods are categorized and briefly summarized next.

1.4.1 Local Measurement Based Methods

Rate of Change of Impedence Method :

During a power swing, electrical quantities such as voltage, current, and frequency change. Because of the change in voltage and current, impedance values seen at various location of the power system also change.

Blinder Scheme: One conventional technique [6,16] is based on the rate of change of impedance. The scheme continuously monitors the change in impedance at the relay location. Power swing detection is based on the time taken for the impedance to travel between pre-set impedance elements called blinders. The time taken by the impedance is compared with the pre-set timer to differentiate between a power swing and a fault. The scheme is called a blinder scheme. Setting the blinders and determining a pre-set delay are two major tasks in this technique. References [16, 17] describe some techniques to set these blinders, where the settings are system specific, depend on system loading conditions, and are only applicable up to a two-machine system. Setting blinders requires extensive system stability studies, and designing a relay using blinders to work for all possible system conditions is impossible. The settings are therefore made with certain assumptions of expected load conditions and oscillations following major disturbances. The settings perform well for assumed system conditions, where the system continuously goes through changes in its structure and loading patterns. Continuous updating of the settings is required to cope with changing system conditions. However, this is not done in most power systems because of scheduling difficulties and lack of manpower [10]. Moreover, the time delay setting for the relay depends on the slip frequency. Relays set for low slip frequencies will not work for high slip frequencies [6].

Quad Scheme: Modern distance relays offer quadrilateral characteristics, the resistive and reactive reach of which can be set independently. It therefore provides better resistive coverage than any mho-type characteristic for short lines. A quadrilateral distance characteristic consists of four elements. Each side of the quadrilateral characteristic represents a different element: the reactance element (top line), positive and negative resistance boundaries (right and left sides, respectively), and the directional element (bottom line). A concentric quadrilateral (quad scheme) for power swing detection is used in the GE N60 relay [15]. The concentric quadrilateral consists of outer and inner characteristics for both blocking and tripping functions and works on the same principle as dual blinder schemes. If the measured impedance remains between the two impedance measurement elements for a predetermined time, then the swing is considered a stable swing; otherwise it is an unstable swing. A power swing blocking signal is issued in the case of a stable swing and an out-of-step tripping signal

is issued in the case of an unstable swing.

Scheme based on Continuous Impedance Calculation: Prior network studies are necessary to find accurate setting for blinders in rate of change of impedance-based methods. The settings remain unchanged unless the operator makes the change and cannot adapt to fluctuating system conditions. Lack of proper grid studies, i.e., those not covering the worst-case scenario, can cause misoperation during swing and out-of-step conditions. Also, the logic that a power swing is a symmetrical phenomenon and asymmetrical current (or voltage) could be used to release the distance protection function is not possible in some of the complex applications. Reference [18] proposes a power swing detection function based on continuous impedance calculations that require no settings for operation. The algorithm described calculates new R, X values for each phase and compares them with historical values (memorized values). To distinguish a power swing from a fault, the continuity, monotonicity, and smoothness are checked. Monotonicity determines the direction of the derivatives of R and X, continuity identifies whether the impedance vector is not stationary, and smoothness determines if two successive changes in both R and X are under the threshold to ensure uniform movement of the swing. The referenced paper also suggests tripping out-of-step protection when the impedance crosses the line angle inside the right blinders of the concentric quad, consequently three times from the right side.

Swing Center Voltage Method :

The swing center voltage (SCV) technique discussed in [6] is a voltage based method. The SCV is a point of zero voltage between two source equivalent systems when the angular separation becomes 180 degrees. The point of zero voltage is called the electrical center. The SCV technique estimates the rate of change of voltage, which will be at a maximum at the electrical center. The detection is usually made at a voltage angle separation close to 180 degrees. If tripping is initiated under this condition, it causes twice the rated stress for the circuit breaking device. Hence the operation of the circuit breaker is deferred to a later instant when the voltage angle separation is less. Also, the estimate of the SCV using local measurements of the voltage phasor will only be valid when the impedance angle is 90 degrees.

R-Rdot Method :

An out-of-step relaying scheme with rate of change of apparent resistance augmentation is proposed in [19]. The relay was installed at the Malin substation on the Pacific AC Intertie and Western North American Power System in February 1983. The relay characteristic is a modified version of the blinder scheme where the rate of change of apparent impedance is replaced with the apparent resistance augmented with the rate of change of apparent resistance and the relay characteristic is defined in the R-Rdot plane. The technique involves setting a piecewise linear resistive element on an R-Rdot plane. The scheme also requires extensive simulation studies under various contingency conditions to set the relay characteristics and has similar types of demerits as the blinder scheme.

Equal Area Criterion in Time Domain :

Reference [20] proposed an out-of-step protection using equal area criterion (EAC) conditions in the time domain. EAC is a method that uses power-angle curves to evaluate the transient stability of a power system, hence, it is regarded as a stability assessment in the power-angle domain. The proposed technique only uses local output electrical power (Pe) information and does not require power system parameter information (line impedances, equivalent machine parameters etc). The electrical output power, Pe over time is calculated from local voltage and current information measured at the relay location. The transient energy which is the area under the electrical power output-time ($P_e - t$) curve is computed and the swing classified as stable or out-of-step based on the findings. However, the method has a shortcoming in that it is not predictive and detect instability after the generator pole slip occurs.

Energy-Based Transient Stability :

Out-of-step detection schemes using transient energy calculation are also proposed in the literature. Reference [21] implements Lapunov's direct method to predict the out-of-step condition of a generator using local substation measurements. For a particular fault scenario mentioned in [21], the detection angle is 136.7 degrees, which results nearly in twice (1.9 times) the stress for out-of-step breakers. The technique is limited to local generator protection and does not cover wide-area instability issues. Moreover, the technique does not provide critical clearing time (CCT) information, which is an important piece of information

for relaying and stability study purposes.

Reference [22], discusses a transient stability monitoring method utilizing synchrophasors. It utilizes a dynamic state estimator (obtained from PMU measurements) from which a real time estimated dynamic equivalent of the generator is found. The dynamic equivalent model is used for the stability analysis of the generator using Lyapunovs direct method. The dynamic state estimation is done in a substation utilizing synchronized and non-synchronized local measurements. When multiple generators are connected to the substation, the information is utilized by the referenced work to identify the center of oscillations of the system. The method is initialized whenever a disturbance is detected. Once the center of oscillations is known, a simplified equivalent system is derived that represents the dynamic oscillations of the actual system. The simplified equivalent is updated continuously with the dynamic state estimator and is further used for the characterization of the stability of the system. In the reference paper the monitoring scheme is utilized for predictive generator out-of-step protection. The net energy of the generator is continuously monitored and the total energy stability limit is computed. If total energy exceeds the stability limit then an instability is indicated and a trip signal is transmitted to the generator.

Third Zone Distance Blocking Scheme :

Third zone distance relaying has been recognized as one of the major causes of cascading outages in power systems. The unwanted third zone operations caused by large loading conditions have often contributed to cascading outages eventually leading to a major blackout. The 14 August, 2003 blackout is the most notable, recent event in North America demonstrating the vulnerability of zone 3 protection [23, 24]. Reference [23] reexamines the application of zone 3, to describe situations where it can be properly utilized, where it can be removed without reducing the reliability of system protection and, if used, how it can be modified or set. The concept of critical locations is also discussed to assist the planning engineers in determining if potential zone 3 undesirable operations are a serious problem to the system and if the expense and difficulty of removing zone 3 or changing the relay or its associated station are justified.

The protection against tripping of the third zone due to a power swing has been proposed

in reference [25] using a third zone distance blocking scheme. At the relay location, the entire system is represented by a single machine infinite bus (SMIB) equivalent system. This scheme uses the local measurements at the relay location to calculate the relative speed of an equivalent machine. The stability of the swing is determined by employing the first zero crossing(FCZ) concept where zero crossing of the relative speed classifies the swing as a stable swing otherwise the swing is classified as unstable. The proposed scheme has benefits of minimum calculations involved using local measurements and no need for prior stability studies to find relay settings.

Frequency Deviation of Voltage Method :

Reference [26] proposes an out-of-step detection technique using a frequency deviation of the voltage method. The technique estimates the frequency using voltage angle calculated at the local bus. Further the angular acceleration is calculated using the calculated frequency. An instability is detected when the frequency measured at the point, where acceleration changes its sign from negative to positive, is greater than zero; otherwise, the system will be stable. One of the major benefits of this technique is that it can detect not only the first swing instability but also the multi-swing instability. Also, the method for finding the out of step conditions is simple and does not require network parameter information. The method could be used in simulation studies but may pose practical issues when implemented in a relaying application. First, calculating the speed and acceleration from the terminal voltage angles of the generator is prone to errors due to the derivative terms used, significantly amplify the power system noise. Second, the estimated generator rotor speeds from the voltage angle measurements have large errors during the transient period and an appropriate time delay needs to be introduced before accurate estimates of the speed and acceleration are obtained.

Power versus Speed Deviation Method :

Reference [27] proposes a method using online measurement of electrical power and the generator speed as inputs. The equilibrium point is obtained using the electrical power signal where the difference between mechanical power (P_m) and electrical power (P_e) goes from negative to positive assuming that the Pm is constant. The relative speed of the machine where the state changes from deceleration to acceleration determines the stability

of the system. The generator speed and the power are made readily available to the relay for analysis. This method has the advantage that it does not require network admittance matrix reduction or any dynamic model approximations. In addition, it is not affected by any switching transients, as the generator speeds, due to the machine inertia, are characterized by smooth changes even during transient conditions.

Power versus Integral of Accelerating Power Method : Another out-of-step detection technique called 'power vs integral of accelerating power' is explained in reference [28] and uses the local measurement of electrical power. This method addresses the practical difficulties associated with the frequency deviation of voltage method by using the electrical power deviation instead of estimating the rotor acceleration (electrical power deviation has a direct relationship to rotor acceleration); and the integral of accelerating power instead of directly estimating the rotor speed (integral of accelerating power has a direct relationship to generator speed deviation). The electrical power changes are straightforward to measure and the values obtained are more stable during transient conditions. The mechanical power deviations could also be included in the analysis to obtain an accurate estimate of the speed and acceleration changes. Power based and accelerating power based stabilizers have also been reported by the Excitation Controls Subcommittee of the IEEE Energy Development and Power Generation Committee [29]

1.4.2 Wide Area Measurement Based Methods

Post-Disturbance Voltage Trajectory based Out-of-Step Prediction :
Voltage-based methods to predict system stability are presented in references [30] and [31]. In the reference [30], the combined investigation of voltage trajectories from important buses is used to predict system stability status after a disturbance. The work involves estimation of the similarity of post-fault voltage trajectories of the generator buses after the disturbance to some pre-identified templates. The accuracy of this method depends upon the test conditions having voltage trajectories close to a pre-identified voltage template.

The rate of change of voltage (ROCOV) with respect to the voltage deviation (ΔV) post

disturbance is studied in reference [31]. The stability boundary of ROCOV in ROCOV-ΔV plane is defined from the simulation experiments for each generator in the system. An unstable condition in the system is declared when a post-disturbance ROCOV trajectory crosses the stability boundary from the stable region to the unstable region. One of the limitations of this method is an inability to incorporate major topological changes for stability prediction due to pre-calculated stability boundary conditions.

Equal Area Criterion with PMU Measurements :

The conventional EAC using the P versus δ method discussed in the literature for out-of-step protection. It involves the calculation of accelerating and decelerating area using power-angle characteristic curves. During transients, the criterion for a stable condition is when the decelerating area is greater than the accelerating area; the opposite case denotes unstable condition. The approach is directly applicable to an SMIB system [32] and was extended to a multi-machine system by Pavella et al. [33]. The scheme was investigated in a large system configuration when it separates into two oscillating groups during transient conditions. The technique is called extended EAC (EEAC). Reference [34] utilizes PMU measurements from generating stations and calculates the rotor angle of generators in the system. Then the system is reduced to an SMIB equivalent. Once the machine equivalent has been calculated with machine angle information, the EAC is used to assess the transient stability of the system. Also, based on the EEAC, an adaptive out-of-step relay was developed by Phadke et al. [35]. The relay was implemented on the intertie between the states of Georgia and Florida in the USA in October 1993 and was operational until January 1995. The behaviour of the system during power swings is approximated by a two machine equivalent, one of which represents the generators in Florida and the other the generators in the southeastern USA. The generator group in the southeastern USA is a very large system and is assumed to be an infinite bus to the Florida system. The relay estimates input mechanical power using the electrical power and angular separation between these two regions and uses the EEAC for out of step detection. The out-of-step detection using the EAC is simple and well established; however, EAC based techniques cannot simultaneously provide the critical clearing angle (CCA) and CCT for the fault. Calculation of CCT requires step-by-step

integration techniques.

State Plane Analysis :

Reference [36, 37] proposes an out-of-step prediction algorithm using a state plane plot of speed verses power angle. System-wide measurement and communication to the relay have made this method realizable. The generator bus voltages are continuously monitored to find the separation of generators during disturbances. After a disturbance, the generators in a large system separating into two groups are represented with an SMIB equivalent system. The separation of machines is found by real-time coherency analysis. The state-plane analysis (SPA) algorithm is applied to the SMIB equivalent, and the dynamic states of the SMIB equivalent at different stages (during and after the disturbance) are represented using a state plane plot to determine the stability of the system. Through the state plane analysis, the CCA and CCT are calculated and used to predict stable or out-of-step conditions in the power system. The out-of-step tripping is then done on pre-selected lines to restore the stability of the system.

Artificial Intelligence :

Fuzzy logic and neural networks are based on the principle of creating an artificially intelligent system that is able to perform future tasks for which it has been trained. This method can be applied to local measurement schemes as well. This approach is applied to out-of-step detection by training the fuzzy and neural systems with respect to a number of possible power swing scenarios. Reference [38] proposed an out-of-step protection scheme using fuzzy logic and reference [39] proposed a technique using a neural network. Rajapakse et al. [40] propose a rotor angle instability prediction technique using a fuzzy C-means clustering algorithm and a support vector machine. Fuzzy C-means clustering required a large offline simulation study database to identify the variation in voltage at generator buses. The support vector machine also used the same database to build a trajectory template to compare the actual voltage oscillations. These approaches require a large number of offline simulations to train their algorithms. The algorithms work well only if they are sufficiently trained and the training signals are appropriately identified. However, the method becomes cumbersome with increased interconnections and tends to fail for unforeseen conditions in a power system.

Linear Rotor Angle Prediction :

Reference [41] proposed an adaptive out-of-step protection method using wide area measurements. The method uses linear curve fitting of the generator rotor angle and the slope to identify the coherency among generators during a disturbance. After system coherency information was used to calculate the characteristic angle of each coherent group, the differences in angles between the groups were compared with a threshold value to determine the stability. This method could adjust to current system conditions and make stability decisions but lacked the ability to predict out-of-step conditions in the system.

Polynomial Rotor Angle Prediction :

Reference [42] proposes an online transient stability prediction method using PMU measurements. This method is implemented in IBM InfoSphere Streams, a stream processing middleware from IBM Research. The method obtains real-time measurements about rotor angles and power of generators in the system using PMUs and time aligns the measurements. The generator rotor angle trajectories are predicted using the polynomial curve fitting technique using 10-12 samples after a fault in the system. The predicted information for rotor angle is used to identify the critical and non-critical machines. Each group of critical and non-critical machines is converted to an equivalent single machine and stability is evaluated using the acceleration and deceleration areas, a fundamental concept of equal area criteria. Though the computation is carried out in the streaming environment, the implementation involves numerous calculations and the transient stability is also predicted based on only a few sample fault data received by the PMUs.

Finite Difference Based Prediction :

Reference [43] proposes an approach for rotor angle stability prediction that uses PMU measurement of voltage and currents at 50 samples/s to develop generator speed and rotor angle data series. The rotor angle is predicted using the finite difference method for the next 100 ms and real-time data-mining-based clustering is used for identification of critical machines. The power system is then represented by means of an SMIB equivalent model for the cluster groups. The instability margin and the time to instability are used to characterize the transient stability of the system. The technique can provide the instability margin and

time to instability but cannot predict far in advance (prediction only made for 5 samples ahead).

1.5 Objective of the Thesis

The objectives of this thesis are summarized below.

1. Develop a method for predicting the stability of the power systems using the wide area measurement.
2. Determine the optimal PMU locations in the system.
3. Test the proposed scheme in multi-machine system configurations and compare its performance with the conventional rate of change of impedance method and swing center voltage method.
4. Test the proposed scheme using PMUs in a GE commercial relay interfaced with a real-time digital simulator.

1.6 Organization of the Thesis

The thesis is organized into six different chapters.

Chapter 1 explains the concept of power system stability and protection. The importance and necessity of out-of-step protection in power systems are highlighted. Some of the current practices for out-of-step protection and those mentioned in the literature are briefly discussed, and their merits and demerits also pointed out. The motivation and the thesis objectives are also discussed.

Chapter 2 discusses power swing phenomena in power systems and their impact on existing protection elements. It primarily focusses on out-of-step prediction and some of the major schemes to detect power swings. The advantages and shortcoming of existing methods

for out-of-step detection are also briefly described. Chapter 2 also introduces a new approach using power vs. accelerating power to predict out-of-step conditions in power systems.

Chapter 3 starts with an explanation of synchrophasor technology and its importance in power monitoring and control. A brief introduction to PMUs is presented in the beginning of the chapter. Optimal PMU locations for complete observability of the test system are investigated and the results presented. Time series analysis and forecasting of the discrete time data are explained along with the model selection details. Further, the solution to the stability problem in large networks utilizing real-time data from WAMS is explained and the proposed synchrophasor-based out-of-step prediction using a time series swing curve is presented.

In Chapter 4, out-of-step conditions are studied for a large power system configuration. The proposed stability prediction method is implemented for a WSCC 9 bus system using the PMU model in an RTDS. The two blinder scheme is also implemented for the same system and the results compared with the proposed method. The swing locus in the multi-machine system is also evaluated.

In Chapter 5, a commercial GE N60 relay is used to study out-of-step conditions. The interfacing of the relay and the RTDS is explained, where the analogue current and voltage signal from the simulated system in the RTDS act as inputs to the relay. The proposed method is tested for the PMUs in the N60 relay. A WSCC 9 bus test system is used to evaluate the performance of the methods.

In Chapter 6, the research contributions are summarized and future extensions of the work are outlined.

Some of the additional information is included in three appendices. Appendix A gives the test system data and information used in this research. In Appendix B, the guidelines for blinder settings to detect the out-of-step condition are discussed. Appendix C explains analysis of power swing in the multi-machine system.

Chapter 2

Commonly Used Out-of-Step Protection and Power Swing Blocking Methods

2.1 Introduction

There is a long history of recorded out-of-step conditions in power systems spanning almost a century (starting in the 1920s). Earlier power systems had a simple structure and consisted of a generating station feeding a load center over long distances. The main reason at that time for instability was insufficient synchronising torque [44]. Power systems have since have grown in size and complexity; generating stations are now interconnected with each other, and one or more generating stations may lose synchronism with the other generating stations.

This chapter discusses the concept of out-of-step protection in a power system. The impedance swing locus in an R-X plane is discussed at the beginning of this chapter followed by the effect of a power swing on different types of protection schemes. The strengths and limitations of each of the schemes are also discussed. The current practices in out-of-step relaying and the importance of out-of-step relaying at the present time are also discussed.

One of the innovative new ideas to detect out-of-step conditions is using the power versus integral of accelerating power method, which was developed during the course of this MSc research is also discussed in this chapter. This new type of analysis method has been included in the Rotating Machinery Committee (J-5) of the IEEE Power Systems Relaying Committee document report entitled "Application of Out- Of-Step Protection Schemes for Generators, which explains the latest out-of-step protection practices in the industry.

2.2 Power Swing Phenomena and Rotor Angle Instability

During the steady state (normal operating condition), the generators connected to the power system deliver constant power, maintaining a balance between the mechanical input and the electrical output of the machines. Similarly, there is a balance between the electrical power output of the machines and the consumed load. The interconnected generators also run at synchronous speed with a constant relative rotor angle separation between them and the frequency of the system remains close to nominal frequency (60 Hz or 50 Hz) [2, 6]. Figure 2.1a shows a typical current and voltage waveform during the steady state operation of a power system.

However, the power systems are continuously subjected to various types of disturbances such as large changes in loads, power system configuration changes, line switching, loss of generation, etc. Any of these disturbances introduced in the system cause oscillations in the rotating units associated with the system. Due to these disturbances, a sudden change in the electrical power output of the generator occurs. Since the mechanical input to the generators cannot change immediately during this short interval, the generator rotor starts accelerating resulting in electromechanical oscillations in the system. These oscillations cause fluctuation in the magnitude and phase of the voltages and currents throughout the system [45]. As a consequence, the power flow between the various parts of the system also starts oscillating. Such a power system phenomena is known as a power swing [6]. The current and voltage oscillations during a power swing condition are shown in Figure 2.1b.

The standards for the operating limits are laid out in the Power System Reliability Committee (PSRC) report [6]. The power engineers design a system as per the standards to withstand variations in current, voltage, power and frequency as long as it falls within certain desired limits (maximum 5% for voltage, 1% for frequency and so on). Asynchronous operation of generators in the system can take place if the voltage angle separation between the tie line buses in an interconnected system goes beyond 180 degrees. This angular separation ultimately leads to the slipping of generators poles and sustained oscillations of power in

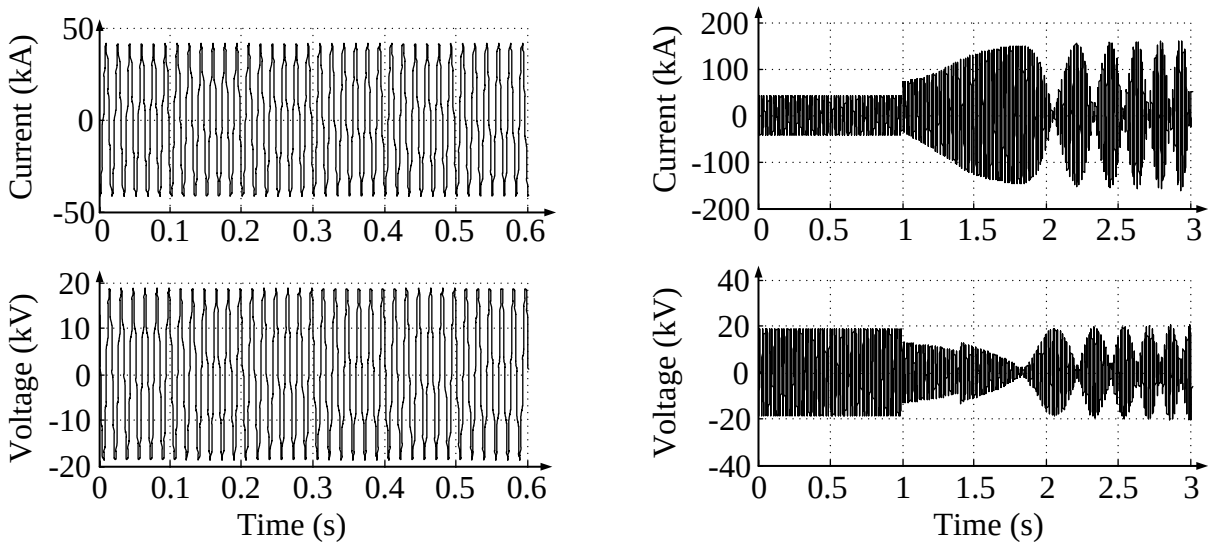

(a) Waveform during steady state

(b) Waveform during power swing

Figure 2.1: Instantaneous voltage and current waveforms

the system. Therefore, the system state after the disturbance depends upon various factors such as the initial operating point, severity of a disturbance, action of the control equipment and the existence of synchronizing and damping torques in each machine [11].

Depending upon the nature of power oscillation, power swings are classified into two categories: stable swings and unstable swings. Whenever the swing damps out and converges to a new steady state point, it is referred to as a stable swing. If the swing goes through a sustained oscillation, it is referred to as an unstable swing. This condition is also referred to as an out-of-step condition or is also referred to as a rotor angle instability [6, 11].

A convenient method for visualizing and detecting a power swing is by looking at the apparent impedance at the relay location [46]. This method came into application in alternative to power swing detection by monitoring the fluctuations in voltage and current, which take several slip cycles to detect. The apparent impedance seen by the relay changes during a power swing and is discussed in Section 2.3.

2.3 Impedance Locus During Power Swing

A distance relay in a power system measures impedance and uses the impedance characteristics to detect faults in the system. The impedance characteristic of a relay is defined in such a way that the impedance enters inside the characteristic only when the fault is within the zone of protection of the relay. During a power swing, impedance seen by the relay changes, and it might enter inside the relay characteristic. It causes unwanted operation of the distance relay. Consider a simplified system diagram, as shown in Figure 2.2, where the generator voltage E_A leads another generator voltage E_B by angle δ. Z_A and Z_B are system impedances and Z_L is the line impedance which connects the two generators. R indicates the relay location at which the relay measures voltage V_R and current I_R.

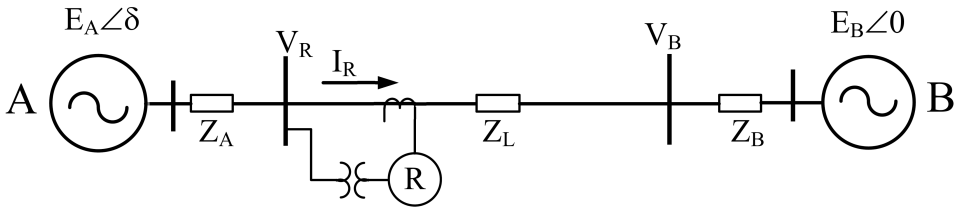

Figure 2.2: Two machine system used to illustrate impedance trajectory

In Figure 2.2, current and voltage measured by the relay is given by Equation (2.1) and (2.2), respectively.

$$I_R = \frac{E_A\angle\delta - E_B\angle 0}{(Z_A + Z_L + Z_B)} \tag{2.1}$$

$$V_R = E_A\angle\delta - I_R * Z_A \tag{2.2}$$

The impedance measured at the relay location is,

$$Z_R = \frac{V_R}{I_R} = \frac{E_A\angle\delta - I_R * Z_A}{I_R} = \frac{E_A\angle\delta}{I_R} - Z_A \tag{2.3}$$

$$= \frac{E_A\angle\delta((Z_A + Z_L + Z_B))}{E_A\angle\delta - E_B} - Z_A \tag{2.4}$$

Let $Z_T = Z_A + Z_L + Z_B$ and the ratio of two voltage magnitudes $\frac{E_A}{E_B}$ is n, then Z_R can be

written as

$$Z_R = n\frac{(n-\cos\delta) - j\sin\delta}{(n-\cos\delta)^2 + \sin^2\delta} Z_T - Z_A \tag{2.5}$$

Assume n=1, then

$$Z_R = \frac{Z_T}{2}(1 - j\cot\frac{\delta}{2}) - Z_A \tag{2.6}$$

The Equation (2.6) gives the impedance value seen by the relay during power swing which

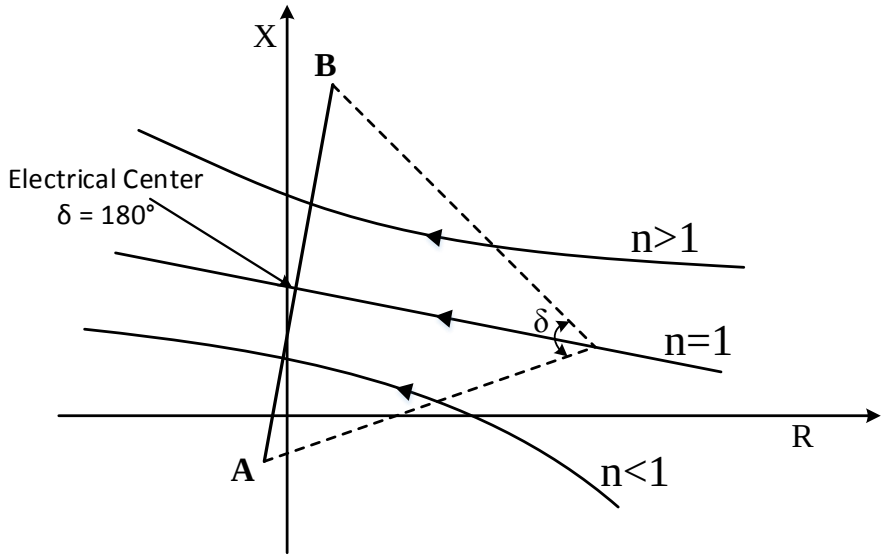

Figure 2.3: Impedance trajectory during a power swing for different values of n

depends on the phase angle between the sources. The geometrical interpretation of the trajectory can be seen in Figure 2.3. For n=1, the impedance locus becomes a straight line which passes perpendicularly through the midpoint of the system impedance between A and B. If n is greater or less than 1, the trajectory becomes a circle with the center on the extension of the total impedance line AB [46].

2.4 Impact of Power Swing in Relaying

As discussed before, during a power swing, the voltage angle between two interconnected systems might reach 180 degrees and the voltages down to a minimum and the currents to

a maximum. Such an electrical condition appears like a fault to the relay. The relays which operate during the fault may operate during a power swing. The current differential relay used to protect generators, transformers, buses and lines does not respond, as the swing appears as an external fault condition to them, but the other types of relays such as an overcurrent, directional overcurrent, undervoltage, distance relays may operate during a power swing [6, 12, 46].

During an unstable swing also termed as out-of-step condition, the current magnitudes can be greater than the pick up setting of the overcurrent relay when V_A leads V_B by 180 degrees. A stable swing also results in higher current magnitudes than the normal current but is much less than that during an unstable swing and hence does not reach the pick up setting value of the overcurrent relay [12].

Distance relays monitor positive sequence impedance and are intended to operate when the impedance lies within the relay characteristics. Figure 2.4 shows a typical relay characteristics of the distance relay. The derivation in section 2.3 shows that the positive sequence impedance at the relay location fluctuates as a function of δ. The swing locus during stable and out-of-step conditions is represented by swing locus c_1, c_2, and c_3, respectively. The unstable swing c_3 enters the operating zone of the the relay and causes it to trip. For stable swing, impedance locus c_2 does not enter the relay characteristics but in some condition even the stable swing might enter the relay characteristics as shown by impedance locus c_1.

Both stable and unstable swing can cause undesirable operation of the protection elements and may have severe impact on the system stability, security and reliability. Unwanted tripping of relays at random locations due to power swings weakens the system and creates imbalance between demand and supply and also may further lead to cascading outage conditions because of loss of generations and loads.

The system can be protected from such an event using out-of-step protection, which is the subject of the next sections.

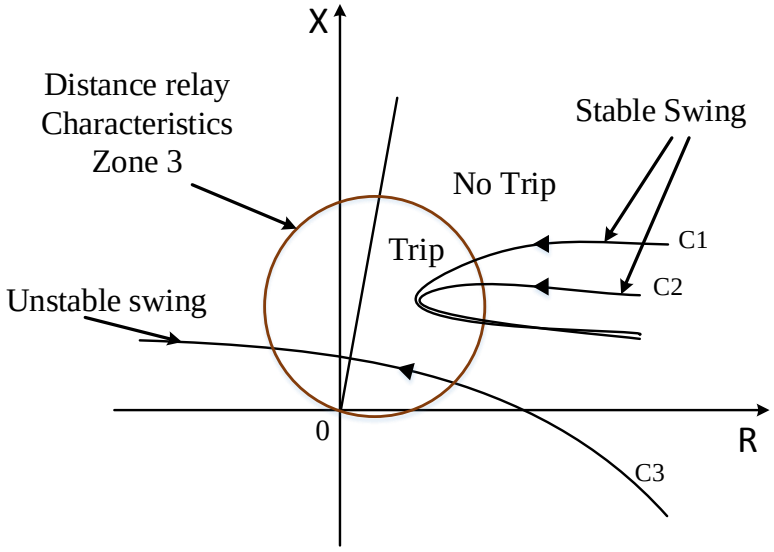

Figure 2.4: Distance relay characteristics and power swing locii

2.5 Out-of-Step Protection

The relay may fail and operate during the stable swing assuming a fault, as discussed in the previous section. It might operate during some stable conditions from which the system can recover by itself. An additional protective function is therefore required to distinguish between a faulted condition and a power swing condition. This protective function has to feature selective blocking of the breaker during a stable swing and send the tripping signal to selected breakers during an out-of-step condition [6, 12, 45, 46].

Therefore the two major functions for an out-of-step relay are:

- Power swing blocking (PSB): This function allows the breakers to operate during fault and blocks all the relay elements that tend to operate during stable or unstable swing.
- Out-of-step tripping (OST) function: It trips selected breakers for an out-of-step condition. The tripping is done to disconnect a generator or a large power system area in order to ensure that the stability is achieved for rest of the generators or areas.

In addition, the out-of-step relay has to be fast enough so that the tripping can be initiated

before 120 degrees of voltage angle separation in order to minimize the voltage stress on the breakers [12]. The fast detection also gives enough time to coordinate between many other protective elements in the system.

During disturbances or fault conditions, the voltage angle difference increases from the pre-fault value and reaches 180 degrees and starts slipping pole. Breakers experience different voltage values at different angles as shown in Figure 2.5. If the breaker operates at a lower voltage angle of separation for an imminent out-of-step condition, breaker life will increase. However, with most of the current out-of-step relaying techniques, the out of step condition is detected at angle values closer to 180 degrees and during this condition voltage reaches as much as twice the normal value creating intense stress in the breaker. The breaker operation is thus performed at a favorable angle. Generator out-of-step tripping is not typically allowed for angles larger than 90 degrees or lower than 270 degrees as per IEEE C37.013 standard [47].

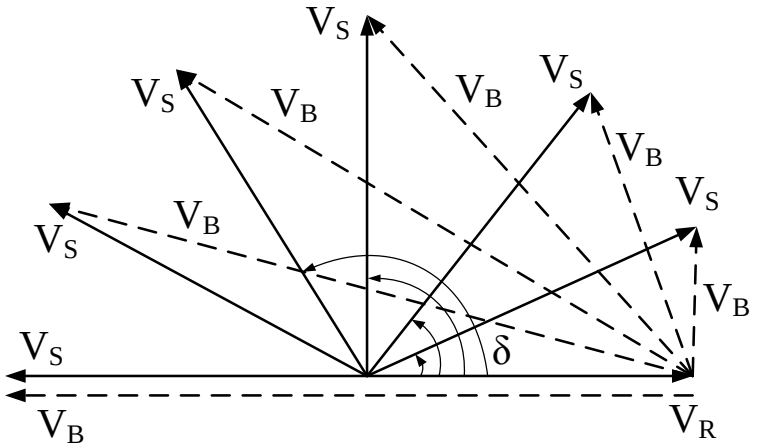

Figure 2.5: Voltage across the breaker during power swing for different values of δ

In Figure 2.5, V_S is the sending end voltage, V_R is the receiving voltage and, V_B is the voltage experienced by the breaker during a power swing. From the figure we can see clearly that the voltage while opening the breaker may reach up to two times the rated voltage. Another useful point to make here is about the restriking voltage. The voltage which appears across the breaker immediately after the breaker operation is called a restriking voltage.

Consider a power system as shown in Figure 2.6. At an instant of the breaker operation,

the input voltage source can be represented by a step voltage V_m. The inductance L and capacitance C represents the equivalent network parameters. If the circuit breaker (CB) is

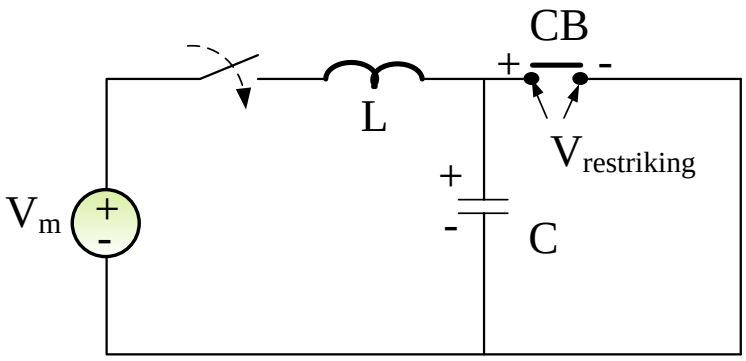

Figure 2.6: Equivalent circuit of a power system at the instant of breaker operation

interrupted at current zero position, the breaker will experience a step voltage of V_m. The restriking voltage for a step input of V_m is given by the Equation (2.7) .

$$V_{restriking} = V_m(1 - \cos \omega_n t) \tag{2.7}$$

where ω_n is the natural frequency of the transmission circuit, which depends on the inductance and capacitance parameter values of the circuit. Equation 2.7 shows that the restriking voltage is proportional to the voltage across the breaker at the time of breaking and the natural frequency of the transmission circuit. Also, if the tripping is initiated at an angle close to 180 degrees, the step voltage experienced by the breaker at the moment of breaking is two times the rated value. The restriking voltage is going to be larger and obviously will lead to more wear and tear of the breaker contacts.

2.6 Out-of-Step Protection Schemes

Various scheme have been reported in literature for out-of-step relaying. One of the conventional and most widely implemented ones is the rate of change of impedance or resistance method. Some other methods include SCV technique, R-dot scheme, fuzzy logic method, neural network and artificial intelligence-based methods, equal area criterion-based

methods, frequency deviation of voltage method and power versus integral of accelerating power method.

These methods are discussed briefly below.

2.6.1 Rate of Change of Impedance Methods (Blinder Scheme)

The PSB and OST schemes have been implemented mostly so far with the rate of change of impedance scheme. It is basically a distance relay with different shapes of impedance elements which measures the positive sequence impedance at the relay location. The scheme is also called as a Blinder Scheme. The relay schemes can be divided into the following types based on the different shapes used:

- One blinder scheme
- Two blinder scheme
- Concentric Characteristics schemes (Mho, Lenticular, Quad)

Figure 2.7 shows the concentric scheme and the two blinder scheme. The choice of the scheme depends on the loading conditions, power system parameters and the desired performance but the operating principle is the same for all. All the methods measure apparent impedance and time between the two measuring elements [16]. The method uses the fact that the rate of change of impedance is different during a fault and a power swing condition. The change is very fast when there is a fault and is slow when the system is experiencing a power swing condition.

To understand the basic operating principle of these relays, let us consider the two blinder scheme as shown in Figure 2.7d. The inner and outer blinders are set according to the guidelines explained in Appendix B. The relay measures the time taken by the impedance locus to travel between the two blinders. A timer is started when the impedance enters outer characteristics or blinder. If the time exceeds the pre-set value of time delay, the relay detects the case to be a power swing and the PSB elements is operated to block the

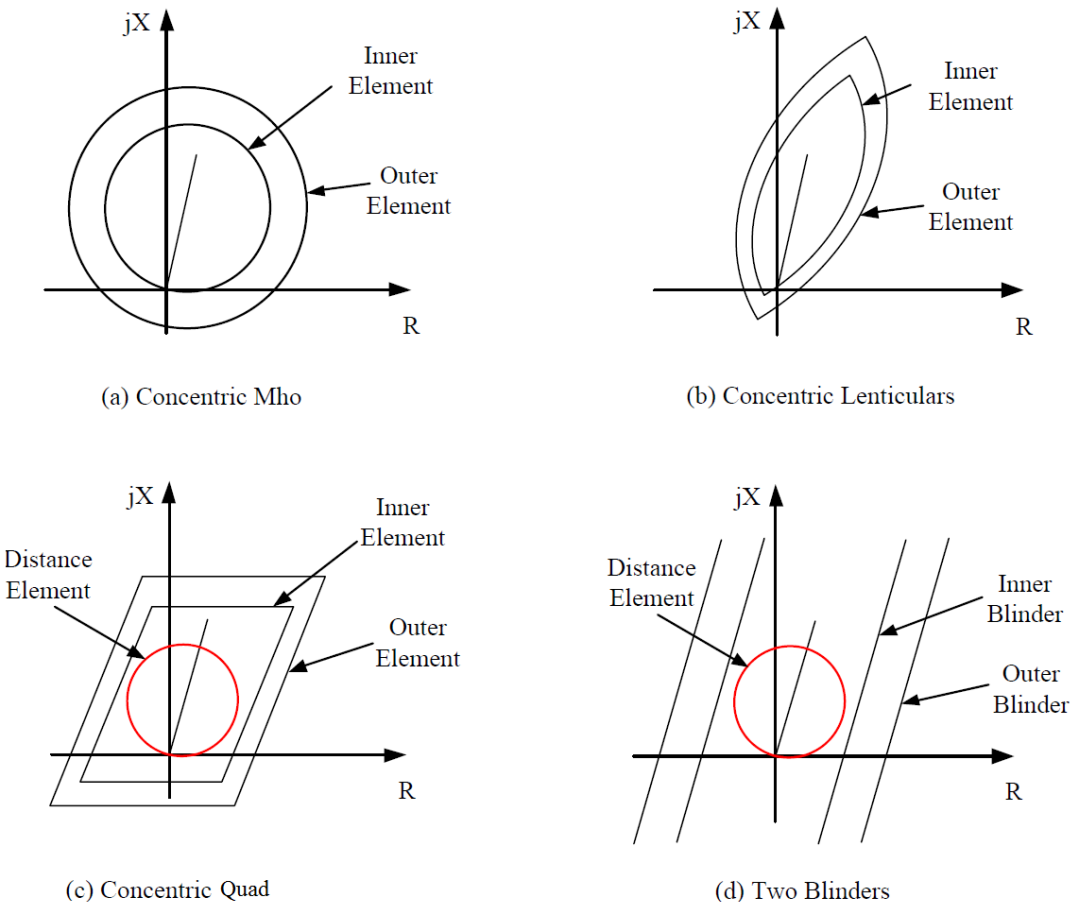

Figure 2.7: Various types of out-of-step relay characteristics

selected distance elements. An out-of-step condition is detected only when the impedance locus passes through both the blinders within pre-set timer. The OST element can trip the distance element any time after this point. Depending on voltage angle separation, tripping is delayed until the voltage reaches a favourable value to minimize the stress on the breakers.

The principle of operation of the scheme is simple and straightforward, but the implementation of the scheme involves extensive and time-consuming stability studies [16]. The inner blinder should be outside the distance relay characteristics under consideration and the outer blinder should be set inside all the possible loading conditions. Setting the separation between the two elements is a tedious and time consuming task. It depends on the slip frequency during the transient and the slip depends on the accelerating torque and machine

inertia. Setting the blinders is quite difficult for heavily loaded long transmission lines where the load region lies very close to the operating characteristics of distance relay. The method is prone to false detection when there is significant change in system and transfer impedance values [6, 16].

2.6.2 Rdot Scheme

Another scheme which hold same principle to the blinder scheme is Rdot scheme. In this scheme, apparent resistance and rate of change of apparent resistance is used instead of using the apparent impedance. The Rdot scheme is given by Equation (2.8) [19].

$$P_1 = (R - R_1) + T_1 \frac{dR}{dt} \leq 0 \tag{2.8}$$

where, P_1 is the control output, R is the apparent resistance measured by the relay and R_1, T_1 are the relay-setting parameters. Figure 2.8 shows the rate of change of resistance versus the resistance and the relay characteristic. The relay characteristic is a straight line having a slope of T_1 which passes through (R_1,0) in R-Rdot plane. In Figure 2.8, the slope T_1 is equal to (-$\Delta\dot{R}/\Delta R$). If the control output P_1 during swing is negative, relay trips the breakers to separate the lines [48]. Since the technique again involves the setting of relay parameters (R_1 and T_1) using transient stability studies, it faces similar issues as that of the rate of change of impedance method.

2.6.3 Swing Center Voltage (SCV) Method

Principle of swing center voltage can be well explained with two machine equivalent system as shown in Figure 2.2. During a power swing, when the voltage angle separation between the two equivalent sources becomes close to 180 degrees, the voltage at a point between the two sources tend to become zero. The voltage at that center point of the two machine equivalent system is called SCV . Figure 2.9 shows the voltage phasor diagram of the system where the vector OO$'$ represents the SCV [6]. Assuming the equivalent source

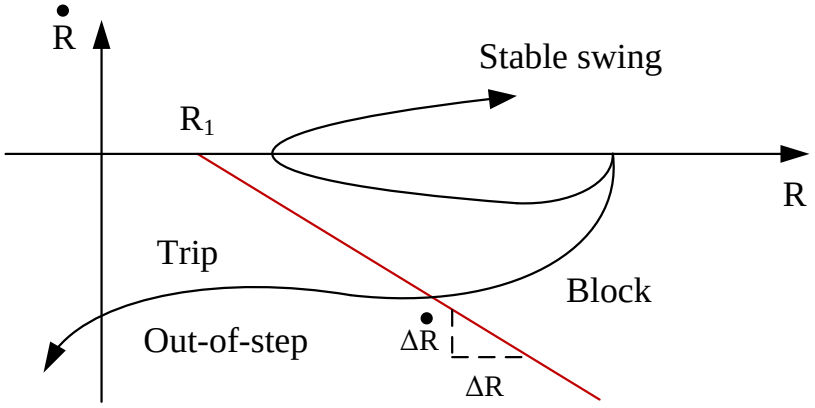

Figure 2.8: Illustration of Rdot method

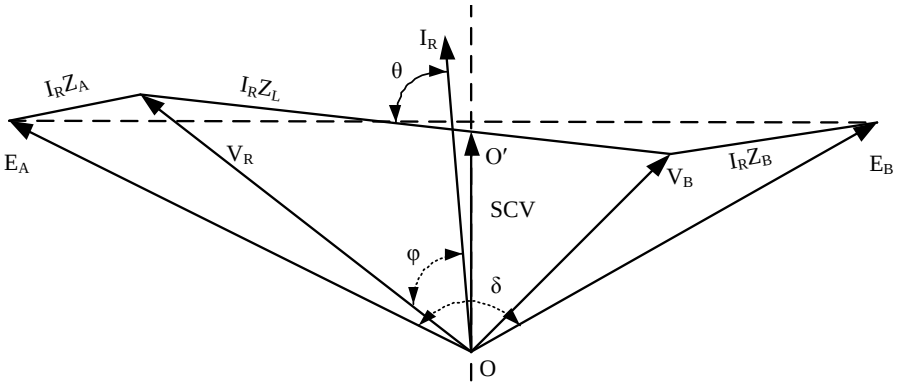

Figure 2.9: Swing Center Voltage (SCV) phasor diagram for a two machine system

voltage magnitude as E, the SCV is given by Equation (2.9) [49].

$$SCV(t) = \sqrt{2}E\sin(\omega t + \frac{\delta(t)}{2})\cos(\frac{\delta(t)}{2}) \tag{2.9}$$

The SCV does not lie exactly at relay location (i.e., R) where the measurements are taken, but can be approximated from the voltage phasor V_R available at the relay location. The approximation of SCV using V_R is given by Equation (2.10).

$$SCV \approx |V_R|\cos\varphi \tag{2.10}$$

noindent where φ is the phase angle between V_R and I_R. The quantity $|V_R|\cos\varphi$ approximates the magnitude of SCV for a homogeneous system with system impedance angle(θ)

close to 90 degrees. Figure 2.10 shows the approximate calculation of SCV which is the projection of V_R on the axis of I_R.

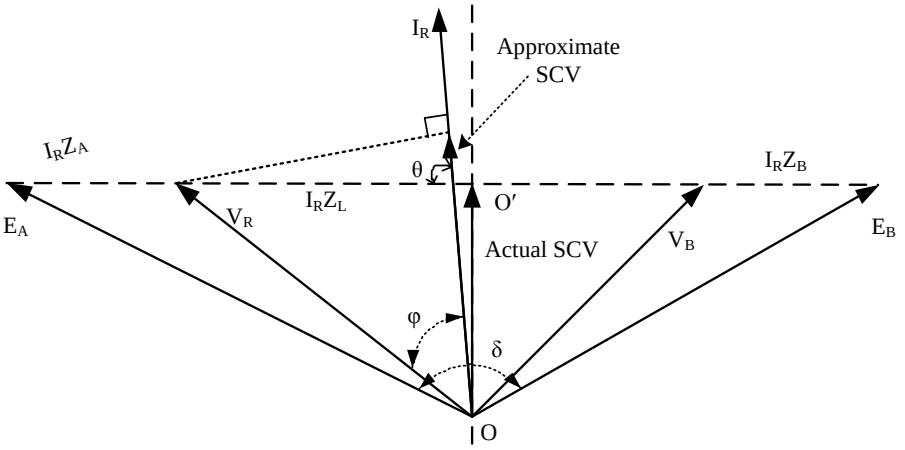

Figure 2.10: Estimating SCV using local measurements

Equation (2.10) can be written in a simplified form using the phase angle difference δ as,

$$SCV \approx |V_R| \cos \frac{\delta}{2} \tag{2.11}$$

The rate of change of SCV is used for detecting the power swing.

$$\frac{d(SCV)}{dt} \approx \frac{|V_R|}{2} \frac{\delta}{dt} \cos \frac{\delta}{2} \tag{2.12}$$

The rate of change of SCV is zero when δ is 0 or 360 degrees and will be maximum when δ is 180 degrees. The method has an advantage that it is independent of source and line parameters and requires no settings. However, the estimate is based on the local measurement available at substation and is close to actual SCV only when impedance angle of the line is 90 degrees. Moreover, the local estimate of the SCV has a sign change when δ goes through 0 degree which causes discontinuity in the estimated SCV; whereas the system SCV does not have such a discontinuity [49].

SCV method can be implemented using the wide area measurements from optimal PMU locations in the test system. After the disturbance introduced in the system, separating coherent groups of generator represents the two oscillating equivalent system in opposite direction. The two equivalent machine representation of machine and their difference of COA

is used as a measurement to determine the stability of the system. The SCV algorithm detect the power swing based on the absolute value of SCV1, rate of change of SCV1 (dSCV1) and the output of the rate of change of dSCV1 (discontinuity detector). This method also requires extensive stability studies to set a threshold for the rate of change of SCV to differentiate between stable and out-of-step-conditions.

2.6.4 Post-Disturbance Voltage Trajectory based Out-of-Step Prediction

Rotor angle instability is predicted using the post distubance voltage magnitude trajectory in reference [30,31]. In reference [30], the combined investigation of the voltage trajectories from important buses are used for the prediction of the system stability status after disturbance. The method tries to find the similarity of post-fault voltage trajectories of the generator buses after the disturbance to pre-identified templates and then does a prediction using a classifier (the similarity values calculated at the different generator buses are used as inputs to the classifier). The accuracy of this method depends upon the test condition having voltage trajectory close to pre-identified voltage templates. Also the methods need a database of simulation cases with various probable contingencies in order to identify templates and then train the classifier.

The rate of change of voltage (ROCOV) with respect to the voltage deviation (ΔV) post disturbance is studied in reference [31] to predict the transient stability of the system. Implementation of this method involves the identification of incidents which tend to marginally destabilize the generators, determination of their stability boundary in ROCOV-ΔV plane and detection of severe disturbances and initiation of the prediction algorithm after the successful detection. For a stable case, the operating point moves in a spiral trajectory inwards and settles to a point on the ΔV axis. For an unstable case, the trajectory starts diverging; the point moves away from the origin further into the unstable region of the ROCOV-ΔV plane passing through the boundary limits. The stability boundaries are obtained from simulation studies.

The advantage of this method is that it utilizes the generator terminal voltage magnitude because of its convenience in measurement but determining the stability boundary for each generator can become tedious for studies in large system configurations. Also the method would suffer in case of major topology changes due to the preset stability boundary condition.

2.6.5 Fuzzy Logic and Neural Network based Out-of-Step Detection

Fuzzy logic and neural network (NN)-based out-of-step detection techniques have been reported in the literature [38, 39]. The detection procedure explained in the literature [38] uses a set of input signals to train the fuzzy inference system (FIS). The output of the FIS is then compared with some threshold value to make a decision. Figure 2.11 shows the block diagram of FIS based out-of-step detection procedure.

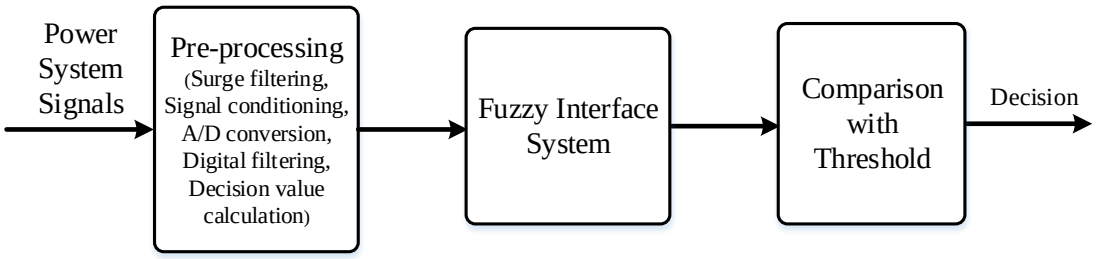

Figure 2.11: Block diagram of FIS based out-of-step detection

With the machine angular frequency deviation and impedance angle at machine terminal as input signals, the FIS was trained for over 108 fault cases in this reference paper. The FIS produces output equal to 0 for stable cases, and 1 for unstable cases. A threshold value of 0.5 was used to compare the output of FIS. The output lower than 0.5 is classified as stable swing and that greater than 0.5 is classified as out-of-step.

Reference [39] uses a feed-forward model of neural network based on stochastic back propagation training algorithm to predict an out-of-step condition in a power system. The schematic diagram of NN used for out-of-step detection is shown in Figure 2.12.

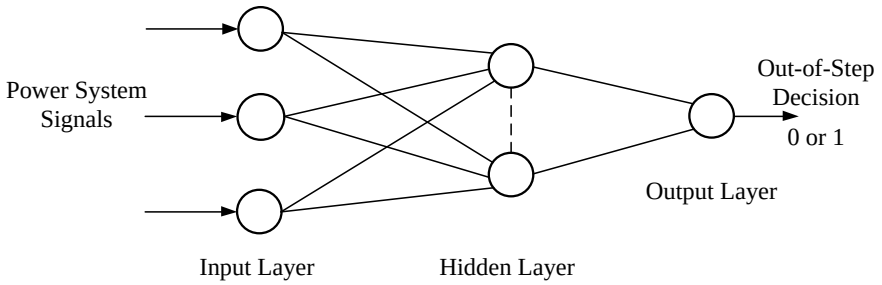

Figure 2.12: NN for out-of-step detection

For training purposes, three input signals – mechanical input power, kinetic energy deviation and average kinetic energy deviation were chosen. A nine bus test system was used with three machines and three randomly distributed loads. The NN was trained using 162 simulation runs with the fault applied at six different locations and three different initial loading conditions for different fault durations. A test case was identified as out-of-step, if the rotor angle of the generator approached 180 degrees within 1 second and was given a stability index of 0; otherwise, the case was classified as a stable swing and was given a stability index of 1. One of the advantages of this method is that all the required signals are locally measured at the generator to be protected.

The above discussed methods make correct decisions only when the new test cases have close resemblance to the trained cases. The methods need training for a wide variety of operating conditions and require a huge computer memory for the storage of their databases.

2.6.6 Conventional Equal Area Criterion (EAC)

The equal area criteria offers a graphical depiction of the transient stability problem. This method portrays the accelerating (kinetic) energy, the rotor gains when disturbances is introduced in the system as well as decelerating (potential) energy the system has available to overcome the acceleration effect. This method has most often been used to assess the stability of a single machine infinite bus system or a single machine infinite bus equivalent of a multi-machine system. The power-angle curve for the pre-fault, during-fault, and post-fault condition are shown in Figure 2.13. The well known EAC uses the power-angle curve.

It calculates the accelerating area(A_1) during the fault, and the decelerating area (A_2) after the fault. The area A_1 depends on fault clearing time. The longer the fault clearing time, greater will be the area A_1. According to EAC, whatever accelerating energy added to the system during fault must be removed after the fault to restore the synchronous speed. The EAC hence determines the stability of a system as follows,

a. If $A_1 < A_2$ Stable swing

b. If $A_1 = A_2$ Critical condition

c. If $A_1 > A_2$ Unstable swing or out-of-step condition

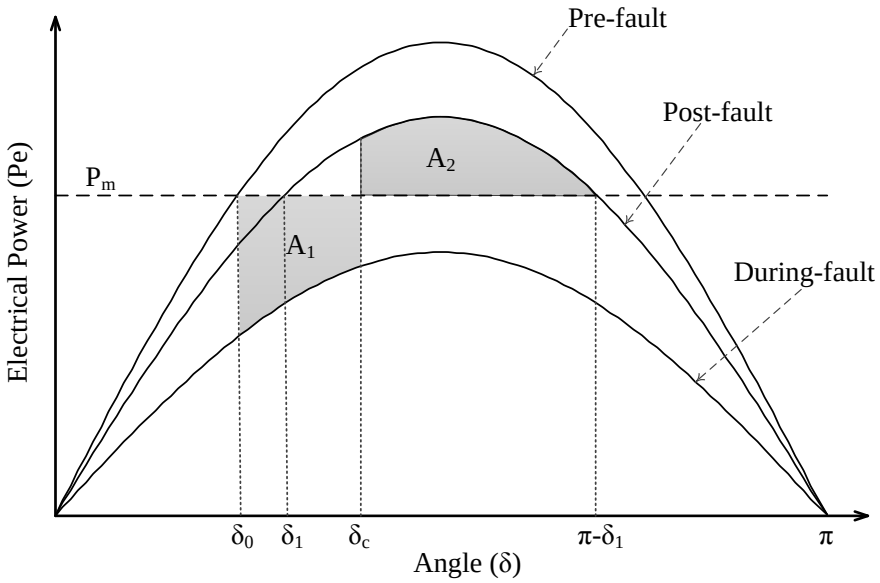

Figure 2.13: Power-angle characteristics

The equal area criteria is a energy equilibrium concept explained in textbooks mostly for a SMIB system and needs additional equivalenting procedures to apply it to multi-machine interconnected real system. The extended equal area criteria (EEAC) developed by Ribbens Pavella in 1980's provides a means to apply this concept to a larger power system which is basically an extension of the EAC for a multi-machine system. Out-of-step protection methods in [37, 50] use the EEAC approach to determine the critical clearing time (CCT) and critical clearing angle (CCA) of the system using wide area measurements. The work

described in [50] was carried out after the EEAC work carried out at the University of Saskatchewan [**?**]. Though EEAC is one of the most popular technique to study the stability of the multi-machine system, the main difficulty associated with EEAC is that as the size of the system increases, the number of calculations increase to reduce system to SMIB equivalent and critical clearing time calculations, requiring a larger computational effort.

2.6.7 Equal Area Criterion in Time Domain

Equal area criterion in time domain is indirectly derived from the concept of equal area criterion in power versus angle domain. The time domain equations are also derived from the swing equation and the accelerating area A_1 and decelerating area A_2 are calculated as given by Equations (2.13) and (2.14), respectively [20].

$$A_1 = \int_{t_0}^{t_1} (P_m - P_e)dt = \frac{M}{\omega_s}(\omega_r \mid_{t_1} - \omega_r \mid_{t_0}) \tag{2.13}$$

$$A_2 = \int_{t_1}^{t_{max}} (P_m - P_e)dt = \frac{M}{\omega_s}(\omega_r \mid_{t_{max}} - \omega_r \mid_{t_1}) \tag{2.14}$$

Where t_0 is fault inception time at power angle δ_0, t_1 is the time when P_e exceeds P_m and t_{max} is the time when $\delta = \delta_{max}$.

The total area for stable and out-of-step condition are given as

$$Stable\ condition: \ A = A_1 + A_2 = \int_{t_0}^{t_{max}} (P_m - P_e)dt = 0 \tag{2.15}$$

$$Out - of - step\ condition: \ A = A_1 + A_2 = \int_{t_0}^{t_{max}} (P_m - P_e)dt > 0 \tag{2.16}$$

Equations (2.15) and (2.16) are the expressions for EAC in time domain, which tells that during the transient, if area A1 and A2 are equal in a P-t curve, the system becomes stable as shown in Figure 2.14. But if area A1 becomes greater than area A2, the system goes to an out-of-step condition as shown in Figure 2.15. The area under the P-t curve represents energy; thus this concept can be referred as the energy equilibrium criteria in time domain.

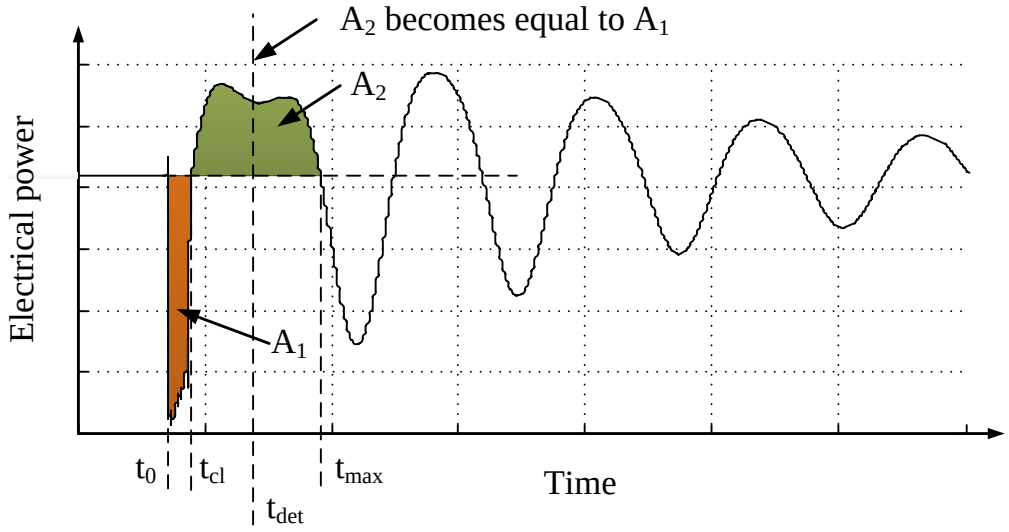

Figure 2.14: Electrical power versus time curve for stable case

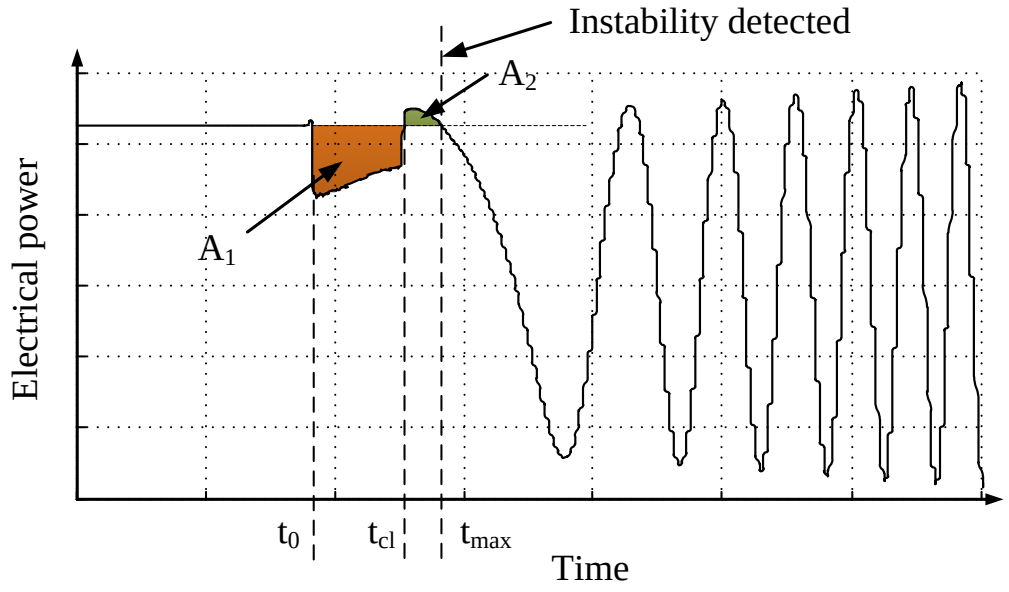

Figure 2.15: Electrical power versus time curve for unstable case

A balance of transient energy results in a stable swing; whereas an unbalance of transient energy causes an out-of-step swing. This method eliminates the numerical computations required to find the critical clearing time to detect the out-of-step condition. However, the method has a shortcoming of not being predictive and detect instability after the generator pole slip occurs.

2.6.8 Frequency Deviation of Voltage Method

Reference [26] explains a method using frequency deviation of voltage to detect an out- of-step condition. Methods based on frequency measurement are based on the definition of the instantaneous frequency as the angular velocity of the rotating voltage phasor. The voltage is measured at the local bus, and the frequency is estimated from the voltage signal using discrete Fourier transform (DFT). For a one-cycle sampling window of the basic waveform, the phasor at the i^{th} sample is given by Equation 2.17.

$$\begin{aligned} \bar{V}(i) &= \sum_{k=0}^{N-1} v(i+k-N+1)e^{-j(\frac{2\pi}{N})} \\ &= V_r(i) + jV_i(i) \end{aligned} \tag{2.17}$$

where $v(i+k-N+1)$ is the discrete time voltage signal and, $V_r(i)$ and $V_i(i)$ are the real and imaginary part of voltage phasor $\bar{V}_i$, respectively.

In the method described in the reference paper, the angular velocity is first calculated using two successive phase angle values of voltages as given by Equation (2.18).

$$\omega_k = \frac{arg(V(k)) - arg(V(k-1))}{T} \tag{2.18}$$

The average ω is then obtained over a 2N+1 data window as given by Equation (2.19):

$$\omega_{avg} = \sum_{k=-N}^{N} \frac{arg(V(k)) - arg(V(k-1))}{T} \tag{2.19}$$

The acceleration of the voltage is then calculated from two successive angular velocity values as given by Equation (2.20), and an average value of acceleration is obtained as given by Equation (2.21):

$$\alpha_k = \frac{\omega_k(k) - \omega_k(k-1)}{T} \tag{2.20}$$

$$\alpha_{avg} = \sum_{k=-N}^{N} \frac{\omega_k(k) - \omega_k(k-1)}{T} \tag{2.21}$$

where T is the sampling period and k is the sample number of voltage signals.

Instability detection is done by observing the angular velocity of the voltage when the acceleration (α_{avg}) goes from negative to positive. If the angular velocity at this point is greater than the nominal angular frequency (ω_0), then an unstable condition is detected. This method is illustrated for stable and unstable case in Figure 2.16 and Figure 2.17, respectively.

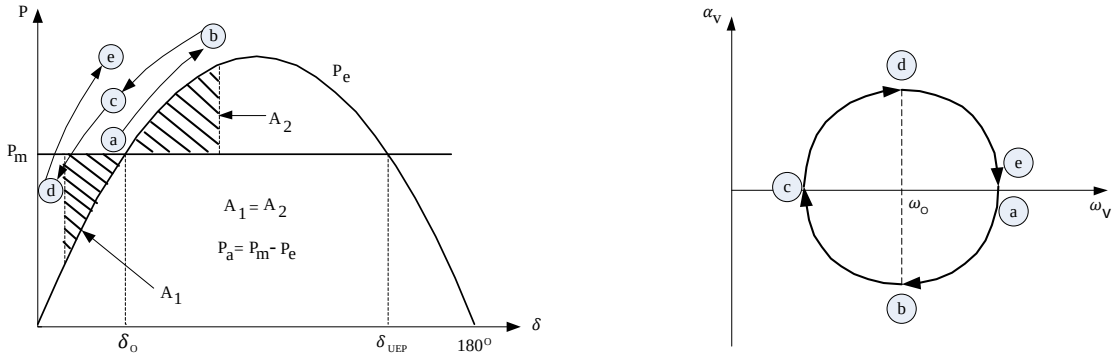

(a) Power-angle curve

(b) Plot of α_v vs. ω_v of v(t)

Figure 2.16: Stable Swing

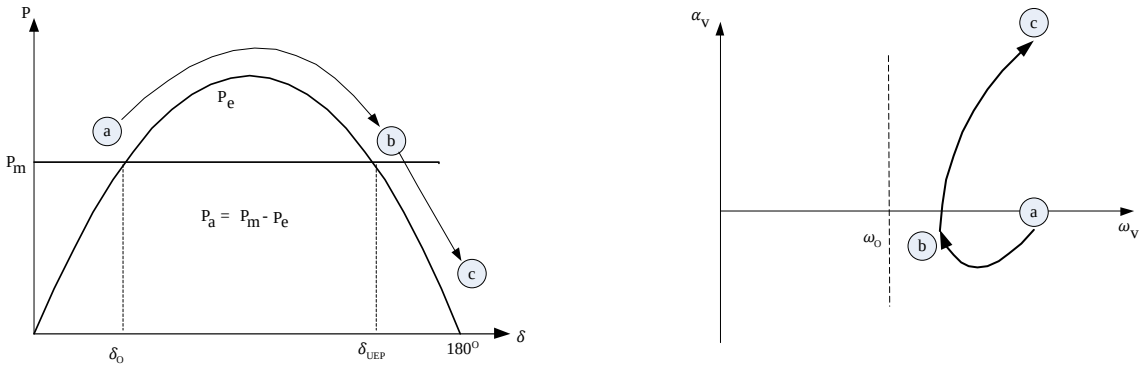

(a) Power-angle curve

(b) Plot of α_v vs. ω_v of v(t)

Figure 2.17: Unstable Swing

This method detects a generator out-of-step condition using the voltage signal at the generator substation. In the course of this research, the voltage signal was found to rapidly fluctuates during a transient condition, and hence the algorithm is susceptible to an incorrect operation during the switching transients. Second, the above method was found to be useful in simulation studies but may pose practical issues when implemented in a relaying device. Calculation of the speed and acceleration from the terminal voltage angles of the generator is prone to errors due to the derivative terms, which significantly amplify the power system noise.

The averaging of speed and acceleration reduce these errors, but the problem with averaging is that the transient changes get cancelled out. To solve this problem, in this research a polynomial curve fitting approach was applied to the sampled values of the phase angles. The angular velocities are then determined from the curve-fitted values. The angular acceleration is determined by taking the slope of the instantaneous speed values. The study was carried out on the SMIB system shown in Figure 2.22.

2.6.8.1 Stable Case

A three-phase fault is applied to the middle of the second transmission line at 2 s and removed at 2.2 s. The angular speed and acceleration of the generator are analyzed during and after the fault. At the point where angular acceleration changed its polarity from negative to positive, the angular velocity (ω_v) was found to be less than the base velocity (ω_o); the method correctly detected it as a stable swing at 2.56 s, as shown in Figure 2.18.

2.6.8.2 Unstable Case

A three-phase fault is applied to the middle of the second transmission line at 2 s and removed at 2.4 s. The plot of angular acceleration versus angular velocity is shown in Figure 2.19. The angular velocity (ω_o) is found to be greater than base velocity (ω_v) at the point where the angular acceleration changes its polarity from negative to positive, and therefore the relay detects it as an unstable swing at 2.4390 s.

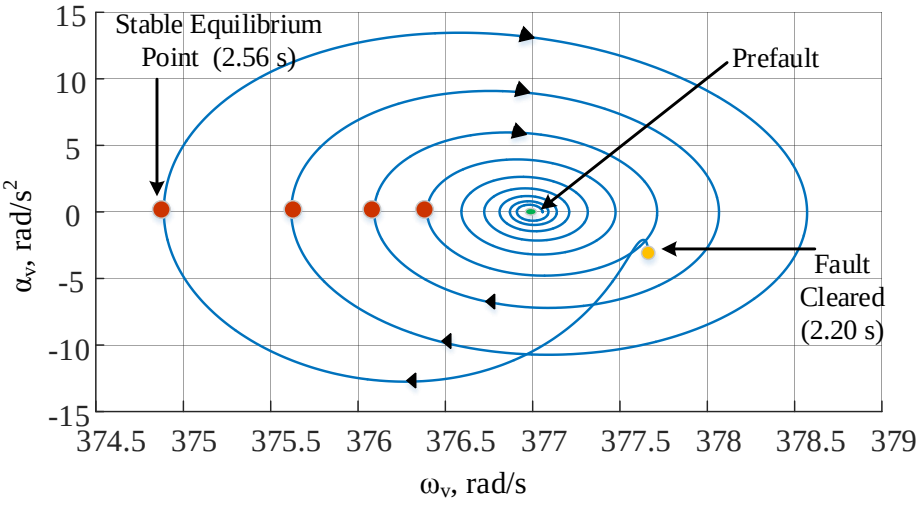

Figure 2.18: Angular acceleration vs. angular velocity for a stable swing

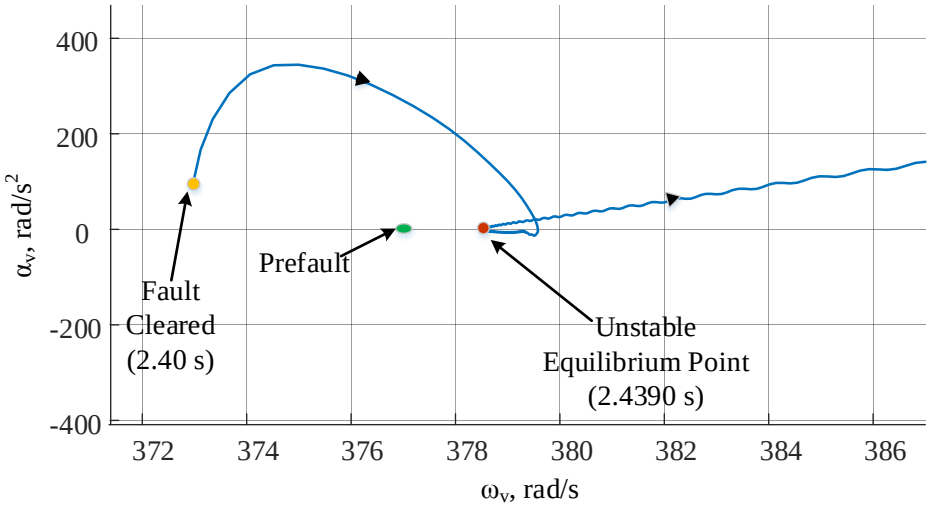

Figure 2.19: Angular acceleration vs. angular velocity for a stable swing

This technique relies on local measurements. However, an algorithm suitable for detecting instability at the system level is necessary for interconnected power networks.

2.6.9 Power versus Speed Deviation Method

Reference [27] discusses an out-of-step protection method using state plane analysis of generator electrical power and speed deviation. Electrical power and speed (derived from electrical measurement of voltage signals) are used as input variables to the proposed scheme for transient stability analysis. The primary advantage of this technique is that the variables required by the algorithm are easily available. The algorithm does not require system network reduction and uses only the electrical power outputs measurements at each time instant from the generators.

The power-angle characteristics for typical pre-fault, during fault and post fault conditions are shown in Figure 2.20a. Analysis of the curve shows that the generator speed increases during the faulted condition and starts decreasing as the fault is removed. Initially, the machine operates in a steady state condition as shown by point m. After a fault occurs in the system, the operating point moves to point n and the machine starts accelerating until it reaches point o where the fault is removed and the operating point moves to point p. As shown in Figure 2.20b, the speed of the machine is greater than the synchronous speed at point p and the rotor angle (δ) increases as the machine starts to decelerate. The stability of the machine depends on whether or not it regains synchronous speed before reaching point r. If the synchronous speed is regained at point s, then the rotor angle (δ) starts to swing backwards. As it swings back, the state changes from deceleration to acceleration at point q. The relative speed of the generator is negative at point q and settles into a new steady state operating point q after a few oscillations. If the disturbance is large, then the machine may oscillate beyond point s and reach point r where the state changes from deceleration to acceleration. The stability of the machine depends on the relative speed at point r. The machine will be unstable if the relative speed is positive at point r. The generator relative speed (ω_r) for both stable and unstable conditions is shown in Figure 2.20b .

In reference [51], this method is implemented for the IEEE 12 bus system configuration shown in Appendix A.3. A three phase fault was applied at the middle of line 1-6 to create both stable and unstable swings in generator G4. In this test scenario, generator G4 was

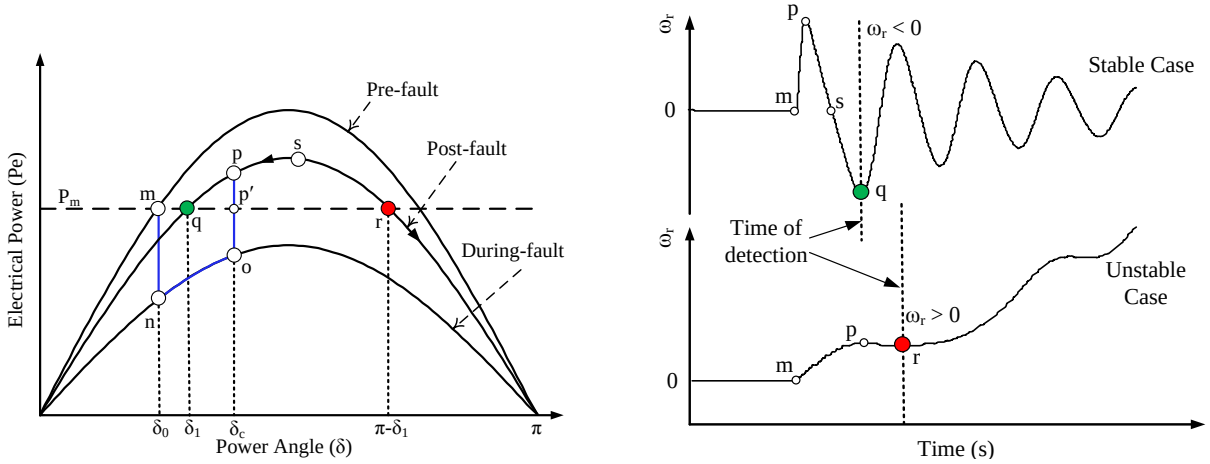

(a) Power-angle characteristics (b) Generator relative speed versus time

Figure 2.20: Generator power angle and relative speed illustration

loaded to 95% of its maximum capacity and generators G2 and G3 were loaded to 75% and 70% of their installed capacities, respectively. Figure 2.21a shows the plot of power deviation versus speed deviation for a sustained three phase fault applied for a duration of 22 cycles (0.3665 s). The relative speed at the first equilibrium point is ω = - 0.0214 pu (368.94 rad/s), and the swing is determined to be stable.

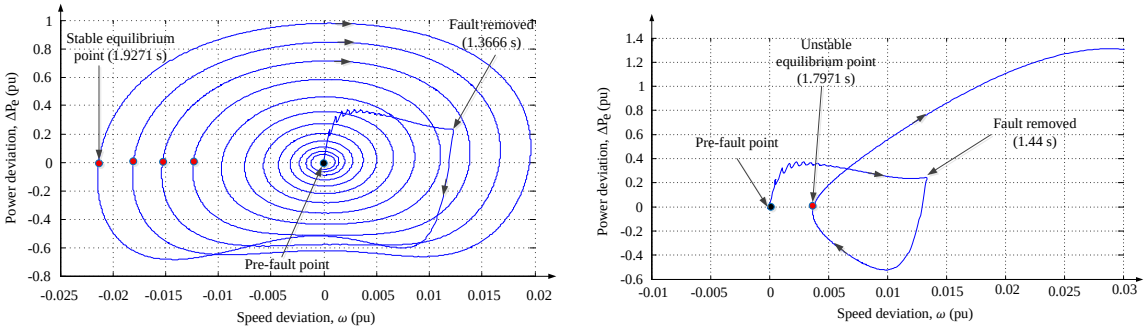

(a) Fault duration of 22 cycles (b) Fault duration of 26.4 cycles

Figure 2.21: Plot of power deviation vs. speed deviation for a stable swing for generator G4

Figure 2.21b shows the plot of power deviation versus speed deviation for a sustained three phase fault applied for a duration of 26.4 cycles (0.44 s). At the equilibrium point, the speed of the machine is ω = 0.00374 pu (378.41 rad/s), which is greater than the base speed and hence the unstable swing is detected. The detection time was found to be 0.7971 s after

fault inception.

This method uses online measurement of electrical power and the generator speed as inputs to the relay. The algorithm first determines the equilibrium point at which the relative rotor speed is evaluated to determine stability. This method addresses the numerical issues that can arise during practical implementation of frequency deviation of voltage method. However the frequency deviation of voltage method suffers from several disadvantages due to the derivatives involved in finding angular acceleration and angular speed especially during the transients.

2.6.10 Proposed Power versus Integral of Accelerating Power Method

The practical difficulties discussed for the frequency deviation of voltage method can be overcome using the electrical power deviation instead of estimating the rotor acceleration. The electrical power deviation has a direct relationship to rotor acceleration (Equation 2.22) and the integral of accelerating power can be utilized to calculate the rotor speed (Equation 2.23). The electrical power changes are straight forward to measure and the values obtained are more stable during transient conditions. The mechanical power deviations could be also included in the analysis to obtain an accurate estimate of the speed and acceleration changes.

$$\frac{d}{dt}\Delta\omega = \frac{1}{2H}(\Delta P_m - \Delta P_e) \tag{2.22}$$

$$\Delta\omega = \frac{1}{2H}\int(\Delta P_m - \Delta P_e)dt \tag{2.23}$$

where Δ represent the small change, H is the inertia constant, $\Delta\omega$ is the angular speed deviation, ΔP_m is the change in mechanical input power, and ΔP_e is the change in electrical output power.

The instantaneous values of the electrical power and the integral of accelerating power were determined at every discrete instance of time. The acceleration and the speed deviation were determined from the power and the integral of accelerating power values, respectively.

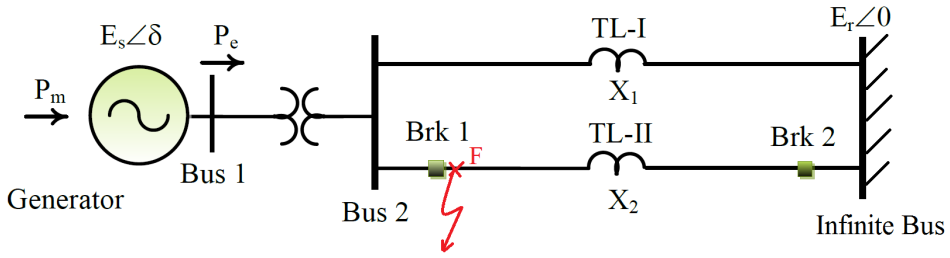

Figure 2.22: Single machine connected to infinite bus

This method was implemented using SMIB test system shown in Figure 2.22 and the system data is given in Appendix A.1. This method is going to be a part of IEEE PSRC J5 Working Group document on 'Application of out-of-step protection schemes for generators'. The instantaneous values of the electrical power and the integral of accelerating power are calculated.

2.6.10.1 Stable Case

A three phase fault is applied in the second transmission line right after the breaker at 0.2 s and cleared at 0.266 s. At the point where angular acceleration changed its polarity from negative to positive, the angular velocity (ω_v) less than the base velocity (ω_o) and the method correctly detected it as a stable swing at 1.282 s. The angular velocities are determined from integral of accelerating power. The angular acceleration is determined from the electrical power deviation. The acceleration and the speed deviation are determined from the power and the integral of accelerating power values, respectively and plotted in Figure 2.23.

2.6.10.2 Unstable Case

A three phase fault is applied in the second transmission line right after the breaker at 0.2 s and removed at 0.27 s. Figure 2.24 shows the plot of angular acceleration versus angular velocity. At the point where the angular acceleration changes its polarity from negative to positive, the angular velocity (ω_v) is greater than the base velocity (ω_o) and therefore the

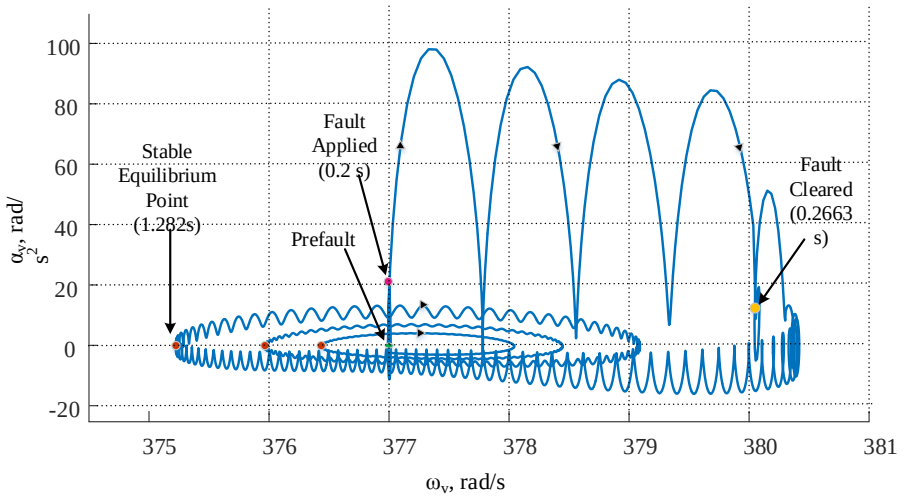

Figure 2.23: Plot of angular acceleration vs. angular velocity for a stable swing scenario with power and integral of accelerating power values

relay detects it as an unstable swing at 0.85 s.

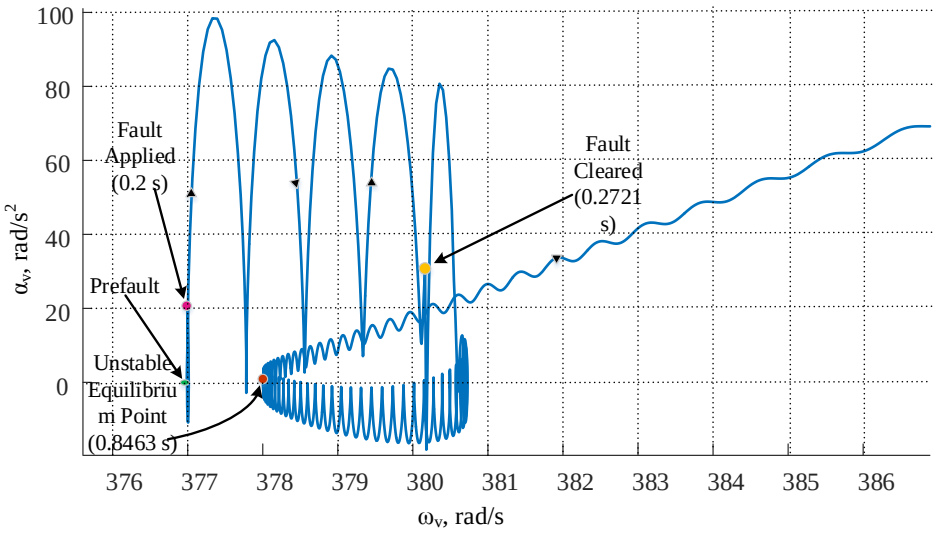

Figure 2.24: Plot of angular acceleration vs. angular velocity for an unstable swing with instantaneous power values

2.7 Summary

This chapter explained the power swing phenomena in power system and the importance of out-of-step protection. The nature of impedance trajectories during a power swing condition were explained and how a power swing affects the various protection elements such as distance relays, overcurrent relays in power system. This chapter also discussed the out-of-step protection functions (OSB and OST) that are implemented in out-of-step relays. Different techniques such as the rate of change of impedance method, SCV technique, fuzzy logic and neural network methods, conventional EAC, EAC in time domain, frequency deviation of voltage method, power versus speed deviation method, power versus integral of accelerating power method were discussed along with their advantages and shortcomings.

The power versus integral of accelerating power method which was investigated in the course of this research for SMIB was also discussed in this chapter. This method has potential of practical application since input to the relay can be measured easily and the method is less prone to errors during transient conditions. The next chapter explains a PMU based method for out-of-step protection. Optimum PMU locations and proposed synchrophasor based method to predict out-of-step conditions are also discussed in this thesis.

Chapter 3

Synchrophasor Based Out of Step Analysis

3.1 Introduction

With the advent of modern PMUs using GPS by Virginia Tech in the early 1980s, system model validation, post-event analysis, and real-time monitoring have become possible. However, due to advancement in technology for phasor measurement, precise time tagging using global reference and high speed communication such as SONET have extended the opportunity to using PMUs for protection and control [52, 53]. PMUs have now become a significant component in WAMS and have been deployed in many parts of the world. In this chapter, literature related to the synchrophasor and methods used to analyze the discrete data from PMUs, time series modelling, and forecasting is presented. The optimal PMU location is determined for the test system using integer quadratic programming. This chapter proposes a synchrophasor-based stability prediction method using the swing curve and the time series model.

3.2 Phasor Measurement Unit (PMU)

3.2.1 Introduction

Phasor measurement units also called synchrophasors are the devices that measure phasors that are synchronized in time. The concept of using phasors to describe the power

system operating quantities dates back to 1893 and Charles Proteus Steinmetz's paper on mathematical techniques for analyzing AC networks. More recently, Steinmetz's technique of phasor calculation has evolved into the calculation of real-time phasor measurements synchronized to an absolute time reference. The latest standard for synchrophasor measurement for the power system is published in IEEE Std C37.118.1-2011 [54]. As per the synchrophasor standards, the sinusoidal waveform defined in Equation (3.1)

$$x(t) = X_m cos(\omega t + \phi) \tag{3.1}$$

is commonly represented as a phasor as shown in Equation (3.2)

$$\begin{aligned} \boldsymbol{X} &= \frac{X_m}{\sqrt{2}} e^{j\phi} \\ &= \frac{X_m}{\sqrt{2}} (cos\phi + jsin\phi) \\ &= X_r + jX_i \end{aligned} \tag{3.2}$$

where root mean square (rms), $\frac{X_m}{\sqrt{2}}$ is the magnitude of the wave form and the subscripts r and i signify real and imaginary parts of the complex value in the rectangular components. The value of ϕ depends on the time scale, *t=0*.

Mathematically, the synchrophasor representation of signal *x(t)* in Equation (3.1) is the value $\boldsymbol{X}$ in Equation (3.2) where ϕ is the instantaneous phase angle relative to a cosine function at the nominal system frequency synchronized to Coordinated Universal Time (UTC). In this definition, ϕ is the offset from the cosine function at the nominal frequency synchronized to UTC. A cosine has a maximum at *t=0*, so the synchrophasor angle is 0 degrees when the maximum of *x(t)* occurs at the UTC second rollover and -90 degrees when the positive zero crossing occurs at the UTC second rollover. Figure 3.1 illustrates the phase angle/UTC time relationship.

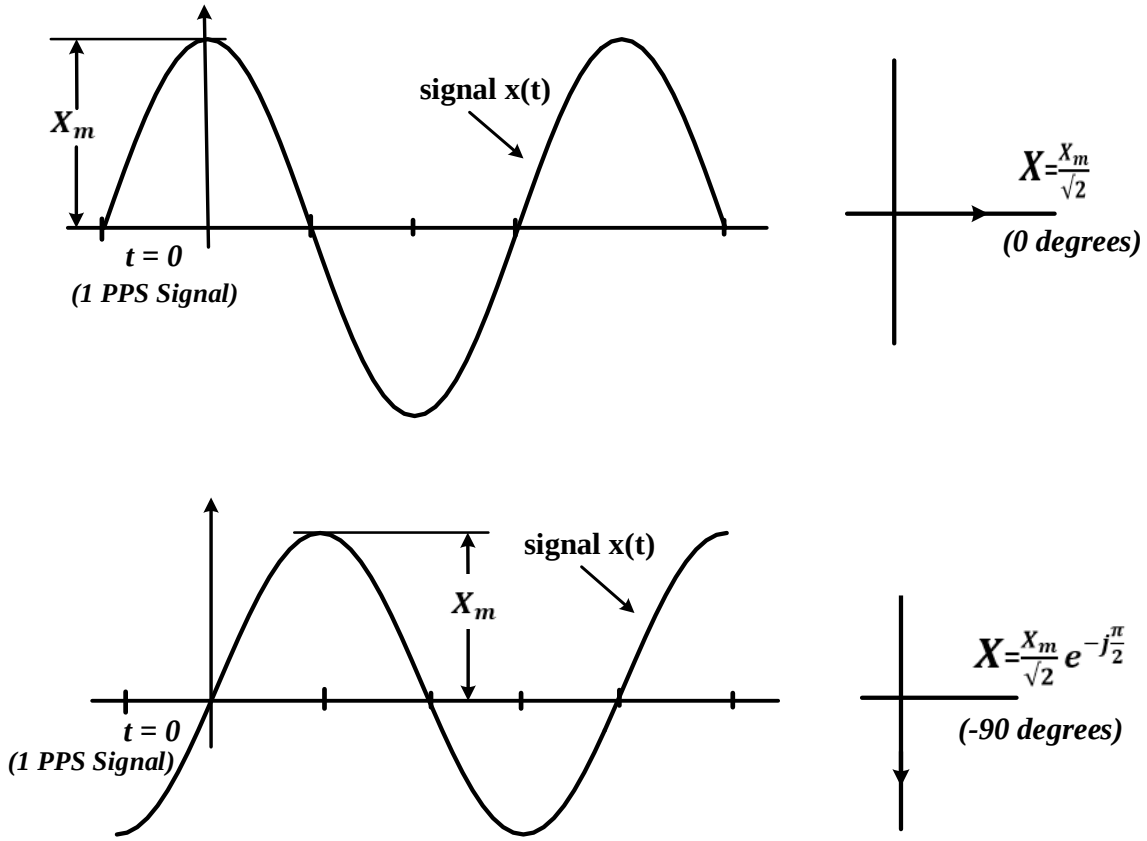

Figure 3.1: Convention for synchrophasor representation

3.2.2 PMU Architecture

PMUs have made possible the measurement of voltages and currents at different locations in the power network at the same time. PMU are placed at the strategic bus locations in the grid called optimal location as explained in detail in section 3.3. The provision of time-tagging to the measurement samples has assisted system operators and planner to measure the state of electrical system and manage power quality. Synchronization of time is aided by the use of Global Positioning System (GPS) satellites. The GPS clock is received once every second from the satellites. As the measurements are truly synchronized, they can be used to access the system state in real time. The typical functional block diagram is shown in Figure 3.2.

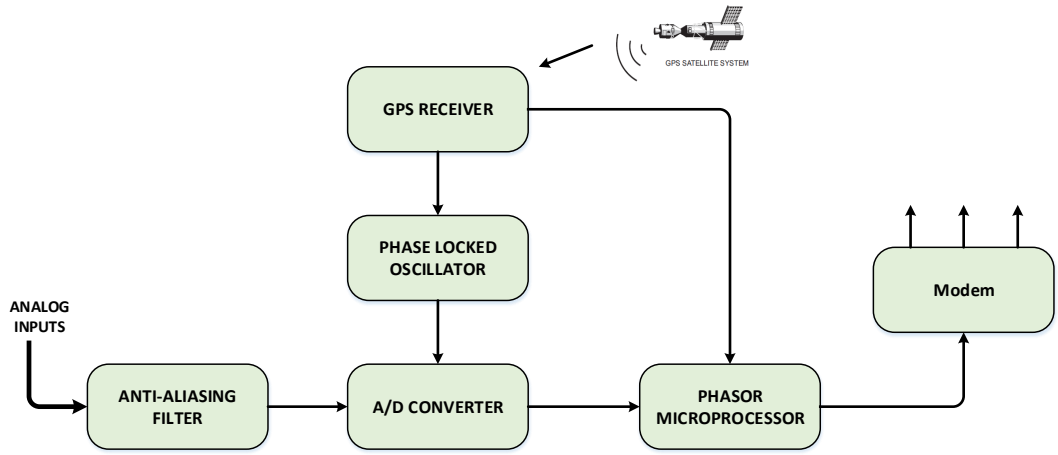

Figure 3.2: Functional block diagram of phasor measurement unit

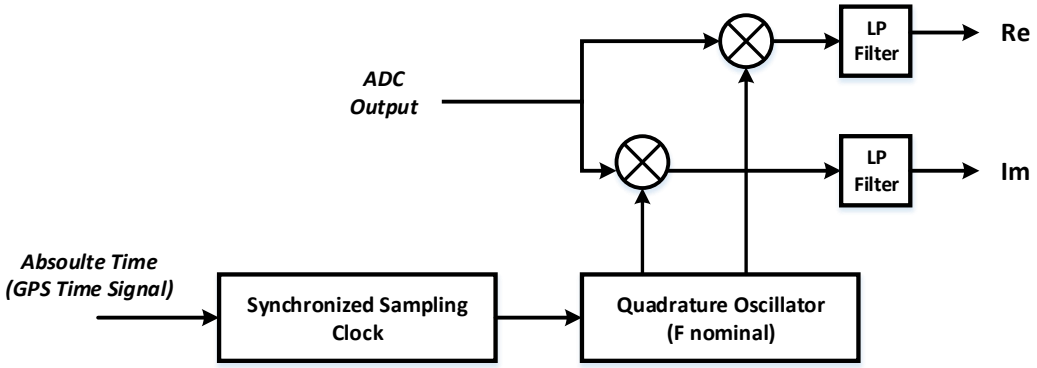

Figure 3.3: Single phase section of phasor microprocessor

The secondary power system voltages and currents are filtered by analog anti- aliasing filter and are converted by A/D converter at the sampling instance defined by the phase locked oscillator. Phasor microprocessor utilize the DFT algorithm to calculate the phasor at each interval using Equation (3.3), (3.4) [54] as shown in Figure 3.3. The low pass filters are used to remove the double frequency component thus leaving the Re and Im part of the original input signal and phasor estimate at the center of the estimation window. Low pass filters are classified into P and M class depending upon the windowing technique. The P class has 2 cycle FIR window; while the M class window varies in length with the reporting rate [55]. With the proper decimation, phasors are transmitted at the specified reporting

rates.

$$\boldsymbol{X(i)} = \frac{\sqrt{2}}{Gain} \times \sum_{k=-N/2}^{N/2} x_{(i+k)} \times W_{(k)} \times e^{-j(i+k)\Delta t \omega_0} \tag{3.3}$$

$$Gain = \sum_{k=-N/2}^{N/2} W_{(k)} \tag{3.4}$$

where, $\omega_0 = 2\pi f_0$ and f_0 is the nominal system frequency.

N= FIR filter order

Δt= 1/sampling frequency

x_i = sample of the waveform at time $t = i\Delta t$

$W_{(k)}$ = low-pass filter coefficients depending on the P or M class filter

3.2.3 PMU Reporting Rates

As per current $IEEE\ C37.118.1^{TM} - 2011$ standard, PMUs should support data reporting at sub-multiples of the nominal power system frequency. Table 3.1 list the reporting rates defined in the current standard.

Table 3.1: Standard PMU reporting rates

System frequency	Reporting rates (Frames per second)
50 Hz	10, 25, 50
60 Hz	10, 12, 15, 20, 30, 60

With the advancement in technology, current commercial relay consist of PMU that has capability to use higher reporting rate as encouraged by the IEEE standard. The PMU in GE N60 relay supports upto 120 Hz for 60 Hz system and 100 Hz for the 50 Hz system [15],

where as the PMU model in $RTDS^{TM}$ can support upto 240 Hz for 60 Hz system and 200 Hz for the 50 Hz system [55].

The synchrophasor reporting rate is an important parameter for the time series analysis used in the proposed protection scheme. Higher sampling rate of PMU provides the detailed granular data and reveal new information about dynamic stability event of the grid. Higher message rate facilitates more observation points for a given period of time in the time series and help in more precise predictions. The preferred solution is to select the reporting rate as high as possible depending upon the feasibility constraint of communication bandwidth, storage and application. A reporting rate of 120 samples per second is implemented in the research work.

3.3 Optimal PMU Location in Power System

3.3.1 Introduction

PMU provides time synchronized measurements of the voltage and current phasors at a bus with very high accuracy utilizing SMT [56]. The high resolution of the measurement data from PMU provide detailed information, especially during transients which were not possible using the supervisory control and data acquisition (SCADA) system. However, placement of PMUs throughout buses in network is rarely feasible due to cost or non-existence of communication facilities in some substations. Depending upon the measurement channels and features, a PMU can be expensive and setting up communication networks can increase the primary substation installation cost. The average costs per PMU along with supporting infrastructure (cost of procurement, installation, and commissioning) range between $40,000 and $180,000. The supporting infrastructure include CT, PT and communication network setup. A PMU device cost is as low as 5% of the installation cost [57]. Therefore there is need to determine the optimal location of the synchronized measurement device so that the number of PMUs required to make system completely observable is minimized. Installation of PMUs is a gradual process, requiring decisions on the best strategic location for a limited

numbers of PMUs at the beginning.

3.3.2 Strategic PMU Placement for Full Observability

The measurement placement identification is described as a process of selecting locations to place measurement device in a way that certain objectives and constraints are satisfied with in a network [56]. Placement identification has been a research topic in the field of operation, control and optimization.

Among different method to find the minimum number of PMUs and their optimal locations, integer quadratic programming is used to achieve the following goals.

- Minimize the required number of PMUs.
- Maximize the measurement redundancy.

The PMU placement methodology used for the optimal PMU placement ensures that the system is topologically observable during normal operating conditions and possible loss or failure of the PMUs is not considered. PMU placed at a bus can measure the voltage phasor at that bus and neighboring buses using current phasors and line parameters. It is assumed that the PMU has a sufficient number of channels to measure the current phasors through all the branches incidental to the bus at which it is placed.

3.3.2.1 Formulation

The elements of the binary connectivity matrix **B** for a power system, used in the formulation of the optimization problem, is defined as:

$$\mathbf{B}(i,j) = \begin{cases} 1 & i = j \\ 1 & \textit{if } i \textit{ and } j \textit{ are connected} \\ 0 & \textit{otherwise} \end{cases} \tag{3.5}$$

The binary vector is defined depending upon the PMU placement at the bus in the network, referred as PMU placement set and is given by:

$$p_i = \begin{cases} 1 & \textit{if a PMU is placed at bus } i \\ 0 & \textit{otherwise} \end{cases} \tag{3.6}$$

The number of times a bus is observed by the PMU placement set defined by $\mathbf{p}$ is given by the element of product $\mathbf{Bp}$. Integer quadratic program is used to optimize the objective function $O(\mathbf{p})$ given by Equation (3.7) [56].

$$O(\mathbf{p}) = \lambda(\mathbf{N} - \mathbf{Bp})^T\mathbf{R}(\mathbf{N} - \mathbf{Bp}) + \mathbf{p}^T\mathbf{Qp} \tag{3.7}$$

where λ is a weight and is used as a normalizing factor such that $\lambda = (\mathbf{N}^T\mathbf{RN})^{-1}$
$\mathbf{N}$ is vector representing the upper limits of the number of times that each bus can be observed by the PMU placement set $\mathbf{p}$ and equals the number of incident lines to the corresponding bus plus one. $\mathbf{R}$ and $\mathbf{Q}$ are diagonal matrix and has diagonal entries representing the significance of each bus and PMU installation cost at different bus location, respectively. Considering

equal significance of each bus and same PMU installation cost, $\mathbf{P}$ and $\mathbf{Q}$ are set equal to identity matrix $\mathbf{I}^{n\times n}$ in the research.

There are two parts in the Equation (3.7). The first part computes the difference between the maximum number of times that the bus can be observed ideally and the actual number of times it is observed by the PMU placement set. Minimization of this difference is therefore equivalent to maximizing the measurement redundancy. The second part represents the total cost of PMU installation. When the installation cost of all PMUs are considered to be the same, minimizing this part is equivalent to minimization of total number of PMUs in the system. The objective function in the Equation (3.7) can be expanded to formulate in an integer quadratic programming framework as

$$Minimize \quad \frac{1}{2}\mathbf{p}^T\mathbf{H}\mathbf{p} + \mathbf{g}^T\mathbf{p} \tag{3.8}$$

$$Subjected\ to \quad \mathbf{B}\mathbf{p} \geq \mathbf{b} \tag{3.9}$$

where $\mathbf{H} = (2\lambda\mathbf{B}^T\mathbf{R}\mathbf{B} + 2\mathbf{Q})$, $\mathbf{g} = (-2\lambda\mathbf{N}^T\mathbf{R}\mathbf{B})^T$, and $\mathbf{b} = \mathbf{I}^{n\times 1}$

The inequality in Equation (3.9) is the constraint for the observability, which ensures that each bus in the system is observed at least once by the PMUs. If a measurement redundancy level of one or higher is desired for some or all of the system buses, the values of the elements in the vector $\mathbf{b}$ can be increased accordingly. The objective function in Equation (3.8) is minimized with respect to $\mathbf{p}$ using integer quadratic programming.

3.3.2.2 Optimal PMU Placement in WSCC 9 Bus System

Optimal PMU placement using formulation in Section 3.3.2.1 is performed in WSCC 9 bus test system. This test system has nine probable locations for the PMU placement. The single line diagram of WSCC 9 bus system is shown in Figure 3.4 [58]. Study is carried out considering the conventional measurements, such as power flow and power measurements are

unavailable. PMU placement for the WSCC 9 bus system without the conventional measurements is explained in this section.

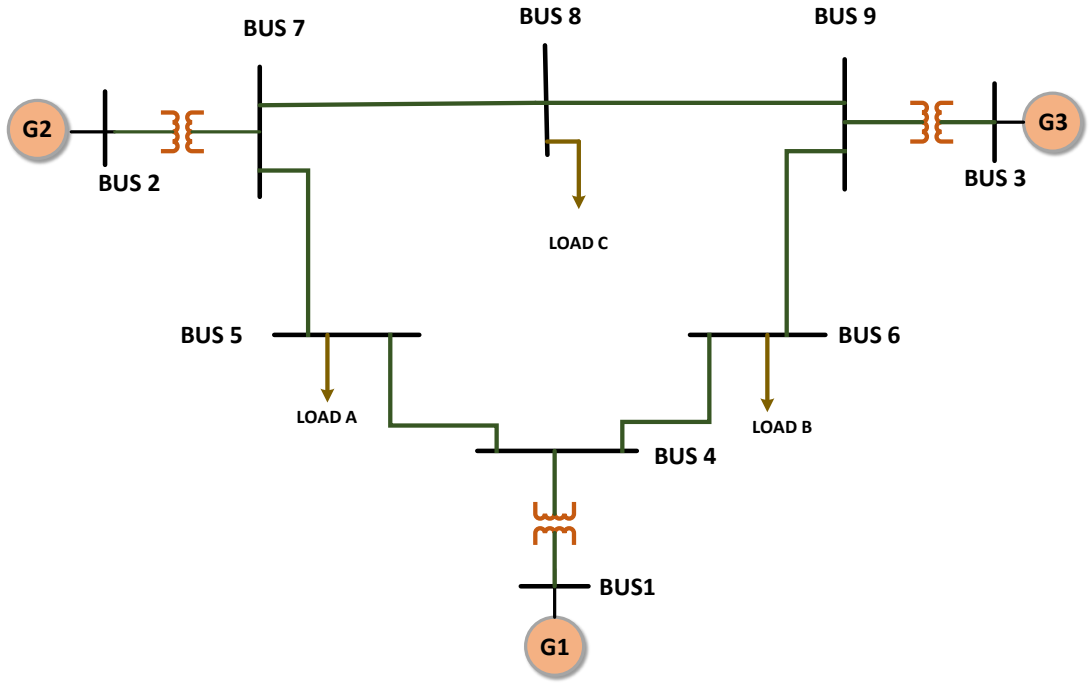

Figure 3.4: WSCC 9 bus test system

The binary connectivity matrix for the WSCC 9 bus system is shown below

$$\mathbf{B} = \begin{bmatrix} 1 & 0 & 0 & 1 & 0 & 0 & 0 & 0 & 0 \\ 0 & 1 & 0 & 0 & 0 & 0 & 1 & 0 & 0 \\ 0 & 0 & 1 & 0 & 0 & 0 & 0 & 0 & 1 \\ 1 & 0 & 0 & 1 & 1 & 1 & 0 & 0 & 0 \\ 0 & 0 & 0 & 1 & 1 & 0 & 1 & 0 & 0 \\ 0 & 0 & 0 & 1 & 0 & 1 & 0 & 0 & 1 \\ 0 & 1 & 0 & 0 & 1 & 0 & 1 & 1 & 0 \\ 0 & 0 & 0 & 0 & 0 & 0 & 1 & 1 & 1 \\ 0 & 0 & 1 & 0 & 0 & 1 & 0 & 1 & 1 \end{bmatrix} \tag{3.10}$$

In the system, since the bus number 1 is connected to bus number 4, the 1^{st} and the 4^{th}

element in the first row of binary connectivity matrix are set to 1. For every combination of PMU placement set, the objective function and the inequality constraint is evaluated as given in Equation (3.8) and Equation(3.9), respectively. The inequality in Equation (3.11) is the constraint for the observability that each bus in WSCC 9 bus system is observed at least once by the PMU placement set.

$$\begin{bmatrix} \mathbf{b1} \\ \mathbf{b2} \\ \mathbf{b3} \\ \mathbf{b4} \\ \mathbf{b5} \\ \mathbf{b6} \\ \mathbf{b7} \\ \mathbf{b8} \\ \mathbf{b9} \end{bmatrix} \mathbf{p} = \begin{bmatrix} 1 & 0 & 0 & 1 & 0 & 0 & 0 & 0 & 0 \\ 0 & 1 & 0 & 0 & 0 & 0 & 1 & 0 & 0 \\ 0 & 0 & 1 & 0 & 0 & 0 & 0 & 0 & 1 \\ 1 & 0 & 0 & 1 & 1 & 1 & 0 & 0 & 0 \\ 0 & 0 & 0 & 1 & 1 & 0 & 1 & 0 & 0 \\ 0 & 0 & 0 & 1 & 0 & 1 & 0 & 0 & 1 \\ 0 & 1 & 0 & 0 & 1 & 0 & 1 & 1 & 0 \\ 0 & 0 & 0 & 0 & 0 & 0 & 1 & 1 & 1 \\ 0 & 0 & 1 & 0 & 0 & 1 & 0 & 1 & 1 \end{bmatrix} \mathbf{p} \geq \begin{bmatrix} 1 \\ 1 \\ 1 \\ 1 \\ 1 \\ 1 \\ 1 \\ 1 \\ 1 \end{bmatrix} \tag{3.11}$$

The optimal PMU placements for the WSCC 9 bus system for i) normal operating conditions, without maximizing the measurement redundancy; ii) normal operating conditions, maximizing the measurement redundancy is shown in Table 3.2. The first part of objective function $O(\mathbf{p})$in Equation (3.7) tend to maximize the number of times a bus is observed by the PMU placement set. The number of times the buses 1 to 9 in the WSCC 9 bus system being observed by the PMU placement sets with minimum number of PMUs are presented in the Table 3.3.

For the three PMU placement sets $\{3, 4, 7\}$, $\{2, 1, 9\}$ and $\{1, 7, 9\}$, only the number of PMUs is minimized and is equal to 3, without maximizing the measurement redundancy. For the PMU placement set $\{4, 7, 9\}$, the number of PMUs is minimized and the measurement redundancy at the buses is maximized. Evidently, the latter one results in a more desirable distribution of measurement redundancy and has been used in the research.

Table 3.2: Optimal PMU locations for WSCC 9 bus system

System configuration	Number of PMU	Optimal PMU locations
Normal operating conditions without maximizing the measurement redundancy	3	3,4,7 2,1,9 1,7,9
Normal operating conditions maximizing the measurement redundancy	3	4,7,9

Table 3.3: PMU measurement redundancy for WSCC 9 bus system

PMU Locations	Number of PMU	Number of times each bus is observed
3,4,7	3	1,1,1,1,2,1,1,1,1
2,1,9	3	1,1,1,1,1,2,1,1,1
1,7,9	3	1,1,1,1,1,1,1,2,1
4,7,9	3	1,1,1,1,2,2,1,2,1

3.4 Out of Step Analysis in WAMS

In large integrated networks, the stability studies are complex. A promising solution for the stability problem in large networks utilizing the real time data from WAMS can be formulated in three steps [59].

- Identification of optimal placement sites
- Real-time coherency determination
- Approach to determine swing outcome

3.4.1 Identification of Optimum Placement Sites

PMU measures the phasor quantities at the optimum bus location. The importance of the measurement can be of very high degree at some of the optimal places and are called critical buses. Optimal placement of the PMUs is described in detail in Section 3.3.

3.4.2 Real-Time Coherency Determination

This section explains the voltage and current measurements from PMUs and the rotor angle estimation using the PMUs measurement and network information. In the later part of this section, the idea of determining the coherent groups using the dynamics of system which is prominent during oscillations is explained.

3.4.2.1 Synchronized Voltage and Current Phasors and Rotor Angle

The synchronized voltage and current phasor measurements are taken at the optimal bus location as shown in the Figure 3.5. The voltage and current measured by phasor measurement unit in one of the PMU location, bus 7 is shown in the Figure 3.6 and Figure 3.7, respectively.

The voltage of the generator buses are back calculated using the PMU measurement of current and voltage and the transformer impedance. With the information of the voltage and current, the rotor angle of the machine calculated using generator classical model for a transient period is given by Equation (3.12). A similar methodology is used for deriving the internal voltage in the excitation control schemes for generators in reference [60].

$$E'\angle\delta = V_t\angle\theta_v + j(Ra + X'_d)I_t\angle\theta_I \tag{3.12}$$

Where E' is generator internal voltage, V_t is generator terminal voltage, X'_d is generator transient reactance, I_t is generator terminal current, and δ is generator rotor angle. During a power swing, the generator operates within transient and then synchronous impedance characteristics, both has significantly different value of impedance. Hence, the appropriate

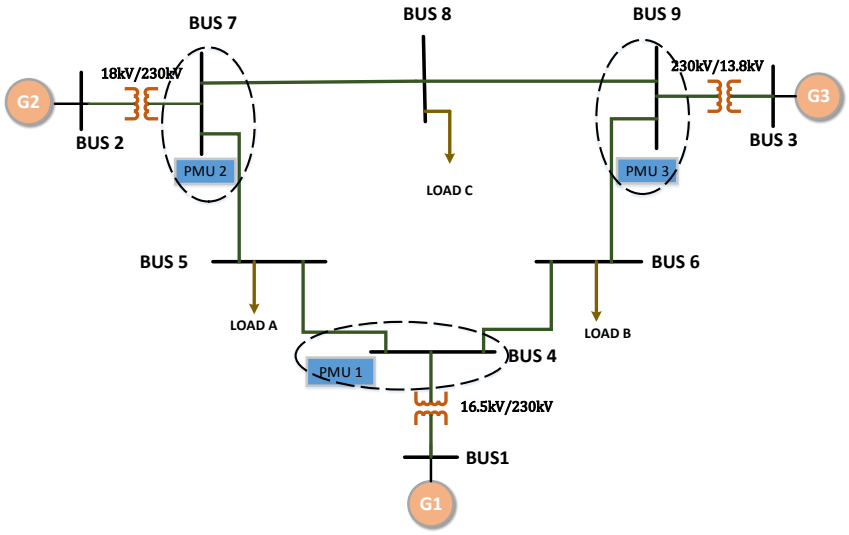

Figure 3.5: PMU measurements at optimum bus locations in WSCC 9 bus system

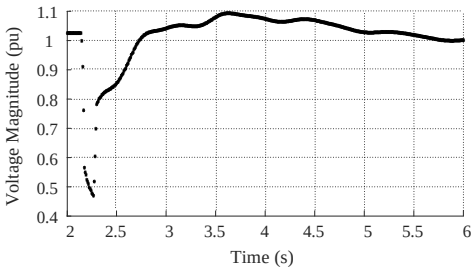

(a) Voltage magnitude samples

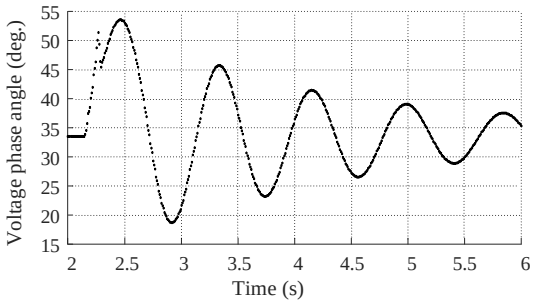

(b) Voltage phase samples

Figure 3.6: Synchronized voltage measurement at PMU bus 7 for 6 cycles fault at bus 5

impedance value is selected when calculating the generator internal voltage. During the calculation of the generator internal voltage, the time for transient period is calculated using the available generator reactances (X_d and X'_d) and the generator open circuit time constant (Tdo') as given in Equation (3.13). The short circuit time constant for the three generators in WSCC 9 bus system are listed in Table 3.4.

$$T'_d = \frac{X'_d}{X_d} Tdo' \tag{3.13}$$

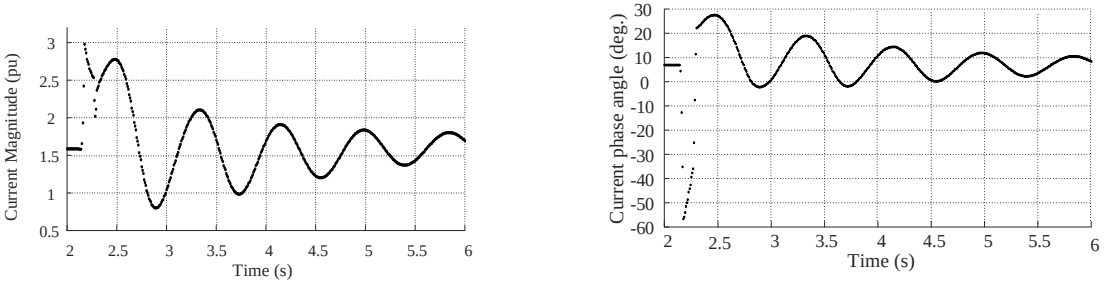

(a) Current magnitude samples

(b) Current phase samples

Figure 3.7: Synchronized current measurement at PMU bus 7 for 6 cycles fault at bus 5

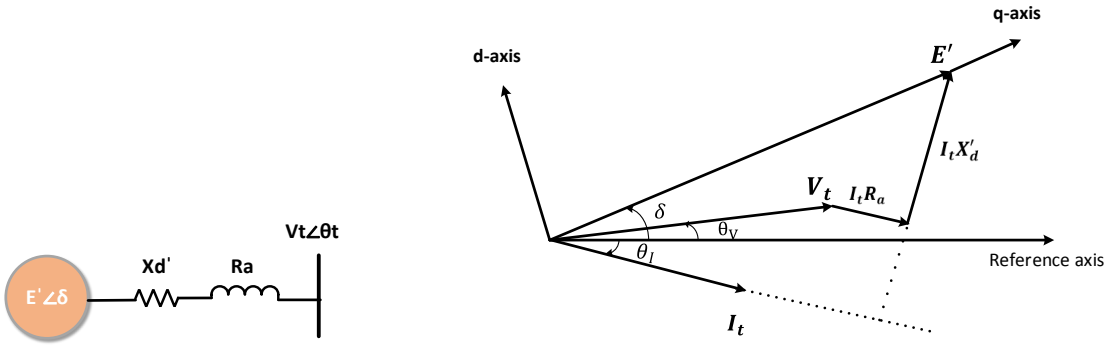

(a) Voltage behind transient reactance model

(b) Synchronous generator phasor diagram

Figure 3.8: Rotor angle estimation

Table 3.4: WSCC 9 bus system generators short circuit time constant

Machine	$X_d(pu)$	$X'_d(pu)$	Tdo' (s)	Td' (s)
Generator 1	0.1460	0.0608	8.9600	3.7313
Generator 2	0.8958	0.1198	6.0000	0.8024
Generator 3	1.3125	0.1813	5.8900	0.8136

3.4.2.2 Coherent Groups Formation

Real-time coherency identification is a stage when the progressive swings of all the generators of significant size is observed over a reasonable observation window. In most of the practical scenarios, time required to identify the coherency of generators is about $0.2 - 0.4$ second after the instance of disturbance. The formulation of coherently swinging groups is carried out from the time instance that the coherency between machines is determined [10]. This concept of coherency determination is illustrated in Figure 3.9. Group of generators which swing together against some other generator or group of generators, form a coherent group and can be represented by the equivalent generator.

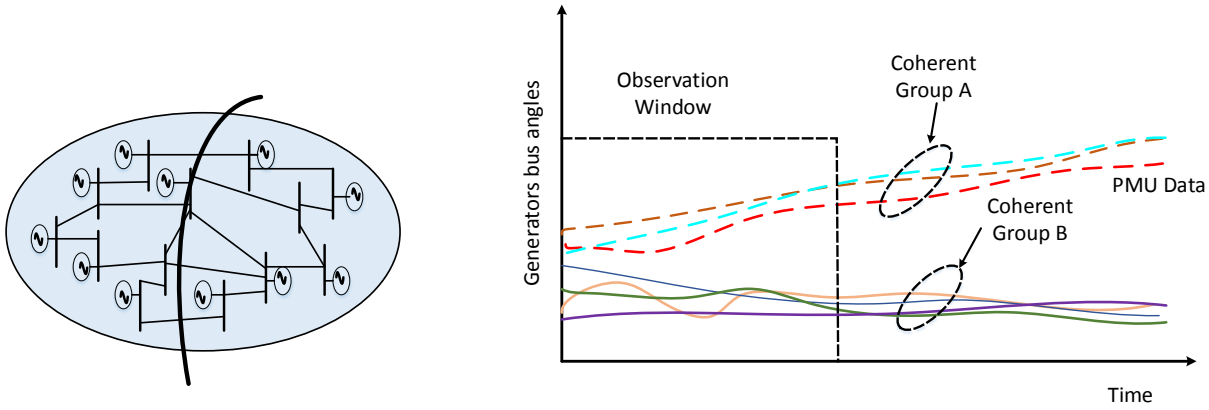

(a) Generators seperating into two groups after disturbance

(b) Generators bus phase angles after distubance

Figure 3.9: Real time coherency determination

3.4.2.3 Coherent Group Identification

The power system states can be more accurately monitored with wide area measurements communicated to the central control center. Real time visibility of the measured synchronized phasor can be utilized in identifying the coherent groups of generators. After a disturbance, the generators in a coherent group swing together against another generator or group of generators. A real time coherency study uses online measurement of generator bus voltage

angles to determine the coherency in the early part of the post fault condition [37].

In this subsection, test system (WSCC 9 bus system) is investigated using time domain simulation and the generator bus voltage angle separation from a reference generator bus is measured at every simulation time step. The coherency is identified in the test system with the assumption that the machines will separate into two groups. This is a fairly valid assumption, because whenever a disturbance occurs in the power system, a group of generators tends to oscillate with another group of generators, forming two coherent groups. The criterion to check whether the generator being compared falls in the same group with respect to the reference generator forms a group is given by Equation (3.14). Those generators which violates the criterion forms a new group.

$$\Delta\theta_i - \Delta\theta_r < \epsilon \tag{3.14}$$

where ϵ is the specified tolerance in degrees, i represents the machine being clustered, and r represents the reference generator. A tolerance of 5 degrees is selected for this study. Coherency determination in WSCC 9 bus test system test system are discussed below.

For three phase fault applied at the middle of transmission line between bus 5 and bus 7 for a fault of 5 cycles, the generator bus voltage swing curve with respect to the reference generator at bus 1 is shown in Figure 3.10.

The generators at bus 2 and 3 begin to separate out from the reference generator bus after the fault and during the post fault condition as the generators bus voltage angles separate beyond 5 degrees, the coherency between the generators at bus 2 and bus 3 is identified. The coherency between the generators at bus 2 and bus 3 is detected at 75.01 ms. Similarly, for the fault at bus 7 and fault cleared after 9 cycles, the generators bus voltage angle with respect to the reference bus is shown in Figure 3.11. The generators at bus 2 and bus 3 separate from the reference bus at bus 1. The time measured for the 5 degree angular separation of bus 2 and bus 3 voltage with the reference bus is 59.01 ms.

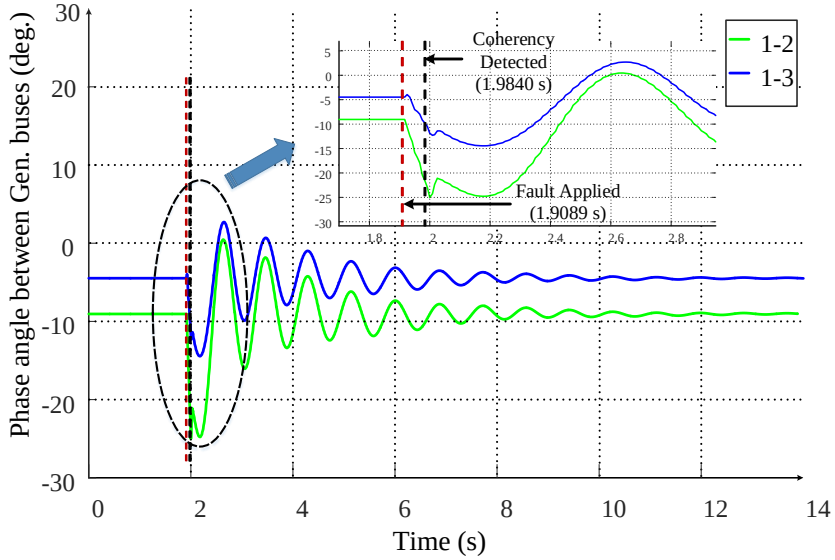

Figure 3.10: Generator bus voltage angle difference for three phase fault at middle of line between bus 5 and bus 7 and fault of 5 *cycles*

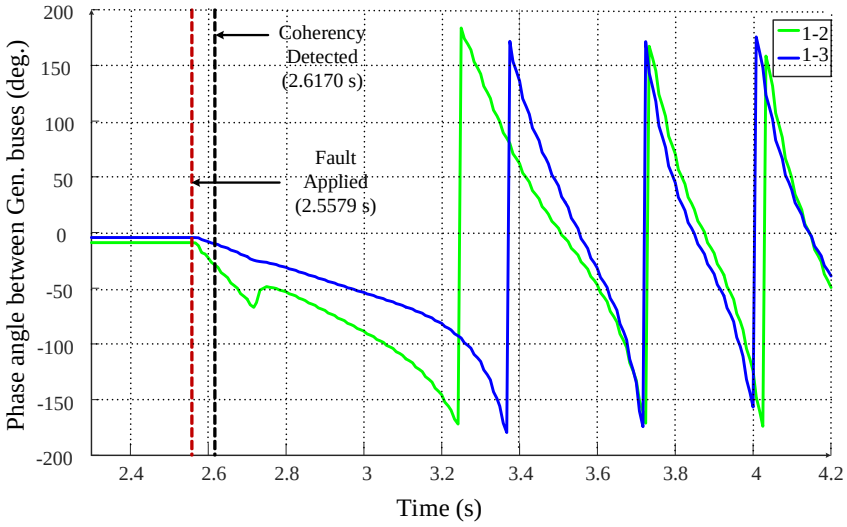

Figure 3.11: Generator bus voltage angle difference for three phase fault at bus 7 and fault of 9 *cycles*

3.4.2.4 Center of Angle of a Coherent Group

For systems which behave like a two-machine system, after the coherency among the generators in a group is identified, the system is reduced to two machine equivalent system. The technique explained in [33] is used to obtain two machine equivalent of multi-machine system. Using the assumption that the disturbed multi-machine system separates in two groups, let us define the two groups of machines as Area A and Area B as shown in Figure 3.12.

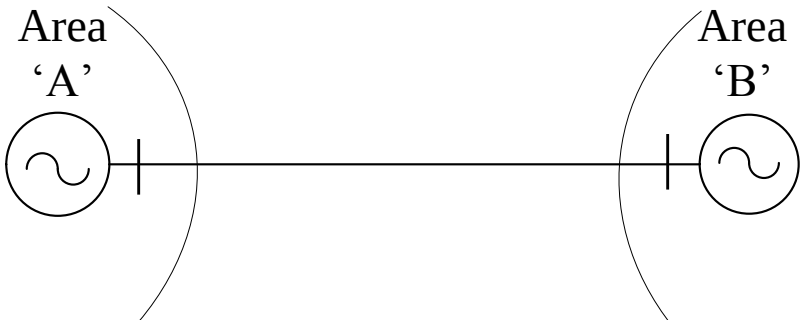

Figure 3.12: Two machine representation

The COA of Area A and that of Area B are given by Equation 3.15.

$$\delta_a = \sum_{i \in A} \frac{M_i \delta_i}{M_a} \tag{3.15a}$$

$$M_a = \sum_{i \in A} M_i \tag{3.15b}$$

$$\delta_b = \sum_{j \in B} \frac{M_j \delta_j}{M_b} \tag{3.15c}$$

$$M_b = \sum_{j \in B} M_j \tag{3.15d}$$

where, δ_a is the COA of the generators in Area A, M_a is the sum of the inertia constants of the generators in Area A, δ_b is the COA of the generators in Area B, M_b is the sum of the inertia constants of the generators in Area B. The COA of a group is assumed to be equal

to the rotor angles of the generators in that group, i.e., :

$$\delta_a = \delta_i \qquad \forall i \epsilon A \tag{3.16a}$$

$$\delta_b = \delta_j \qquad \forall j \epsilon B \tag{3.16b}$$

In WSCC 9 bus system, the generator 1 forms the coherent group A, and generator 2 and 3 form the coherent group B.

3.4.3 Approach to determine swing outcome

In the literature review, different methods using the swing based methods to predict the out-of-step condition using various approach of prediction are presented. Reference [41] used slope of rotor angle calculated by linear curve fitting to identify the coherency. Reference [42] use the polynomial curve fitting to predict the rotor angle for finding the critical and non critical group of generators and use EAC to predict the stability of the system. The difference method is used in reference [43] to predict rotor angle used for identification of critical machines and instability margin and the time to instability are calculated to determine the stability of the system. A new approach of time series based prediction using the time series models and past information is proposed in this thesis and is described next.

3.4.3.1 Proposed Time Series Swing Curves Based Prediction

It is evident that during the disturbance, the rotor angle of generators start to swing due to the output electrical power and input mechanical power imbalance. It is also seen that the system tend to segregate into two groups having similar rotor swing and form a coherent group and swing against another machine or group of machine. Based on similarities in the nature of swing, the group of machine in a group can be represented with the characteristic angle as explained in Section 3.4.2.4. The angular difference of the coherent groups is proposed to predict the transient stability of the power system. The time series models act as a tool to predict the future samples of difference of center of angle (dCOA) between the coherent group. The steps for model selection, parameters estimation and forecasting of time

series are explained in Section 3.5 of this chapter. The analysis is simple, computationally easy and has an ability to predict transient instability faster. The angular separation of two coherent groups is given by Equation (3.17)

$$dCOA = \delta_a - \delta_b \tag{3.17}$$

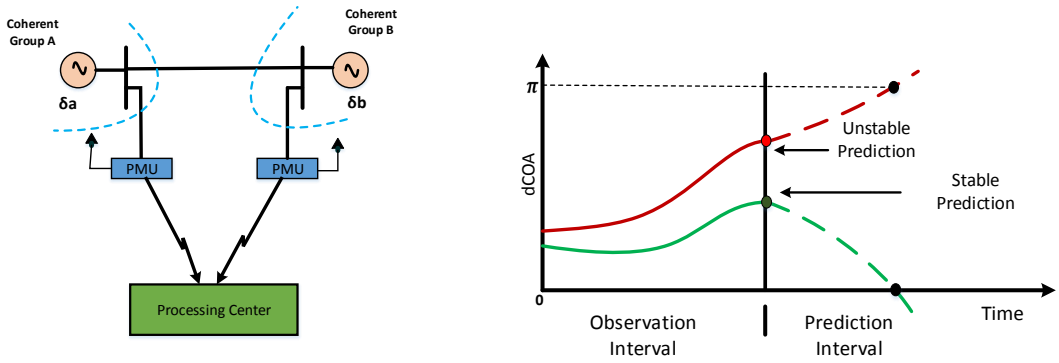

(a) Two machine equivalent

(b) Observation and prediciton of swing curve

Figure 3.13: Time series swing curves and prediction

The measured angular separation between the two coherent groups is predicted as a time-series function. The predicted future values would lead to either of the two conditions, stable or unstable conditions. If the difference of swing curve between the coherent two groups has a zero-crossing for the predicted samples after the disturbance then the system is declared to be stable, whereas if the swing curve is monotonically increasing then this would indicate instability in the system. Figure 3.13 shows the time series swing curve based prediction illustration. The prediction of the stability is based on the forecasted value of the angular separation and categorized as below.

$$if\ forecasted\ dCOA \leq 0: \quad Stable \tag{3.18}$$

$$if\ forecasted\ dCOA \geq 180: \quad Unstable \tag{3.19}$$

3.5 Time Series Analysis and Forecasting

3.5.1 Introduction

Time series is defined as sequence of observations taken sequentially in time. It represents the point-by-point behavior of a variable in power system over a period of time. The fundamental feature of the time series is distinctly characterized by the dependency adjacent observations. The nature of this dependence among observations of a time series can be utilized to forecast the future trend and timely value of the same observation variable. Time series analysis is concerned with techniques for the analysis of this dependence [61]. The development of the stochastic and dynamic models for the time series data and the use of such models to estimate or approximate the behavior of series becomes necessary. This section presents the concept of time series analysis and forecasting. The time series representation, time series model and model selection criteria are explained and play important role in the performance of the proposed WAMS based protection scheme. The swing between coherent groups are used for the time series analysis in the research.

Forecasting is also widely applied in the power industry for predicting the load demand and energy pricing. Forecasting is performed to predict the trend for next day, months or years in advance. Depending up on the prediction result, necessary planning is carried out for the infrastructure development and bids for the best economic power is placed. Forecasting has been extensively used in economics and finance sector. It is used to forecast market trends to make budgeting, planning, investing, and policy decisions [62].

As the utilities integrate more renewable energy into the system, forecasting of wind and solar power availability is also going to be important. The proper amount of renewable energy that can be available need to be known in advance for a given a period of time so that generation from the conventional source can be kept running to meet load demand. These predictions assist in determining the stability of the system. The predicted load demand and generation from renewable will help to operate the power plant to meet the required power demand. Any faults in the power system may also affect the stability of the system. Accurate

forecast models play a key role while analyzing/predicting the stability behavior in power systems. The advanced information about the stability of system will provide sufficient time to take remedial action and save the system from collapsing. This future state of the system after disturbance or any changes introduced in system can be known only by estimation. This is the reason why time series analysis plays an important role in power systems to approximate the state of system in future.

3.5.2 Time Series Representation

The voltage and current measurements from PMU are a discrete time series observation made at times t_1, t_2, t_3,$\cdots\cdots$, t_N and can be represented as

$$v(t_1),\ v(t_2),\ v(t_3),\ \cdots\cdots,\ v(t_{n-1}),\ v(t_n),\ v(t_{n+1}),\ \cdots\cdots,\ v(t_N) \tag{3.20}$$

$$i(t_1),\ i(t_2),\ i(t_3),\ \cdots\cdots,\ i(t_{n-1}),\ i(t_n),\ i(t_{n+1}),\ \cdots\cdots,\ i(t_N) \tag{3.21}$$

These observation are made at a fixed time interval h and for N successive values of such series are measured at equidistant time intervals t_0+h, t_0+2h, t_0+3h, $\cdots\cdots$, $t_0+(n-1)h$, t_0+nh, $t_0+(n+1)h$, $\cdots\cdots$, t_0+Nh. PMU measures the electrical input signals from current transformer and voltage transformer sampled at intervals of 8.33 milliseconds. The magnitude of sample voltage signal is shown in Figure 3.14.

Beside the evolution of measurement in time, times series data can be utilized to forecast the future trend. Time series model can be constructed and analyzed with the available measurements to build the characteristics of the variable and approximate the future trend. Among different time series analysis method, Box and Jenkins methods are commonly used methods and are explained in the following sections.

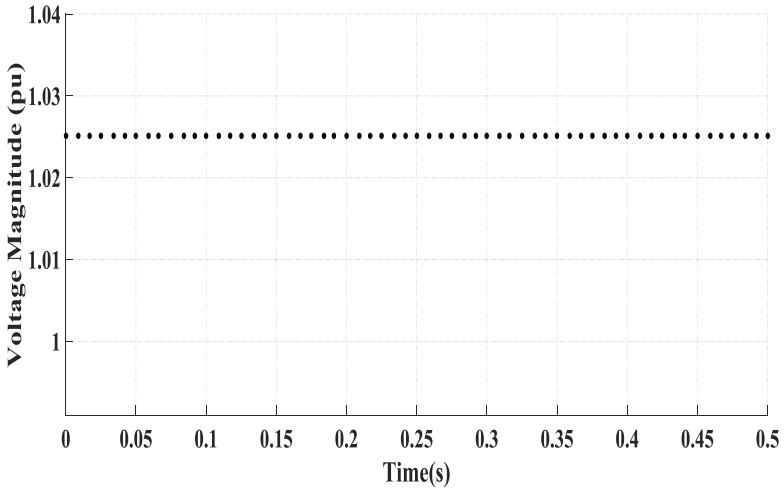

Figure 3.14: Sampled voltage measurement at bus 4 during steady case

3.5.3 Autoregressive Models (AR)

One of the simplest models extremely useful in practically occurring time series systems is the autoregressive (AR) model. This model assumes the future values of the series is a linear aggregate of finite number of previous values in the series and a random error [61]. The autoregressive model of order one for a time series z_t, z_{t-1}, z_{t-2} $\cdots$ can be represented as

$$z_t = c + \phi_1 z_{t-1} + \varepsilon_t \tag{3.22}$$

In Equation (3.22), ϕ_1 is the autoregressive parameter of order one, c is a constant and ε_t is a random error term associated with the data points at time t. The error shows the difference between the actual and estimated values. The notation to represent autoregressive model of order one as in Equation (3.22) is $AR(1)$ and in this model z_t is linear function of its previous value z_{t-1}. Similarly, $AR(p)$ represents the p order autoregressive model where future value depends upon past p values and error as in Equation (3.23).

$$z_t = c + \phi_1 z_{t-1} + \phi_2 z_{t-2} + \cdots + \phi_p z_{t-p} + \varepsilon_t \tag{3.23}$$

3.5.4 Moving Average Models (MA)

In time series analysis, moving-average (MA) model is a common approach for modeling single variable ("univariate") time signal. This model is conceptually a linear regression of future value of the series against the random shocks (error) of one or more previous values of the series [61]. The random shocks at each point are assumed to come from the same distribution, typically a normal distribution [63]. The moving average model of order one for a time series z_t, z_{t-1}, z_{t-2} $\cdots$ can be represented as

$$z_t = \mu + \beta_1 \varepsilon_{t-1} + \varepsilon_t \tag{3.24}$$

In Equation (3.24), β_1 is the moving average parameter of order one, μ is the mean of the series, ε_{t-1} is random error associated to the previous data sample z_{t-1} and ε_t is the random error of the series at the time period equal to t. Higher order of moving average model can utilize q number of previous data points to model future value and are referred as q order moving-average model as given by Equation (3.25)

$$z_t = \mu + \beta_1 \varepsilon_{t-1} + \beta_2 \varepsilon_{t-2} + \cdots + \beta_q \varepsilon_{t-q} + \varepsilon_t \tag{3.25}$$

3.5.5 Autoregressive Moving Average Models (ARMA)

The combination of autoregressive and moving-average model can effectively form a useful class of time series model called autoregressive moving average (ARMA) model. Inclusion of both autoregressive and moving average terms in the model provides greater flexibility in fitting the time series [61]. ARMA model use the finite p previous values and finite q previous random errors to calculate the future value. ARMA(p,q) can be mathematically represented as in Equation (3.26).

$$z_t = c + \sum_{i=1}^{p} \phi_i z_{t-i} + \sum_{j=1}^{q} \beta_j \varepsilon_{t-j} + \varepsilon_t \tag{3.26}$$

where model order p and q refers to the p autoregressive and q moving average terms.

ARMA model is designed for stationary time series whose basic statistical properties; mean, variance and covariance is considered to be constant over time. Stationary time series fundamentally represent a measured variable whose values vary along the mean and does not deviates largely from it. In reality, actual time series data of power swing can have steady, continuous increasing, oscillating or damped oscillatory nature and its stationarity is not guaranteed. Thus, non-stationary series need variable transformation technique called differentiation to make series stationary and transformed stationary series is utilized to build the ARMA model.

3.5.6 Autoregrassive Integrated Moving-Average Models (ARIMA)

Statisticians George Box and Gwilym Jenkins developed a practical approach to build ARIMA model, which best fit to a given time series. Their concept has fundamental importance in the area of time series analysis and forecasting. ARIMA model is generalized ARMA model to incorporate the case of non-stationarity. In ARIMA models, a non-stationary time series is made stationary by applying finite differencing to the data points. A series can be modelled as stationary ARMA(p,q) after the finite d differentiation and is denoted as ARIMA(p,d,q). The first order differentiation of variable in non stationary series is given by the Equation (3.27) and the second order differentiation of the variable of same series is given by Equation (3.28). The general notation for the d differentiation order of time series is $\Delta^p z_t$.

$$\Delta^1 z_t = z_t - z_{t-1} \tag{3.27}$$

$$\begin{aligned} \Delta^2 z_t &= \Delta^1 z_t - \Delta^1 z_{t-1} \\ &= z_t - 2z_{t-1} + z_{t-2} \end{aligned} \tag{3.28}$$

After non stationary signal is transformed to stationary signal with the help of differentiation method, an ARMA model described by Equation (3.29)can be used in order to forecast the future points of the series. An integration to the same order of differentiation is performed over the forecasted variable in Equation (3.29) to get the future value of original

time series.

$$\Delta^d z_t = c + \phi_1 \Delta^d z_{t-1} + \cdots + \phi_p \Delta^d z_{t-p} + \varepsilon_t + \beta_1 + \cdots + \beta_q \varepsilon_{t-q} \tag{3.29}$$

3.5.7 Model Selection

Various time series models have been described in the previous subsection (3.5.3) - (3.5.6), the next step is concerned with the selection of appropriate model that can produce accurate forecast based on a description of historical pattern in the time series data and to determine the optimal model orders. The Box-Jenkins methodology does not assume any particular pattern in the historical data of the series to be forecasted. Rather, it uses a three step iterative approach to determine the best parsimonious model from a general class of ARIMA models as listed [61]:

- *Identification* consists of using the data and any other knowledge that will tentatively indicate whether the time series can be described with a moving average model, an autoregressive model, or a mixed autoregressive moving average model.
- *Estimation* consists of using the data to make inferences about the parameters that will be needed for the tentatively identified model and to estimate values of them.
- *Diagnostic* checking involves the examination of residuals from fitted models, which can result in either no indication of model inadequacy or model inadequacy, together with information on how the series may be better described.

Above three-step process is repeated several times until a satisfactory model is finally selected. Then this model can be used for forecasting future values of the time series.

A crucial step in an appropriate model selection is the determination of optimal model parameters. One criterion is that the sample autocorrelation function (ACF) and partial autocorrelation function (PACF), calculated from the training data should match with the corresponding theoretical or actual values [63]. These statistical indexes provide information regarding patterns in the time series. They are able to portray, in their respective

correlograms, the relationship that exists between the most recent points and the previous data of the series. But, sometime the identification of the time series model becomes more complicated when correlogram graphs follow unusual patterns and are tough to recognize. Other widely used approaches for model identification are Akaike Information Criterion (AIC) and Bayesian Information Criterion (BIC) [61].

3.5.7.1 Akaike Information Criteria (AIC)

Akaike information criteria (AIC) provides the model fit statistic related to the goodness of fit and parsimony. This criteria penalize the sum of squared residuals for including additional parameters in the model. The optimal model order is chosen by the number of model parameters which minimize the AIC value [61]. The definition of AIC is given by Equation (3.30)

$$AIC(p) = n \ln(\hat{\sigma}_a^2) + 2p \tag{3.30}$$

Here n is the number of observations used to fit the model, p is the number of parameters in the model and $\hat{\sigma}_a^2$ is the sum of the sample squared residuals.

3.5.7.2 Bayesian Information Criteria (BIC)

Bayesian Information Criteria (BIC) is almost similar to AIC except BIC imposes a greater penalty for the number of estimated model parameters [61]. This is because BIC is also a function of the sample size along with the residuals as can be seen in the Equation (3.31). Use of minimum BIC for model selection would always result in a chosen model whose number of parameter is no greater than that chosen under AIC.

$$BIC(p) = n \ln(\hat{\sigma}_a^2) + p \; ln(n) \tag{3.31}$$

Here n is the number of observations used to fit the model, p is the number of parameters in the model and $\hat{\sigma}_a^2$ is the sum of the sample squared residuals. The second term in the BIC definition puts additional weight to BIC value for use of higher number of observations.

3.5.8 Parameter Estimation and Forecasting

Once the best fit model is selected, parameters for the model is estimated in such manner that the sum of the squared residuals is minimized. This process is carried out by computer programs using the least square method and the parameters obtained are called estimated parameters. Autoregressive parameters $\phi's$ and moving average parameters $\beta's$ are identified with the fitting sample data for a selected model. The autoregressive model of order 2 with one degree of difference can be written as in Equation (3.32).

$$(1 - \phi_1 L - \phi_2 L^2)(1 - L)z_t = \varepsilon_t \tag{3.32}$$

where $L^m z_t = z_{t-m}$, ε_t is the white noise process, $(1 - L)z_t = z_t - z_{t-1}$ and ϕ_1, ϕ_2 are the parameters of the model. Parameters are estimated by minimizing the sum of square of errors solved in Equation (3.32). This is done by taking the derivatives of the sum of square of errors with respect to the parameters ϕ_1 and ϕ_2 and equated to zero in order to obtain the parameters of the model calculated as in Equations (3.33),(3.34) and (3.35). Parameter estimation follows similar procedure for any other order of models.

$$S(\phi_1, \phi_2) = \sum \varepsilon_t^2 \tag{3.33}$$

$$\frac{\partial S(\phi_1, \phi_2)}{\partial \phi_1} = 0 \tag{3.34}$$

$$\frac{\partial S(\phi_1, \phi_2)}{\partial \phi_2} = 0 \tag{3.35}$$

The forecast of time series for its future value use previous observations available upto the time t. $\hat{z}_t(l)$ denotes the forecast made at the origin point of the series t for future time $t + l$ and is representation for the series at lead time l. This forecast function $\hat{z}_t(l)$ provides the forecast at origin t for all the future lead time l depending upon the information of current and previous values z_t, z_{t-1}, z_{t-2}, z_{t-3}, $\cdots$ through time t. The Equation (3.32) can be rewritten to show the forecast procedure as

$$z_{t+l} = (1 + \phi_1)z_t + (\phi_2 - \phi_1)z_{t+l-1} - \phi_2 z_{t+l-3} + \varepsilon_t \tag{3.36}$$

The predicted values of the series z use the past value upto time t and the l lead time prediction are listed as

$$\begin{aligned}
\hat{z}_t(1) &= (1+\phi_1)z_t + (\phi_2 - \phi_1)z_{t-1} - \phi_2 z_{t-2} \\
\hat{z}_t(2) &= (1+\phi_1)\hat{z}_t(1) + (\phi_2 - \phi_1)z_t - \phi_2 z_{t-1} \\
&\quad . \quad . \quad . \quad . \quad . \quad . \quad . \\
&\quad . \quad . \quad . \quad . \quad . \quad . \quad . \\
\hat{z}_t(l) &= (1+\phi_1)\hat{z}(l-1) + (\phi_2 - \phi_1)\hat{z}(l-2) - \phi_2 \hat{z}(l-3)
\end{aligned} \tag{3.37}$$

The basic building of the time series model for forecasting are shown in Figure 3.15

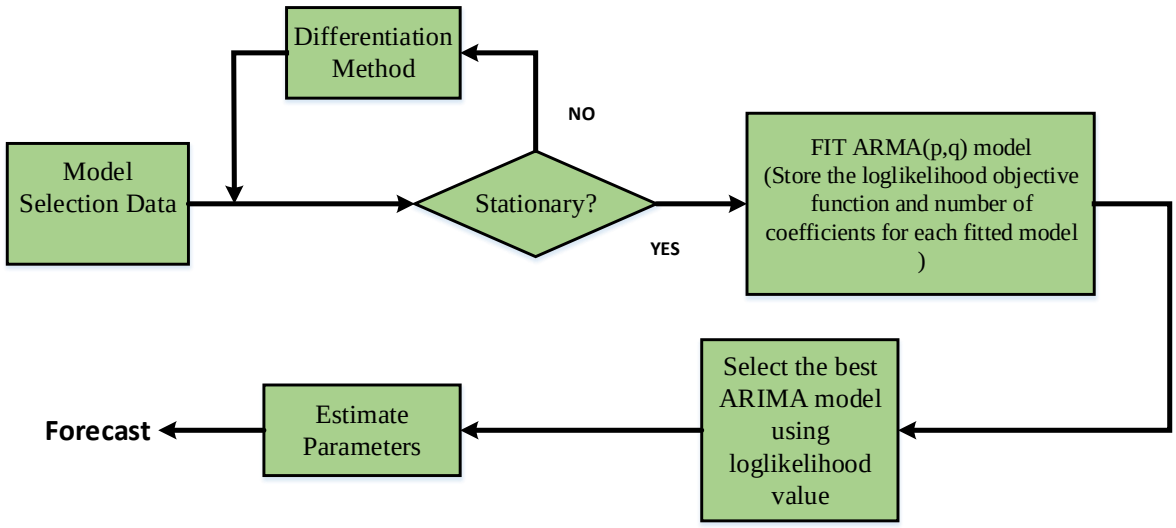

Figure 3.15: Time series model selection and forecasting

3.6 Summary

In this chapter, a brief introduction to the phasor measurement unit along with its architecture and reporting rates was presented. Optimal PMU location studies for the WSCC 9 bus system were carried out using integer quadratic programming. The results for the

optimal PMU location during normal operating conditions with and without measurement redundancy are presented in Table 3.2. Out-of-step analysis using WAMS was discussed and the proposed transient stability prediction method based on the swing of the coherent group using the synchronized measurement was presented. Coherency analysis of the generators in the WSCC 9 bus system was also presented for a three-phase fault at bus 7 for both stable and unstable cases, and the coherency determined within 100 ms. Time series analysis, time series models, and model selection criteria were presented, and used for time series prediction to determine the stability of a system in advance. The ARI model does a differentiation of non-stationary data instead of just modelling as AR process, and best suits the continuously increasing nature of the variables discussed. Reference [64] also discusses a method for predicting the outcome of evolving transient behavior in power systems through adaptive time series coefficients using an auto-regressive integrated model.

After the initiation of a power swing, an auto-regressive model is fitted to the generator power angle and the outcome of that swing predicted for future intervals. The Bayesian information criterion was selected as the model selection tool because it introduces a penalty factor for more parameters. The selected model provides the best fit with a smaller number of parameters and reduces the computational complexity. In the next chapter (chapter 4), a stability analysis is carried out for the WSCC 9 bus system using the proposed method. Time series model selection is studied for stable and unstable swings. Prediction of the angular swing between the coherent groups is derived for different disturbance conditions in the test system and compared with the rate of change of impedance-based scheme (blinder-based scheme).

Chapter 4

Synchrophasor based Out-of-Step Analysis in Multi-Machine Power Systems

4.1 Introduction

The standard practices for out-of-step protection are often implemented in conjunction with the logic used for distance relays, and selective tripping is done to distinguish faults with out-of-step conditions. However, sometimes the tripping might take place at locations that can initiate an unwanted outage of other lines or generators in the system [17]. Application of the conventional blinder method in a large power system requires rigorous transient stability studies with many possible stressed operating conditions; determination of the optimal location for the out-of-step relay is another substantial challenge.

The wide area measurements provide synchronized measurements at critical locations and make it easier to determine the swing trajectories. This is due to the higher reporting rates now available for PMUs (120 Hz in GE N60 [15]), which are capable of capturing the power system steady-state and dynamic behaviors in detail. Implementation of prediction schemes for out-of-step conditions is possible using time-tagged wide area measurements during severe but rare contingencies that cause angular instability between generation stations and the rest of the system. These schemes provide a visualization of phase differences between substations, can predict system stability conditions before the actual out-of-step condition, and allow intended islanding at predetermined locations.

In this chapter, the synchrophasor-based method is implemented in the WSCC 9 bus system and compared with the traditional blinder-based method. The separation of machines

is found by real-time coherency analysis. Each group is represented by an equivalent machine, thereby reducing the two groups of machines into a simple two-machine system. The inertia of the equivalent machines is equal to the respective sum of inertias of all machines in the group, and the angle is equal to the center of angle (COA) of all machines in the group. The proposed method is used to forecast the difference of COAs to predict the instability in the large system.

4.2 Synchrophasor based Swing Prediction using PMU model in Real Time Digital Simulator

4.2.1 Brief Hardware and Software Description

In the research, RTDS^{TM}, the network interface card in RTDS called Giga Transceiver Network Interface Card (GTNET) and Giga Transceiver Synchronization Card (GTSYNC) are used to simulate the power system. A brief introduction to each of them is provided in Sections 4.2.1.1, 4.2.1.2 and 4.2.1.3.

4.2.1.1 RTDS^{TM}/RSCAD^{TM}

RTDS^{TM} is a fully digital power system simulator which is capable of performing electromagnetic simulation in real time. The simulation is done in a fixed simulation time step of 50 μs using a combination of advanced computer hardware and custom software [65], [66]. The main components associated with the simulator are Workstation Interface Cards (GTWIF and WIF), GIGA Processor Card (GPC), PB5 Processor Card (PB5) and a user friendly software RSCAD^{TM}. The simulator hardwares are assembled in a modular unit called a rack. Each rack is provided with processing units such as GPC or PB5 and communication units. The workstation interface card in a rack is a backplane mounted to facilitate computer workstation communication, multi-rack case synchronization, inter-rack data communication paths, backplane communication and rack diagnostic. Both GPC and PB5 cards are used to solve the equations representing the power system and control system components mod-

elled within the RTDS^{TM}. One processor on a GPC/PB5 card within an RTDS^{TM} rack is mainly dedicated to power system network solution. Similarly, one processor on a GPC/PB5 card within a rack is generally assigned to handle the control system components within the RTDS^{TM}. These processors can also be used to for small time-step calculation for power electronics and to connection to the Giga Input/Output (GT I/O) Cards. PB5 is the latest processing card developed by the RTDS^{TM} Inc. with two processors running at 1.7 GHz whereas GPC card consists of two processor running at 1 GHz. More than one GPC/PB5 can be used to compute other power system components in parallel.

Each GPC card consists of the following major components [55],

- Two IBM PPC750GX PowerPC processors
- Core frequency: 1 GHz
- Floating Point computation rate: 1.0 GFLOPs
- Floating Point Numeric Format: IEEE-754 64 bit
- L1 Cache: 32 Kilobyte instruction, 32 Kilobyte data
- L2 Cahce: 1.0 Megabyte
- On-Chip Memory: 2 Megabit static ram

Each PB5 card consists of the following major components [55],

- Two Freescale PowerPC MPC7448 processors
- Core frequency: 1.7 GHz
- Floating Point computation rate: 3.4 GFLOPs
- Floating Point Numeric Format: IEEE-754 64 bit
- L1 Cache: 32 Kilobyte instruction, 32 Kilobyte data

- L2 Cahce: 1.0 Megabyte

RSCAD^{TM} is a graphical user interface of RTDS^{TM} hardware. It consists of two sections: Draft and Runtime. In the draft section, circuits are built with custom power system and control components, parameters of the components are entered and the processor for the components is assigned. The runtime section is used to control the hardware. The control actions, such as starting and stopping simulation, applying disturbance, closing and opening of breakers, etc., are done in runtime section. RSCAD^{TM} communicates with the RTDS^{TM} hardware through either 10 Mbit/s or 100 Mbit/s ethernet connection. GTWIF works as a communication interface between RSCAD^{TM} and RTDS^{TM} processors.

4.2.1.2 GTNET Card

The GTNET card provides a real time communication link to and from the simulator via Ethernet. This card is used to interface a number of network protocols with RTDS^{TM} simulator [55]. The protocols supported by the GTNET are listed below.

- GSE: IEC 61850 GOOSE/GSSE
- SV: IEC 61850 Sampled Values
- DNP3: Distributed Network Protocol
- PLAYBACK: Playback of large data sets
- PMU: IEEE C37.118 datastream output

Among the above available protocols, GTNET-PMU protocal in the card is used to provide the synchrophasor output datastream from the location of interest in modelled power system (WSCC 9 bus system). A single GTNET-PMU model available in the RSCAD^{TM} draft provide output for upto 8 PMU's with symmetric component information related to 3-phase sets of voltage and current using UDP or TCP connections. The GTNET-PMU component output is synchronized to an external 1 PPS, IRIG-B or IEEE 1588 signal via the GTSYNC card described in the section 4.2.1.3 .

4.2.1.3 GTSYNC Card

The GTSYNC card is used to synchronize the RTDS^{TM} simulation timestep to an external time reference (GPS) and to synchronize the device under test. It ensures that the RTDS^{TM} time-step clock remains locked to the reference time signal provided as input to the GTSYNC card.The GTSYNC uses either IEEE 1588 PTP, 1 PPS, or IRIGB unmodulated signals as the synchronization source. In the research, IRIG-B unmodulated signal has been used as synchronizing timing signal from SEL-2407 GPS clock. Figure 4.1 shows the setup of RTDS^{TM} components to provide synchronized datastream from PMU modules in GTNET.

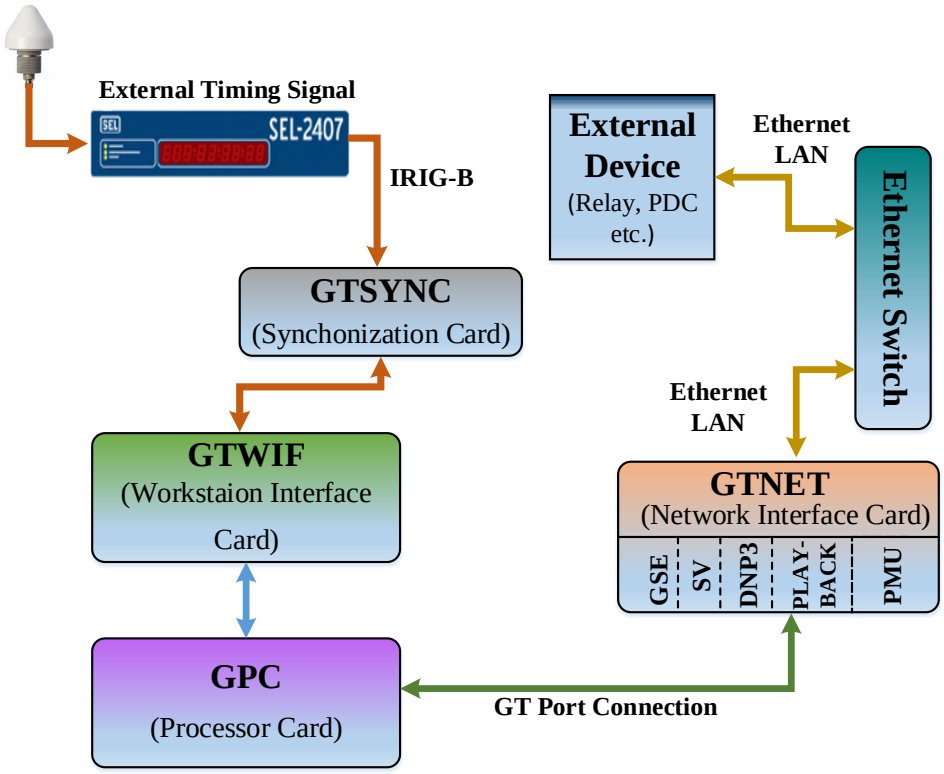

Figure 4.1: Connection of a external protection device to RTDS using GTNET

4.2.1.4 OpenPDC and Matlab

The OpenPDC is a complete set of applications to handle the processing of time series data in real time. The OpenPDC supports the IEEE 37.118 protocol and can be used to

recieve and archive phasor data from PMUs. In the research, the synchrophasor information from the optimal bus locations are managed by the OpenPDC application and stored in the Phasor Data Concentrator (PDC). Matlab is numerical computing platform developed by Mathworks. It includes multiple toolboxes to facilitate numerical calculation related to different application areas. All the analysis including the time series modelling and forecasting is carried out in Matlab.

4.2.2 Case Studies: WSCC 9 bus system

The test system WSCC 9-bus system is simulated in RTDS. Simplified one-line diagram of the test system is shown in Figure 3.4 and the system data are shown in Appendix A. Three phase fault is applied at different buses and the center of transmission lines in the system and the stability of the system is predicted using proposed method based on time series swing curve prediction. The flow chart for detecting the stability condition is shown in Figure 4.2 .

4.2.3 Testing Methodology

Figure 4.3 shows the conceptual view and hardware setup for the proposed OST prediction method. Phasor measurement units are placed at strategic locations in the power system. The synchronized phasor measurements of voltage and current along with time-stamp are sent to a phasor data concentrator supposed to be placed at the central control center. Phasor data concentrator gathers and aligns the time-tagged phasor information from the different PMUs using the application like OpenPDC and make it available to the computer for analysis. The computer program is used to calculate the generator bus voltage with the current and voltage phasors from the PMU bus and the transformer impedance. As soon as the generator bus voltage angles (measured from the initial post fault value) deviates from the reference generator bus voltage angle beyond a certain value (5 degrees were used for the studies), the associated machines are assumed to separate from the reference generator. The reference generator chosen in this study is the generator 1 connected at bus 1. When

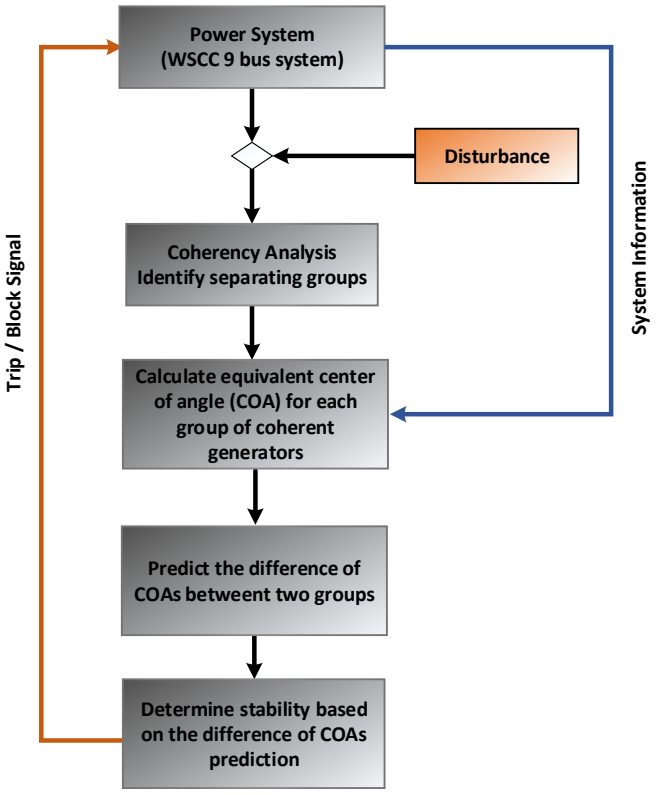

Figure 4.2: Wide area base out-of-step prediction flowchart

the generators separate from the reference generator, equivalent process to find the COAs for two coherent group is carried out. In the same time interval, the difference of COAs (dCOA) is also calculated. Then after computer programming tool is used to run the time series prediction method to forecast 40 points in the future for the difference of COAs. With this prediction, the tripping decision is evaluated to assess the nature of COA's swing curve. The weak lines through which the system separates can be found using either past data or from online simulation studies, and the system can be separated at those lines. If instability is determined, separation can be initiated on those lines by sending a signal to out-of-step relay. On the other hand, if the swing is found to be stable the unnecessary tripping can be avoided by sending a blocking signal to those lines. The study on forming islands of the power system after instability detection is out of scope of this research and hence is not discussed in detail.

The proposed protection scheme predicts the stability of system on the basis of predicted

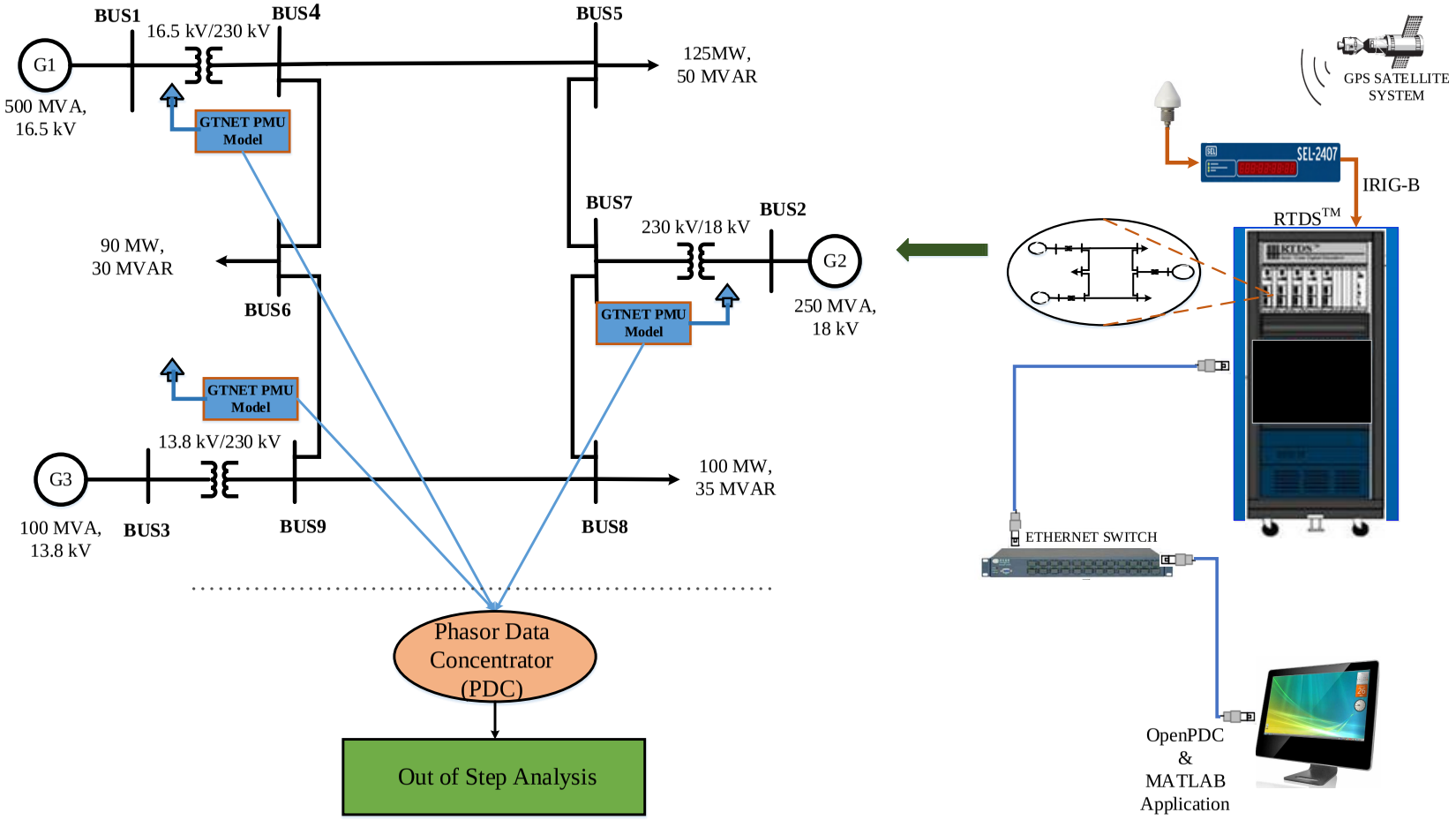

Figure 4.3: Test setup for the time series based swing curve prediction using the PMU model in RTDS™

values of dCOA. The time series modelling, explained in the previous chapter's Section 3.4.3.1 is used for forecasting the difference of COAs. During the implementation of the proposed scheme on out-of-step protection, some considerations are necessarily put forward for time series analysis and decision making. These assumptions and the decisions made for determining the instability are listed below.

- No OST relay action for the first 10 cycles after system separates in coherent group.
- Relays algorithm forecast 40 points in future using the appropriate time series model and it is done for the difference of center of angle (dCOA).
- After the prediction is made, the relay waits for the next set of measurements to arrive and it deletes the first point of the previous sequence of data in every other prediction in order to forecast the following points. 20 samples and then 30 samples for reliable model parameter estimation.
- If the tripping decision is met in three consecutive prediction, an OST condition would be declared and protection action should be initiated. When three consecutive prediction values are below zero crossing, it is declared as a stable condition.

4.2.4 Model Selection and Forecasting

Model selection is important to find the model which provide the best fit to the behaviour of observed dCOA. Among the two model identification techniques AIC and BIC, BIC is not only the measure to rank the fitness of model on the basis of observed data but also check and penalize for the free parameters more strongly introduced in the model. The goodness-of-fit with minimum model order is the fundamental principles of model selection which is obtained by using BIC [62]. Their ability to select the correct model form and produce accurate parameter estimates for the forecast is essential in determining the best model. After the disturbance in power system, the angular separation between generator and reference may increase monotonously, oscillate or oscillate with damping [64].

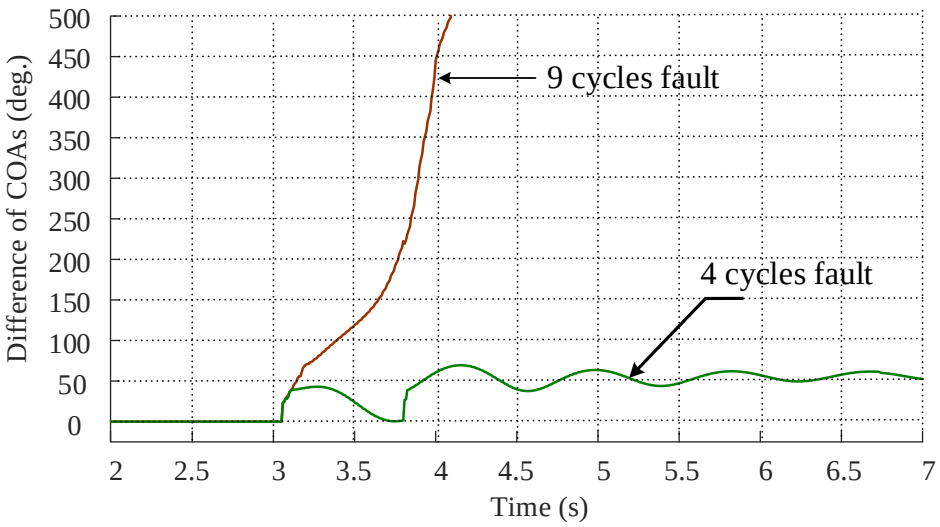

Figure 4.4: Coherent groups angular separation for 4 and 9 cycles fault at bus 7

Figure 4.4 shows the dCOA response for the fault of 4 and 9 cycles at bus 7 in the test system. For the fault of 4 cycle the angular separation between coherent groups oscillates with damping resulting in stable condition. But for the fault of 9 cycles the angular separation increase monotonously to make system unstable. Therefore, Autoregressive models of different orders are tested for the prediction algorithm and the two cases are presented in the Table 4.1. In these cases, a differentiation process of order one is also applied to the collection of data points. The 120 samples of data after coherency is used to calculate the best fit.

Depending upon the characteristics of swing, the highest order model used for model selection is ARIMA(3,1,0). The test cases show that the best fit model for the stable case is ARIMA(2,1,0) and for the unstable case is ARIMA(3,1,0). Between these two models, a comparative selection is performed for a fault scenario at bus 5. Figure 4.5 and Figure 4.6 show the prediction of the protection scheme using an ARIMA(2,1,0) and ARIMA(3,1,0) respectively for a stable condition. The triangular shape points indicates the 20 sample observation window of data used to estimate the time series model parameters. The pentagon shape points are the 40 forecasted values for the dCOA.

Similarly, the prediction of the protection scheme for the unstable condition is performed

Table 4.1: Model selection using BIC

Fault location	Fault dur. (*cycles*)	Decision	ARIMA (p,D,q) Model	BIC value
Bus 5	6	Stable	AR(1)	578.1320
			ARIMA(1,1,0)	569.6117
			ARIMA(2,1,0)	547.1285
			ARIMA(3,1,0)	550.3238
	13	Unstable	AR(1)	683.3347
			ARIMA(1,1,0)	636.4493
			ARIMA(2,1,0)	631.8222
			ARIMA(3,1,0)	560.2741
Bus 9	6	Stable	AR(1)	570.8062
			ARIMA(1,1,0)	560.1348
			ARIMA(2,1,0)	531.6387
			ARIMA(3,1,0)	536.1942
	11	Unstable	AR(1)	693.7625
			ARIMA(1,1,0)	636.7355
			ARIMA(2,1,0)	634.9531
			ARIMA(3,1,0)	589.2192

and showin in Figure 4.7 and Figure 4.8.

The arima model of order ARIMA(2,1,0) seems to have better performance in emulating the future characteristics of the angular data. ARIMA(2,1,0) model is the best prediction model for this power system considering the fact that the prediction results by ARIMA(3,1,0) model is not significantly improved. Also the higher order time series model for prediction mechanism can have more complexity of calculation in parameter estimation and can be avoided in case of insignificant improvement in forecasting outcomes.

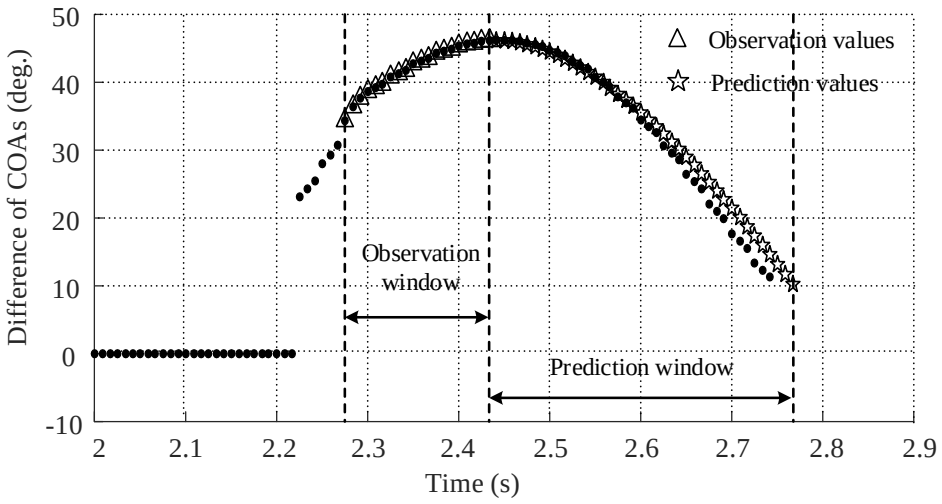

Figure 4.5: ARIMA(2,1,0) stable case

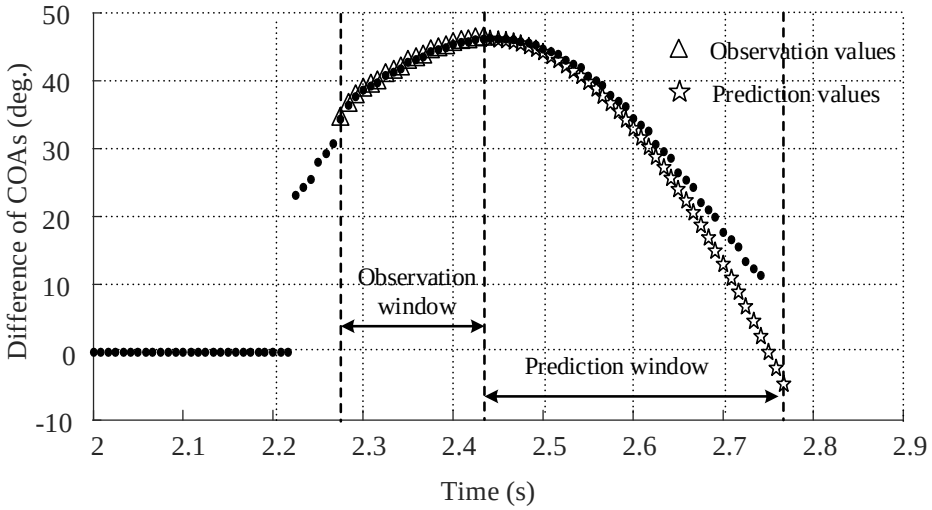

Figure 4.6: ARIMA(3,1,0) stable case

4.2.5 Test Cases: Synchrophasor Based Out-of-Step Prediction

This section presents the test results for 2 cases, each for stable and unstable scenario. A three phase fault is applied at bus 5 for the first case and at bus 6 for the second case. The fault durations are varied to find stable and unstable cases. For the fault at bus 5, the fault is applied at 2.1420 s and is cleared after 6 cycles (0.1 s). The voltage angle swing

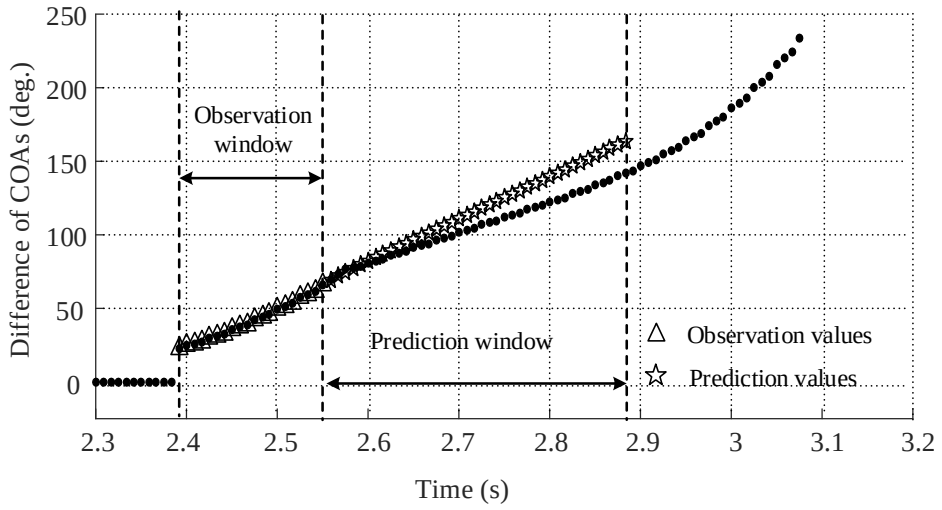

Figure 4.7: ARIMA(2,1,0) unstable case

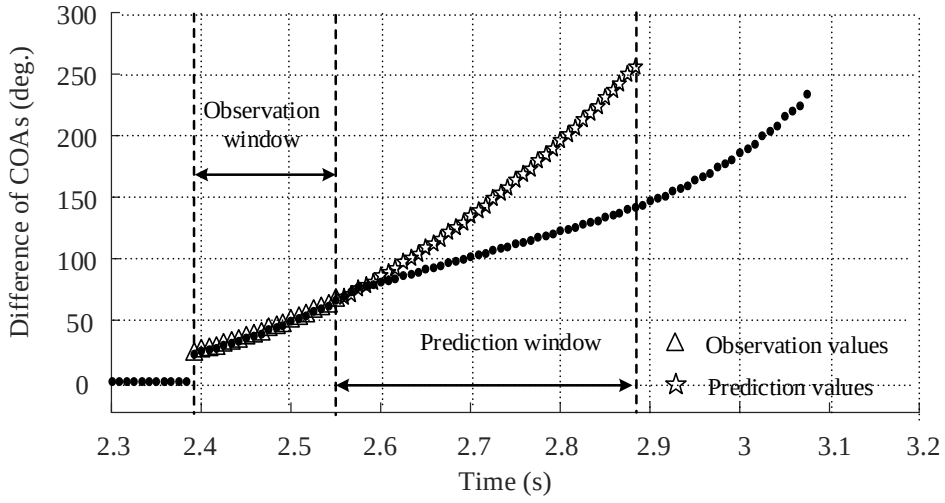

Figure 4.8: ARIMA(3,1,0) unstable case

observed at different generator buses with respect to the reference generator bus are shown in Figure 4.9.

The coherency is declared at 2.2250 s where machine 2 and 3 separate out from the reference machine. At this point, calculations are carried out to find center of angle (COA) of each coherent groups. The difference of COAs (dCOA) is predicted with the previously calculated samples of dCOA, enough to form the observation window of 20 samples after the coherency

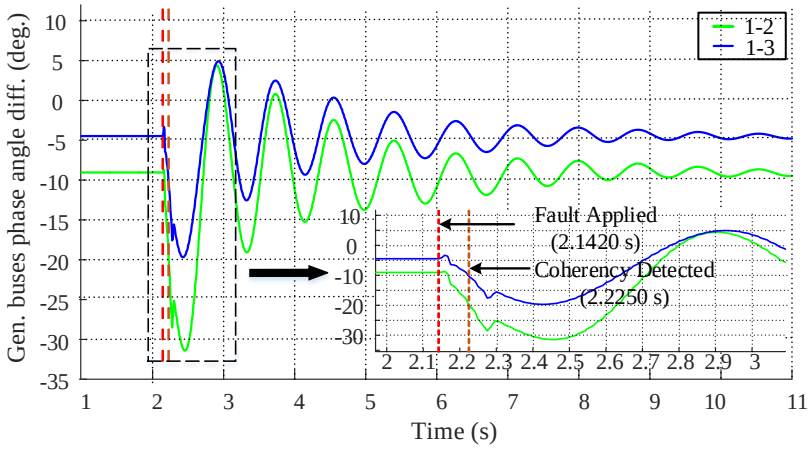

Figure 4.9: Generator bus voltage angles with respect to reference generator bus for the fault at bus 5 and fault cleared after 6 cycles

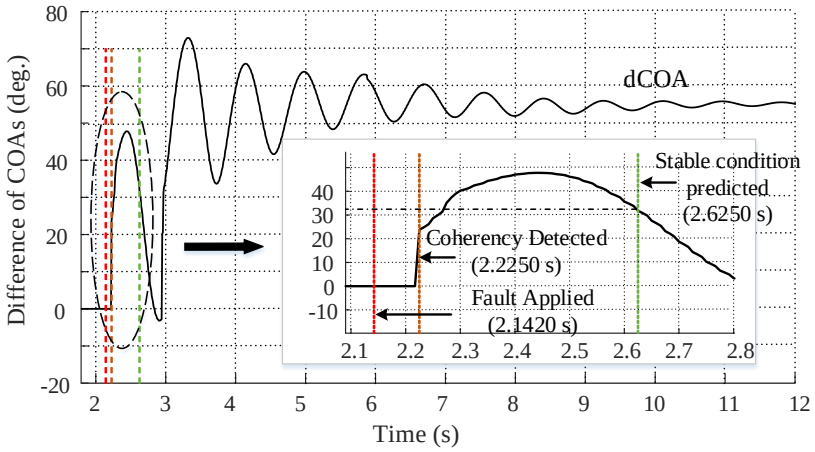

Figure 4.10: Difference of COAs for the fault at bus 5 and fault cleared after 6 cycles

is declared. Figure 4.10 shows dCOA with the instance of fault application, coherency detection and stable condition prediction.

The three consecutive prediction using each of 30 samples observation window that meet the zero crossing to satisfy the stable condition criteria for the proposed method is shown in Figure 4.13. The stable condition was predicted at 2.6250 s and the angular separation between the coherent groups at the instance is 31.7956 degrees.

Now the fault duration is increased to 13 cycles (0.2166 s) for the fault at bus 5. The angular separation of the generator bus angles with respect to the reference generator bus angle is shown in Figure 4.11.

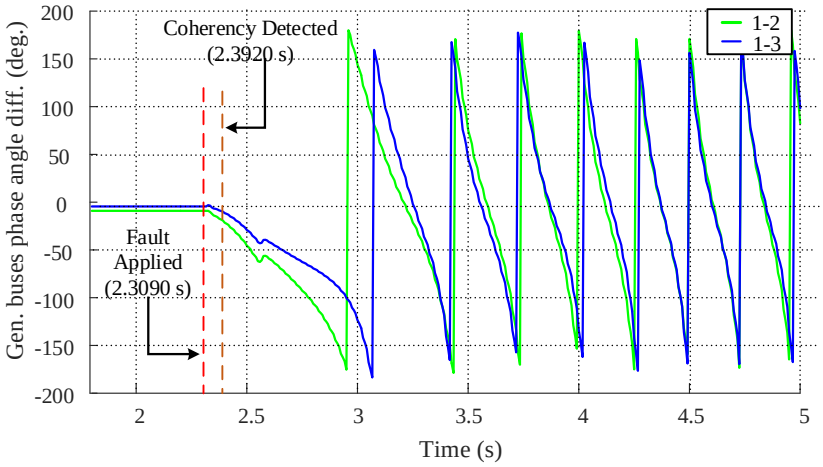

Figure 4.11: Generator bus voltage angles with respect to reference generator bus for the fault at bus 5 and fault cleared after 13 cycles

All the other generator bus voltage angles deviate from the reference bus post the fault applied at 2.3090 s. The separation beyond 5 degrees is detected at 2.3920 s and the COA calculation is started.

The difference of COAs is predicted with the previously calculated samples of dCOA after the coherency is declared. Figure 4.12 shows dCOA with the instance of fault application, coherency detection and unstable condition prediction. Since the three consecutive prediction of difference of COAs has crossed the 180 degrees, the system becomes unstable. The last three observation window and prediction window used to declare the unstable condition is shown in Figure 4.14. The unstable condition was predicted at 2.5920 s well ahead of actual out-of-step condition at 2.9910 s and the angular separation between the coherent groups at that instance is 80.4964 degrees.

A similar study is performed with the three phase fault applied at bus 6 which is cleared after 7 cycles (0.1166 s). The voltage angle swing, observed at different generator buses

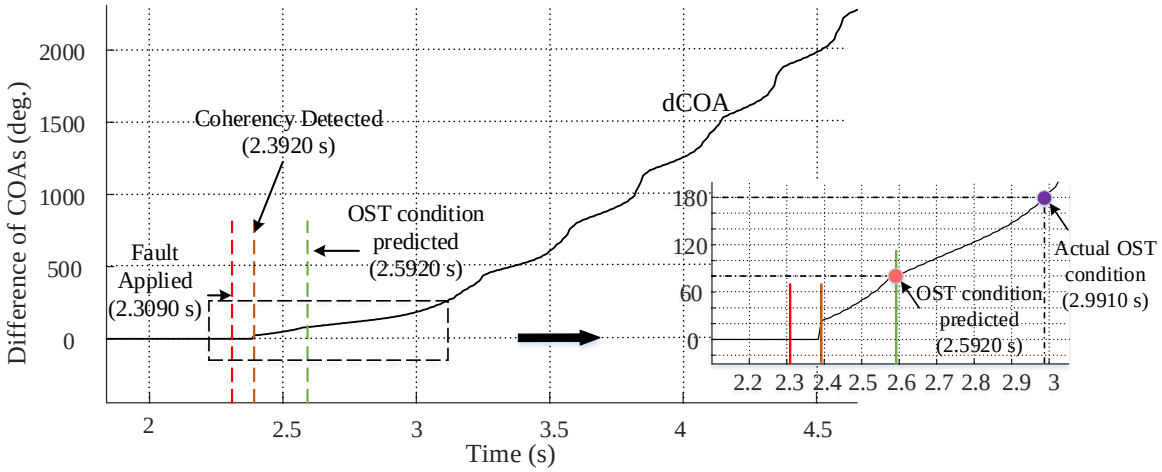

Figure 4.12: Difference of COAs for the fault at bus 5 and fault cleared after 13 cycles

with respect to the reference generator bus, is shown in Figure 4.15. At 2.6409 s, 0.08300 s after fault, machine 1 and 2 separate beyond 5 degrees from the reference machine. At this instance, relay calculates center of angle of each group. The relay predicted the difference of COAs once enough samples for observation window is available. Then the relay continues to perform prediction with arrival of each new sample. Figure 4.16 shows dCOA with the instance of fault application, coherency detection and stable condition prediction. The three consecutive prediction using each of 30 samples observation window that meet the zero crossing to satisfy the stable condition criteria is shown in Figure 4.19. The stable condition was predicted at 3.1409 s and the angular separation between the coherent groups at the instance is 23.6064 degrees.

For the same bus fault, fault duration is increased to 16 cycles (0.2666 s). The plot of generator bus voltage angles for this fault is shown in Figure 4.17.

The difference of COAs with the instance of fault application, coherency detection and unstable condition prediction is shown in Figure 4.18 and the calculations are discussed earlier. Since the three consecutive predictions over reach 180 degrees as shown in Figure 4.20, the system is detected to be unstable and the time of detection is 0.3160 s after the fault well ahead of actual out-of-step condition at 0.7249 s and the angular separation between the coherent groups at that instance is 84.1365 degrees. Using a similar procedure, system

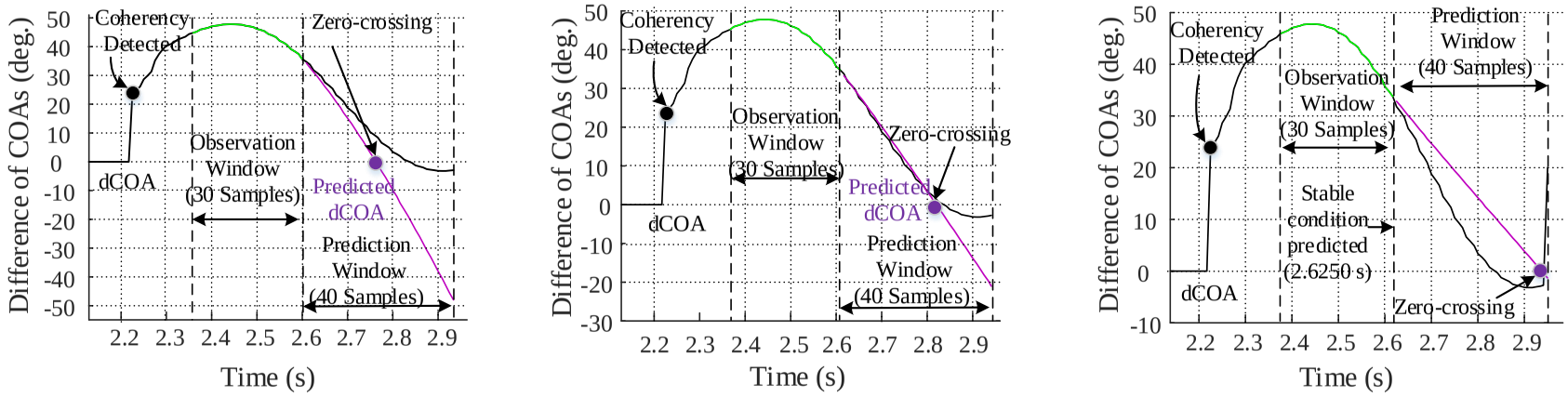

(a) First prediction

(b) Second prediction

(c) Third predicition

Figure 4.13: Three consecutive prediction before stable condition is declared for 6 cycles fault at bus 5

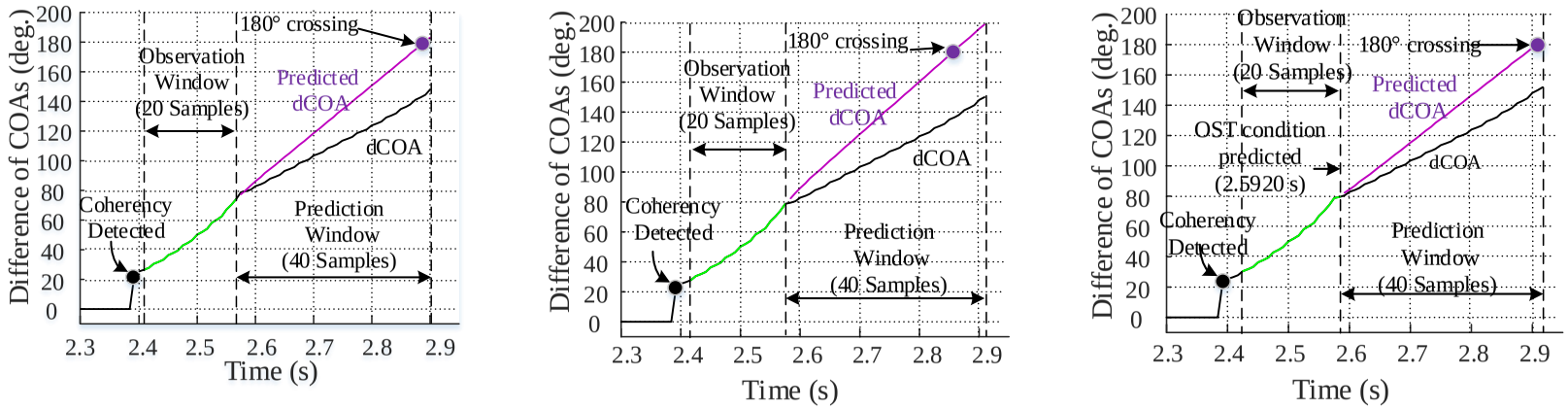

(a) First prediction

(b) Second prediction

(c) Third predicition

Figure 4.14: Three consecutive prediction before unstable condition is declared for 13 cycles fault at bus 5

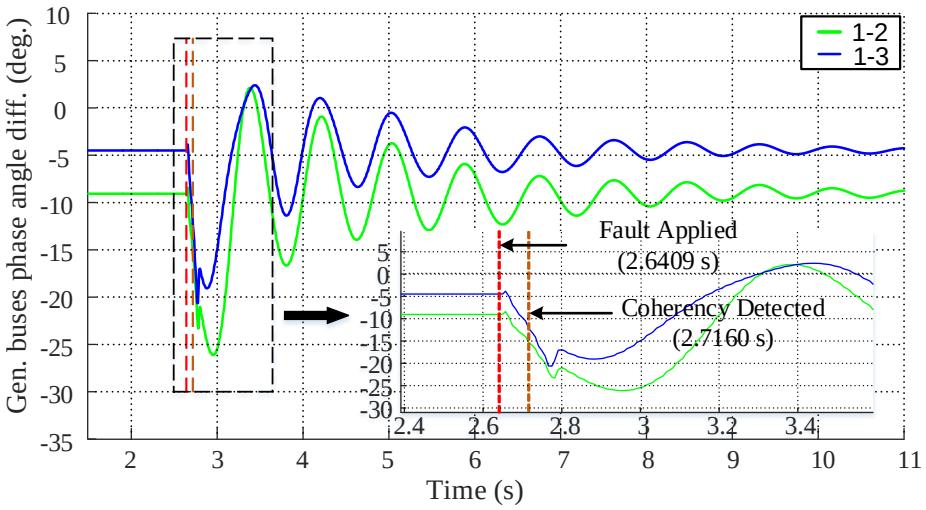

Figure 4.15: Generator bus voltage angles with respect to reference generator bus for the fault at bus 6 and fault cleared after 7 cycles

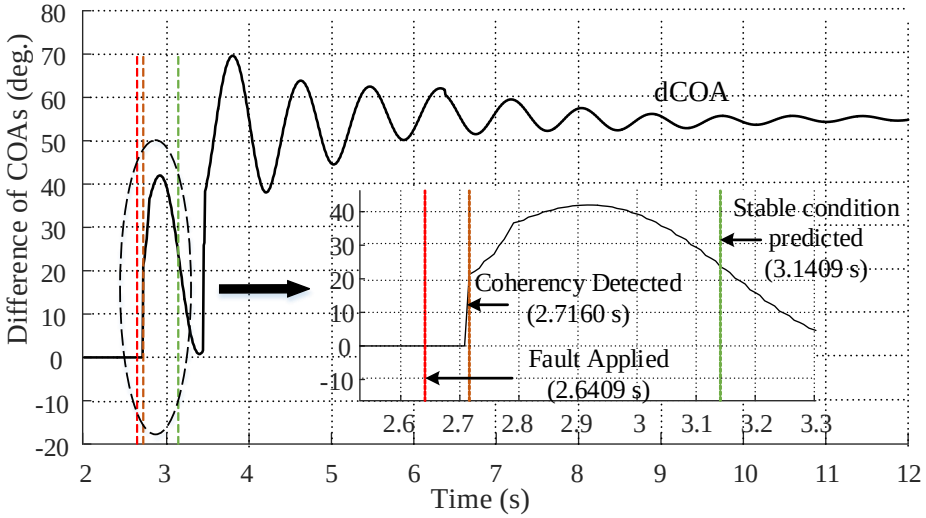

Figure 4.16: Difference of COAs for the fault at bus 6 and fault cleared after 7 cycles

stability is predicted for the fault at different buses and line locations. A summary of those cases are presented in Table 4.2.

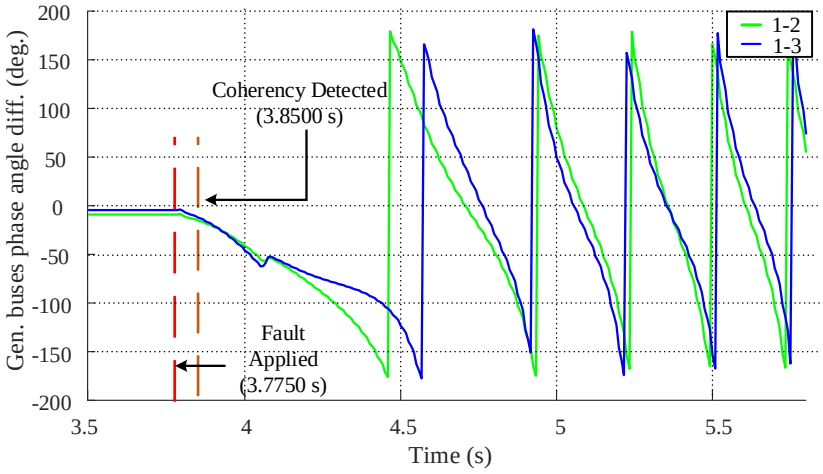

Figure 4.17: Generator bus voltage angles with respect to reference generator bus for the fault at bus 6 and fault cleared after 16 cycles

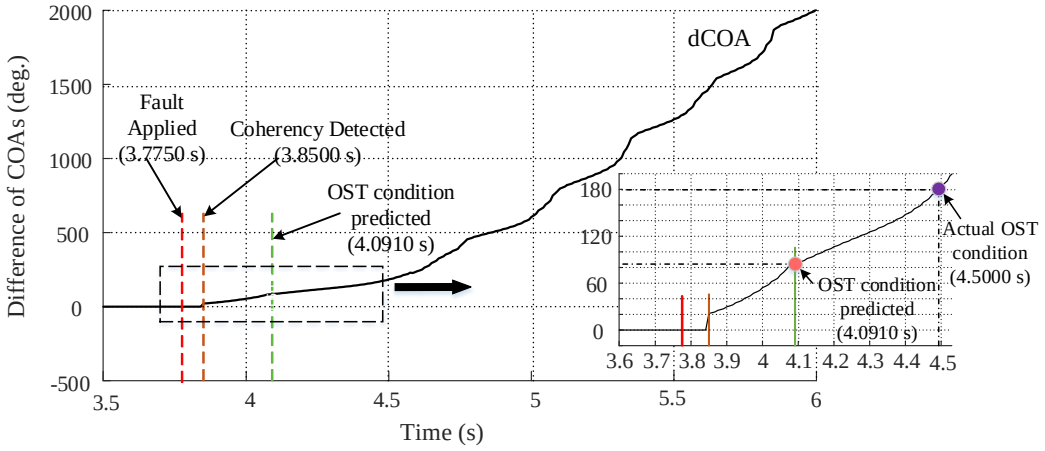

Figure 4.18: Difference of COAs for the fault at bus 6 and fault cleared after 16 cycles

4.3 Generator Pole Slipping During Transients

After severe disturbance, coherent group of generators swing together. Rotor angle of the generator is used to determine the generator coherency [33] as it provides the initial information about the swing. The use of rotor angle for the the selective tripping of unstable generators for transmission line has been applied extensively to improve stability. When a power system is unstable, identification of coherent group of generators and then pole slip-

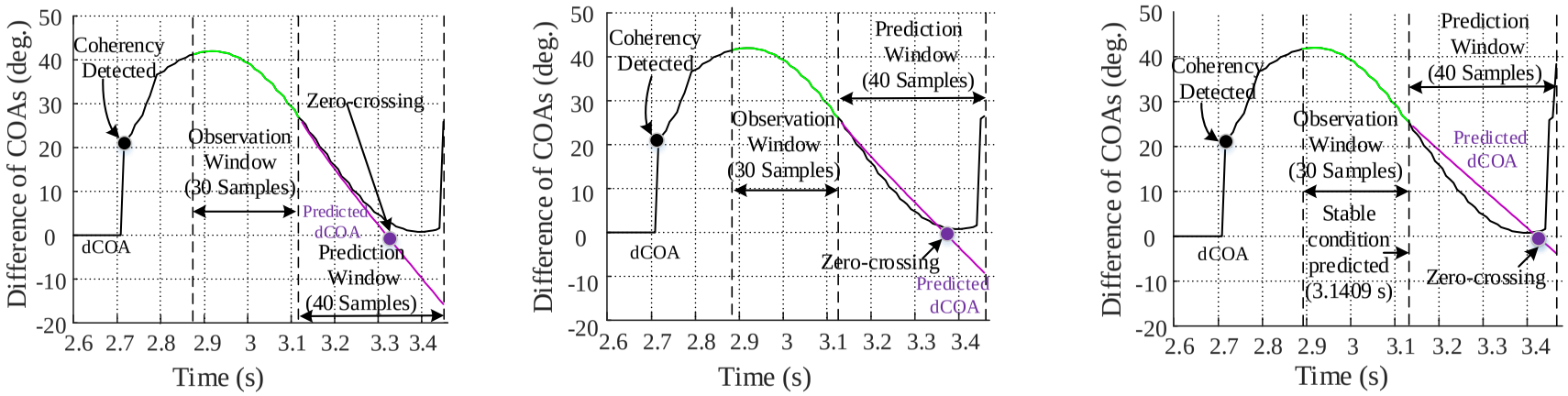

(a) First prediction

(b) Second prediction

(c) Third predicition

Figure 4.19: Three consecutive prediction before stable condition is declared for 6 cycles fault at bus 5

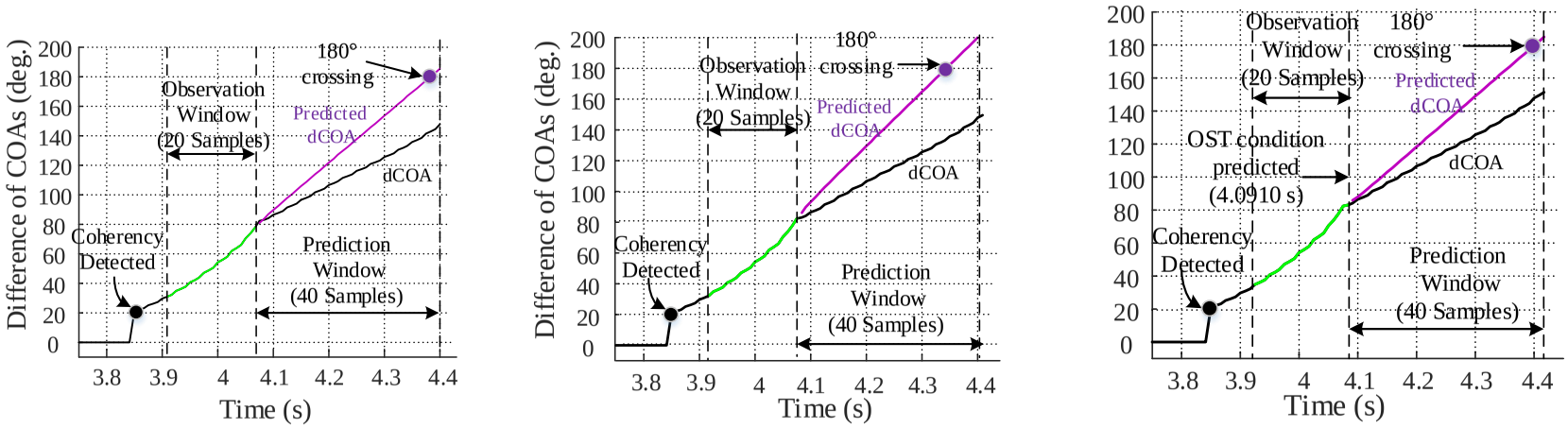

(a) First prediction

(b) Second prediction

(c) Third predicition

Figure 4.20: Three consecutive prediction before unstable condition is declared for 16 cycles fault at bus 6

Table 4.2: Test results of instability prediction using swing curve

Fault Location	Fault dur. (*cycles*)	Coherency detected after fault (s)	Time of prediction (s)	Decision	dCOA (deg.)	Actual OST time (s)
Bus 5	6	0.0829	0.4829	Stable	31.7957	
	13	0.0830	0.2829	Unstable	80.4965	0.6820
Bus 6	7	0.0750	0.5000	Stable	23.6064	
	16	0.0749	0.3160	Unstable	84.1365	0.7249
Bus 8	6	0.0429	0.5090	Stable	30.6397	
	11	0.0500	0.6250	Unstable	137.7929	0.7669
Bus 9	6	0.0410	0.5160	Stable	28.0718	
	11	0.0410	0.3909	Unstable	104.8163	0.6909
Center of line 4-5	7	0.0750	0.5000	Stable	40.9702	
	12	0.0749	0.3750	Unstable	104.8163	0.7499
Center of line 6-9	6	0.0579	0.5079	Stable	24.1207	
	15	0.0670	0.4250	Unstable	104.9575	0.7500
Center of line 8-9	6	0.0329	0.5079	Stable	28.0746	
	12	0.0419	0.3499	Unstable	98.0711	0.6749

ping of the generators in a group against other group is necessary to make the intelligent control strategy. After the unstable condition is predicted, it is possible to trip OST relay at the transmission line forming the electric island with generation and load balance in order to mitigate potential transient instabilities. Two fault case in WSCC 9 bus system is presented to show the pole slipping of generators after the disturbance that makes system unstable.

Figure 4.21 show the rotor angle for 3 generators in WSCC 9 bus system during fault at bus 5. Fault was applied for 13 cycles at 2.3090 s and coherency was determined at 2.3920 s. The coherency analysis determines that generator 2 and 3 forms a coherent group B against generator 1 in coherent group A. The proposed algorithm predicts the OST condition at 2.7 s where the actual OST condition happens between the groups at 2.9910 s. In this case the

generator 2 was found to have early pole slip with reference generator 1 at 2.9420 s followed by generator 3 at 3.1 s. The action that should be applied is requires to trip OST relay in appropriate location to separate the coherent groups of generator.

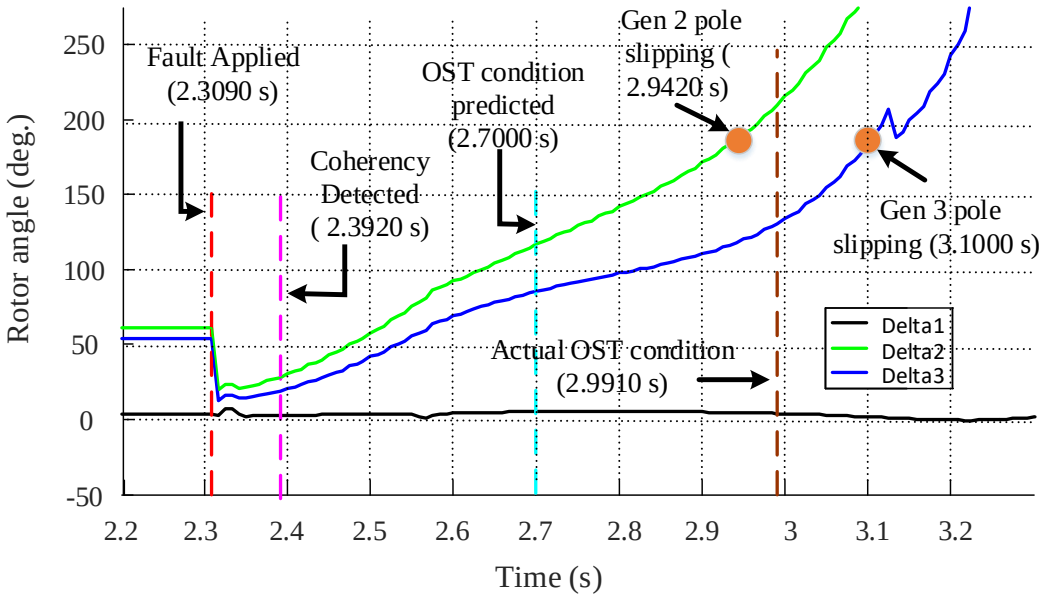

Figure 4.21: WSCC 9 bus generators pole slipping for 13 cycles fault at bus 5

One more case was studied for the fault applied to bus 9 with duration of 11 cycles. Fault to the bus was applied at 2.1089 s and the algorithm was able to determine the coherency at 2.1499 s. The coherency analysis determines that generator 2 and 3 forms a coherent group B against generator 1 in coherent group A. The proposed algorithm predicts the OST condition at 2.6249 s where the actual OST condition happens between the groups at 2.7999 s. The generator 2 in coherent group B was found to have early pole slip with reference generator 1 at 2.7660 s followed by generator 3 at 2.9000 s. The appropriate action is to form the island with generation and load balance since tripping of generators causes the system frequency to drop due to generation-load imbalance.

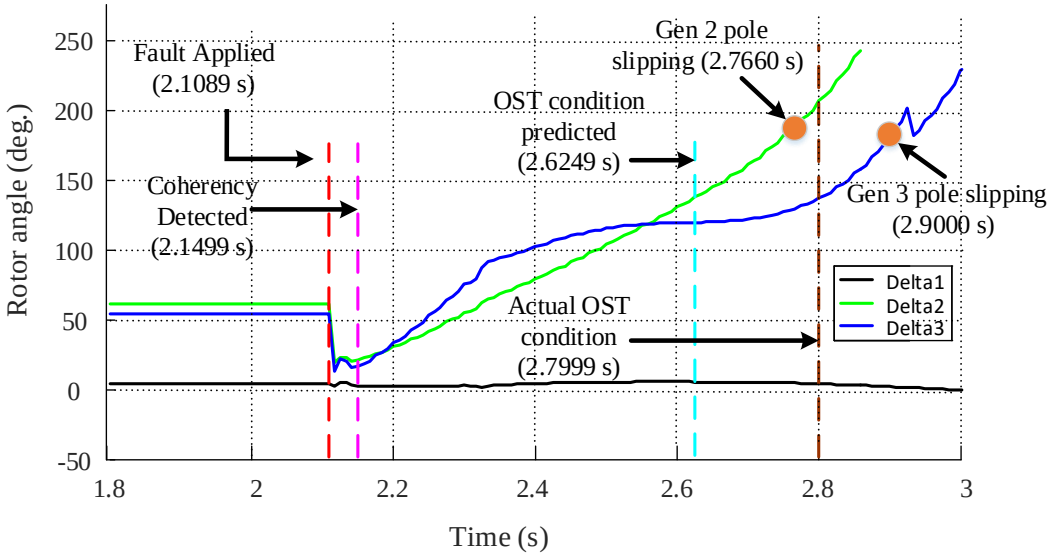

Figure 4.22: WSCC 9 bus generators pole slipping for 11 cycles fault at bus 9

4.4 Swing Locus in Complex System

In large interconnected system, determination of location for the power swing relay can be difficult. Stability studies are carried out to find the location of the critical points in the power system and to measure the stability margin [6]. Sometime, historical data is used to determine the location of separation during disturbances. Impedence-based setting method is suitable for most applications where there are not significant changes in the source and transfer impedances [16]. Reference [6] [67] explains the power swing elements using known system parameters. Reference [67] explains three different methods to find whether the swing locus traverse a particular transmission line during loss of synchronism by reducing the complex system, excluding the line of interest, to a two-source equivalent system as shown in Figure C.1. The method based on forming a matrix having elements of drivingpoint and transfer impedance of the original network is used in the research to determine the parameters of two-source equivalent system. A brief explanation on the procedure along with the determination of power swing in multimachine system is given in Appendix C.

This method is implemented in WSCC 9-bus system to find the transmission lines through which the swing passes. The results are summarized in the Table 4.3. The analysis of the

swing shows that the swing passes through the tramsmission line L75 and L96 as shown in Figure 4.23.

Table 4.3: Determination of swing locus in WSCC 9-bus system

Line	Line impedance (pu)	Point at which line intersected by swing locus (pu)	Swing locus intersect line
L45	0.0855∠83.29°	0.1859∠83.46°	No
L46	0.0935∠79.53°	0.2201∠81.47°	No
L75	0.1641∠78.75°	0.1256∠80.72°	Yes
L96	0.1744∠77.08°	0.1237∠76.92°	Yes
L78	0.0725∠83.27°	0.1258∠85.12°	No
L89	0.1015∠83.27°	0.0277∠-86.77°	No

4.5 Two Blinder Scheme

In most of the power industries, the distance relays for major lines are designed to respond to power swing and out-of-step conditions. The distance relay has a power swing blocking and an out-of-step tripping element to prevent undesired tripping or to allow intentional opening of transmission line [17]. The blinder scheme is the most popularly used technique for power swing and out-of-step detection. It is useful to compare the new relay logic with one of the standard practices being used in an industry. The performance of the proposed method is hence compared with double blinder scheme (Two Blinders Scheme) discussed in Section 2.6.1. Figure 4.24 shows the two blinder scheme where the two blinder elements are indicated by either RRO and RRI or LRO and LRI . Whenever there is fault in the line, impedance immediately jumps from the operating point to short circuit impedance inside the distance relay characteristics. However, during power swing, the impedance vector exhibits a steady progression and its rate of change corresponds to the power swing frequency of the system [68]. The scheme measures the time taken by the impedance trajectory to traverse outer and inner blinders, and compares with a pre-set time to discriminate between a power

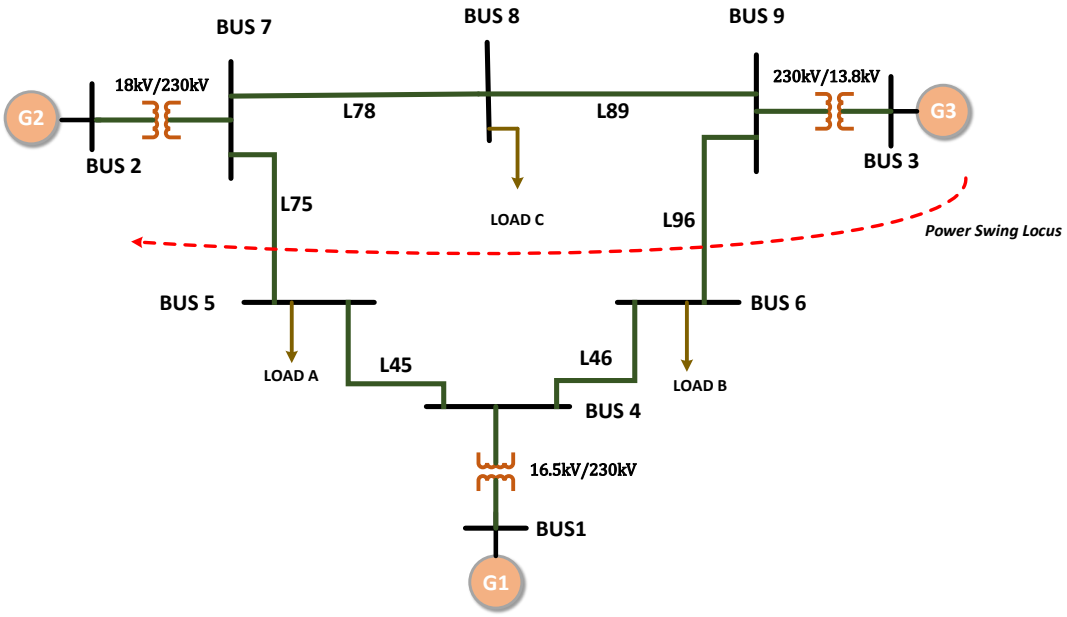

Figure 4.23: Power swing locus in WSCC 9-bus system

swing and fault. If the measured time is less than the pre-set time, then the disturbance is a fault. If the trajectory enters the outer blinder and stays inside the two blinders for more than a pre-set time, then it is a power swing. Now if the trajectory crosses the inner blinder in more than a pre-set time, then it is an out-of-step condition. If the trajectory crosses the outer blinder but does not cross the inner blinder, then the swing is a stable swing [6].

4.5.1 Blinder Setting in Multimachine System

Blinder setting in multi-machine system has been explained in Reference [67] and provides a detailed description on how to set the blinder elements. Setting of blinder starts with by determining the equivalent source and transfer impedance in the area of interest as explained in Appendix C.2. After the equivalent impedances has been calculated, the slip rate is determined by stability studies. Typically, maximum slip frequency is selected anywhere between 4 to 7 Hz [6]. An average slip in cycles/sec is determined analyzing the angular excursions of systems as a function of time. This approach is appropriate since the test systems slip frequency does not change considerably as the systems go out of step. The

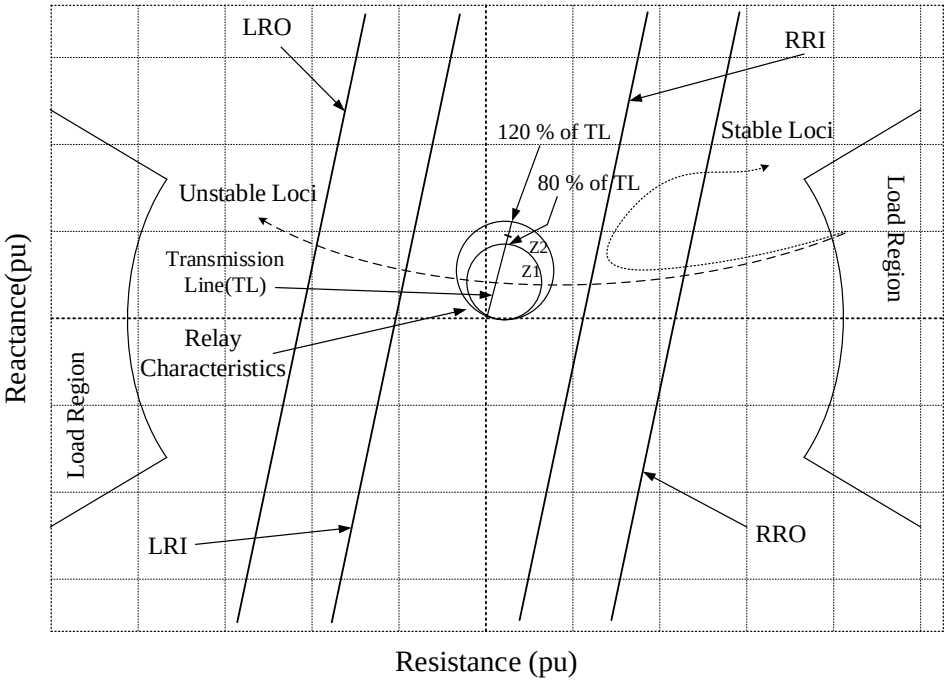

Figure 4.24: A two blinder scheme

slip rate of 4 Hz is used in the research. Figure 4.25 shows the rotor angle swing of three generators with respect to generator bus for the fault at bus 8 for 15 cycles which resulted in out-of-step condition. A brief explanation on the procedure of setting the blinders is given in Appendix B.

4.5.2 Comparison with Two Blinder Scheme

The prediction of stable and unstable swings based on the proposed method is compared with conventional two blinder method. In order to test the performance, an impedance relay R75 with a two blinder scheme placed near bus 7 on the transmission L75 of test system shown in Figure 4.23. Similar test is performed with an impedance relay R96 located near bus 9 on the transmission line L96 separately. The inner and outer resistive blinder reach is set using the procedure explained in Appendix B. The left-side resistive blinder and right-side resistive blinder are set for equidistant value from the center.

The nominal operating voltage for the system under test is 230 kV. The voltage and

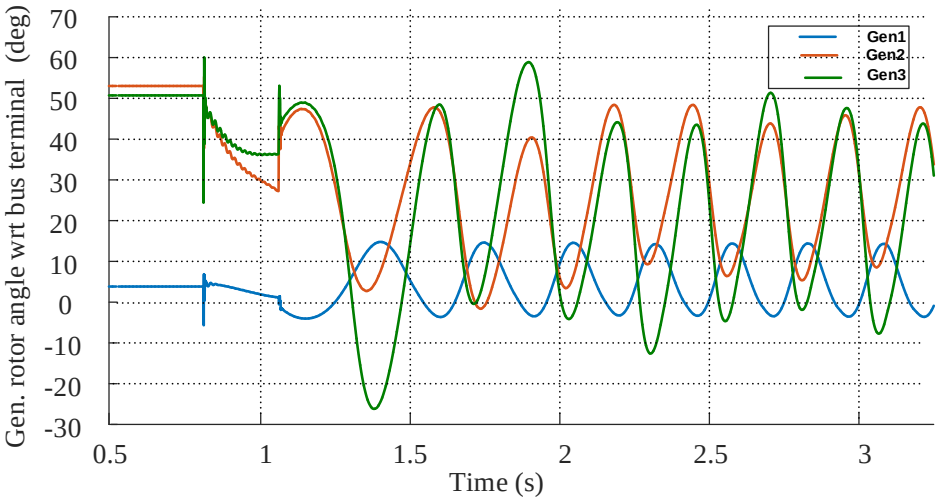

Figure 4.25: Impedance locus for fault at bus 6 for fault cleared after 7 cycles

current transformer ratio is 2000 : 1 and 2000 : 5, respectively. The zone 1 and zone 2 setting of distance element are set to 80 and 120 percent of the transmission line, respectively. Multiple simulations were carried out to compare the proposed technique with the two blinder scheme. The three phase faults at the different buses and at the center of the lines are studied. For both relays R75 and R96, the two test cases have been presented for a stable and an unstable condition.

4.5.2.1 Test Cases: R75

The equivalent source impedances and line impedances as shown in Appendix C expressed in secondary ohms are:

$$Z1S : 13.3882\angle 89.13^\circ\ \Omega$$

$$Z1R : 21.5406\angle 87.18^\circ\ \Omega$$

$$Z1L : 15.3304\angle 78.34^\circ\ \Omega$$

The outer blinder is adjusted to provide a 2.5 cycles PSB delay for a maximum slip rate of 4 Hz. The setting are calculated following the procedure as shown in Appendix B.

Right Resistance-Inner (RRI) = 79.4876 Ω

Right Resistance-Outer (RRO) = 22.9257 Ω

Left Resistance-Outer (LRI) = −22.9257 Ω

Left Resistance-Inner (LRO) = −79.4876 Ω

Figure 4.26 shows the impedance locus for a fault duration of 7 cycles (0.1166 s) at bus 6. The impedance locus enters the region between the two blinders and comes out of the outer blinder at 0.4397 s. Therefore, 0.4397 s is the time taken by relay to detect the swing as a stable swing, whereas the proposed scheme takes 0.5 s for the same swing detection. The times indicated in Figure 4.26 are measured from the instant when the fault occurs in the system. An unstable case is simulated with longer fault duration of 16 cycles (0.2666

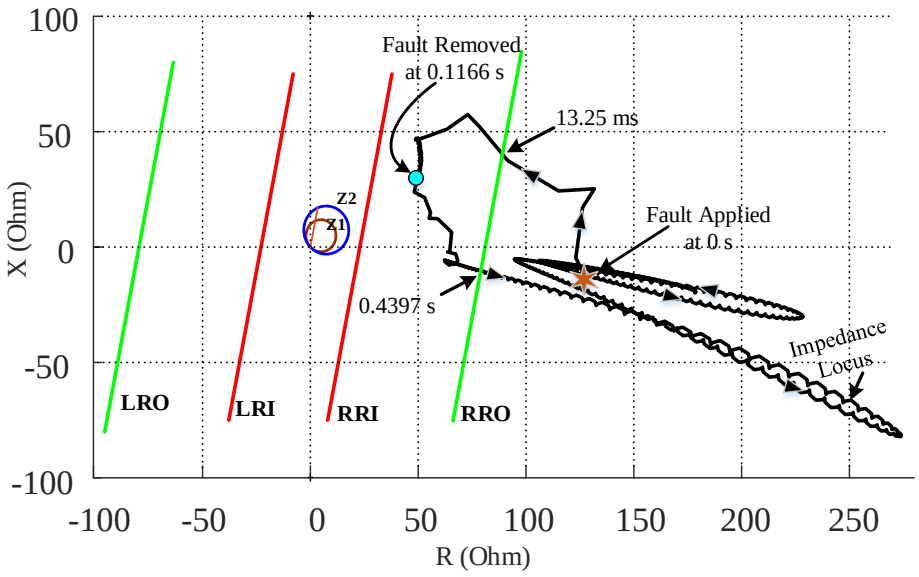

Figure 4.26: Impedance locus for fault at bus 6 for fault cleared after 7 cycles

s). The impedance locus crosses both blinders as shown in Figure 4.27, which means the swing is going to be unstable. The impedance trajectory enters the inner blinder at 0.4097 s. The scheme hence detects the swing as an unstable swing at 0.4097 s; whereas the proposed scheme detects the instability at 0.8080 s. One more case study is carried out for the faults at bus 9 in the system. The impedance locus during and after for fault of 6 cycles (0.1 s) is

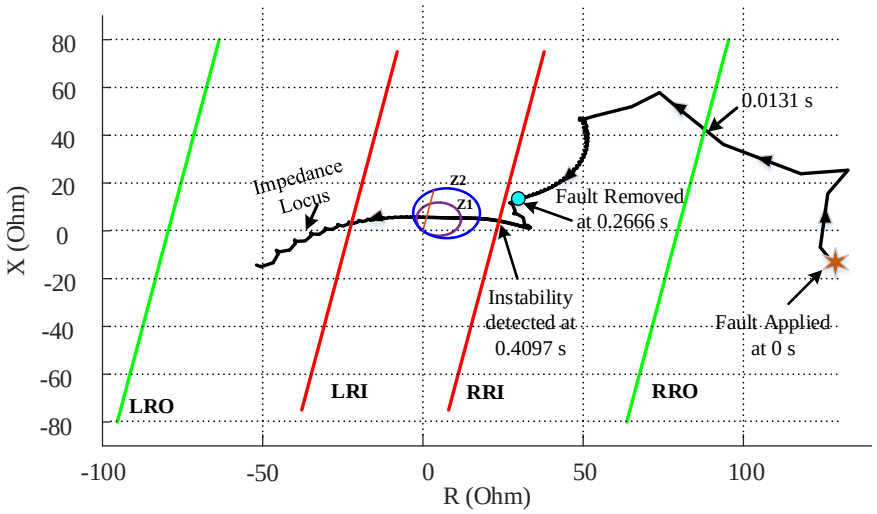

Figure 4.27: Impedance locus for fault at bus 6 for fault cleared after 16 cycles

shown in Figure 4.28. The impedance locus enters the right outer blinder and swings back before reaching the right inner blinder. The swing is detected as a stable swing at 0.5021 s, whereas the proposed scheme detects the swing at 0.5160 s. Now an unstable case is simulated with the fault duration of 11 cycles (0.18333 s). Figure 4.29 shows the impedance locus for the fault duration of 11 cycles. The swing is detected as an unstable swing at 0.3975 s, whereas the proposed technique takes 0.3910 s for detection. Table 4.4 shows the test results for stable and unstable swings using two blinder scheme.

4.5.2.2 Test Cases: R96

The equivalent source impedances and line impedances for relay R96 expressed in secondary ohms are:

$$Z1S : 15.2881\angle 88.93^\circ\ \Omega$$

$$Z1R : 22.0381\angle 85.00^\circ\ \Omega$$

$$Z1L : 16.3566\angle 76.76^\circ\ \Omega$$

The outer blinder is adjusted to provide a 2.5 cycles PSB delay for a maximum slip rate of 4 Hz. The setting are calculated following the procedure as shown in Appendix B.

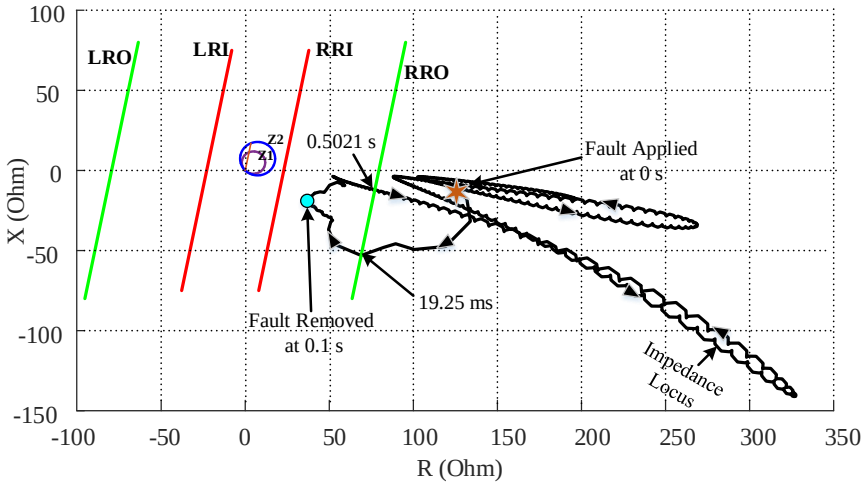

Figure 4.28: Impedance locus for fault at bus 9 for fault cleared after 6 cycles

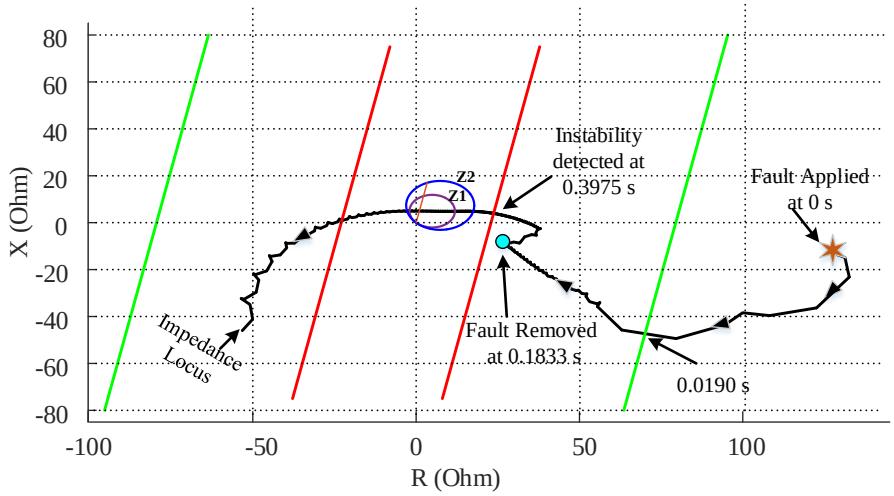

Figure 4.29: Impedance locus for fault at bus 9 for fault cleared after 11 cycles

Right Resistance-Inner (RRI) = 86.8338 Ω

Right Resistance-Outer (RRO) = 24.7692 Ω

Left Resistance-Outer (LRI) = −24.7692 Ω

Left Resistance-Inner (LRO) = −86.8338 Ω

The impedance locus for a fault duration of 6 cycles (0.1 s) at bus 5 is shown in Figure 4.30. The impedance locus enters the region between the two blinders at 0.01475 s and comes out

Table 4.4: Summary of results using a two blinder scheme

Fault Location	Fault duration (cycles)	Fault duration (s)	Decision time (s)	Decision
Bus 4	5	0.0833	0.4304	Stable
	12	0.2000	0.3393	Unstable
Bus 6	7	0.1166	0.4397	Stable
	16	0.2666	0.4097	Unstable
Bus 8	6	0.1000	0.4984	Stable
	11	0.1833	0.3907	Unstable
Between line 4-6	8	0.1333	0.5114	Stable
	15	0.2500	0.3788	Unstable
Between line 7-8	5	0.0833	0.4606	Stable
	10	0.1666	0.3962	Unstable
Between line 8-9	6	0.1000	0.4884	Stable
	12	0.2000	0.16975	Unstable

of the outer blinder at 0.1165 s. Therefore, the moment locus comes out of the right outer blinder, relay detects the swing as a stable swing. The proposed scheme takes 0.4829 s for the same swing detection. The times indicated in Figure 4.30 are measured from the instant when the fault occurs in the system.

Simulation is performed for longer fault duration of 13 cycles (0.2166 s)in the same bus. In this case, the impedance locus traverse through both blinders and indicates that the swing is going to be unstable as shown in Figure 4.31.

The impedance trajectory enters the right inner blinder at 0.4813 s. The scheme hence detects the swing as an unstable swing at 0.4813 s; whereas the proposed scheme detects the instability at 0.2830 s.

One more fault scenario is described for the relay R96. A three phase fault is applied at bus 7 for a duration of 4 cycles (0.0666 s). The impedance locus during and after the

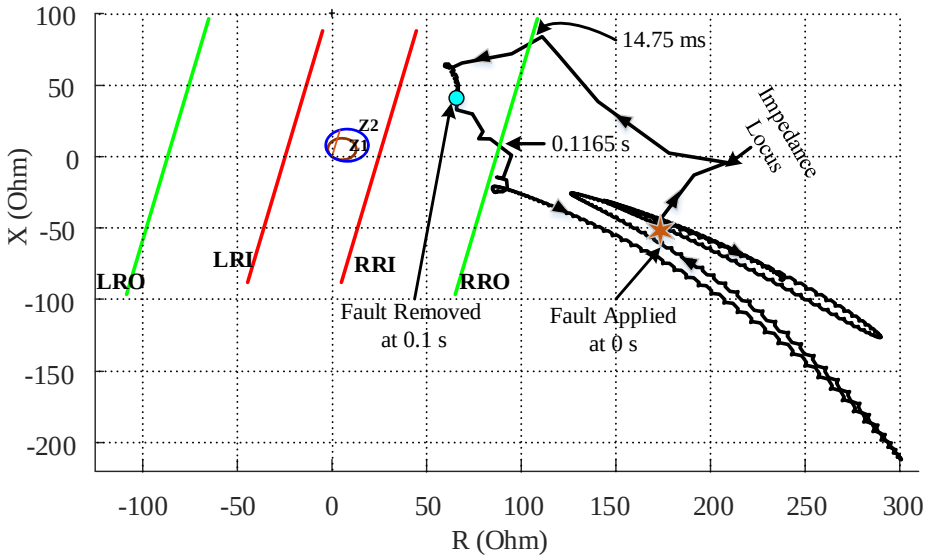

Figure 4.30: Impedance locus for fault at bus 5 for fault cleared after 6 cycles

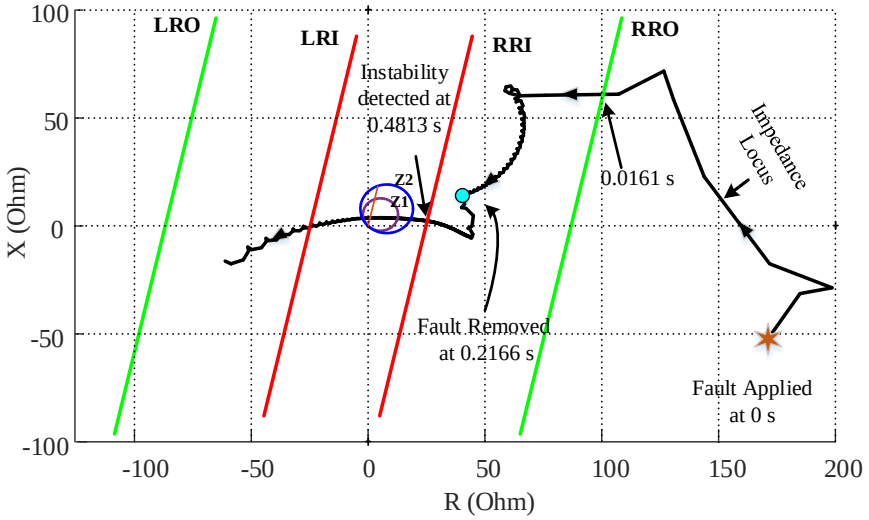

Figure 4.31: Impedance locus for fault at bus 5 for fault cleared after 13 cycles

fault is shown in Figure 4.32. The swing is detected as a stable swing at 0.0930 s, whereas the proposed scheme detects the swing at 0.4999 s. Unstable swing is obtained with a fault duration of 9 cycles (0.15 s). Figure 4.33 shows the impedance locus with this fault. The swing is detected as an unstable swing at 0.5323 s, whereas the proposed technique takes

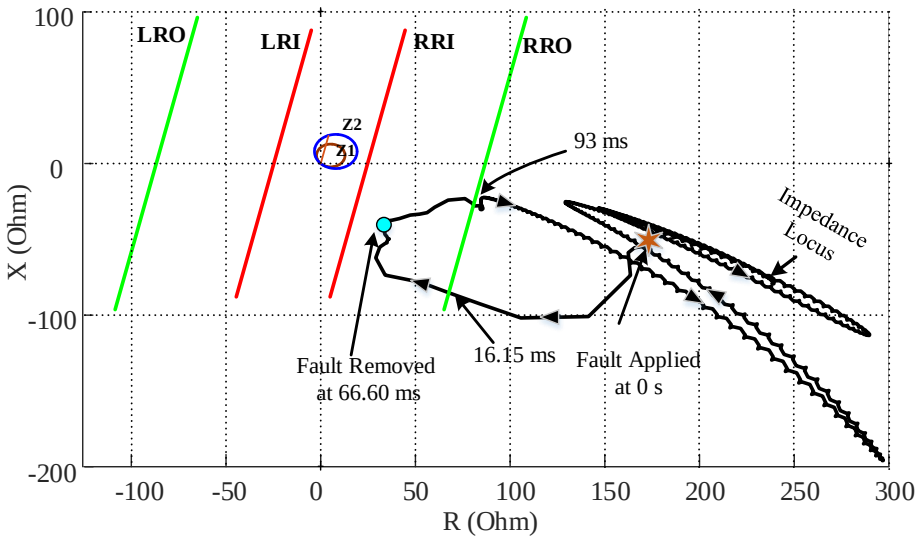

Figure 4.32: Impedance locus for fault at bus 7 for fault cleared after 4 cycles

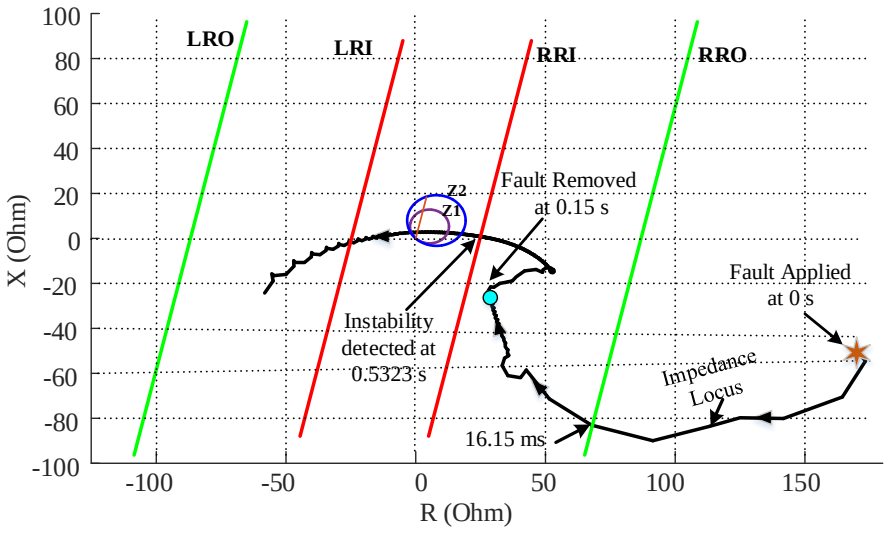

Figure 4.33: Impedance locus for fault at bus 7 for fault cleared after 9 cycles

0.5750 s for detection. Table 4.5 shows the test results for stable and unstable swings using the two blinder scheme.

Table 4.5: Summary of results using a two blinder scheme

Fault Location	Fault duration (cycles)	Fault duration (s)	Decision time (s)	Decision
Bus 4	5	0.0833	0.2861	Stable
	12	0.2000	0.3393	Unstable
Bus 5	6	0.1000	0.1164	Stable
	13	0.2166	0.4813	Unstable
Bus 8	6	0.1000	0.4036	Stable
	11	0.1833	0.6128	Unstable
Between line 4-5	7	0.1166	0.3890	Stable
	12	0.2000	0.5218	Unstable
Between line 5-7	6	0.0833	0.3078	Stable
	12	0.2000	0.6046	Unstable
Between line 8-9	6	0.1000	0.3699	Stable
	12	0.2000	0.4518	Unstable

4.6 Swing Center Voltage

The SCV method is investigated in this thesis for system level out-of-step protection on the WSCC 9 bus system configuration. Using the wide area measurements from optimal PMU locations in the test system, the proposed SCV methodology is implemented at the system level. Once the disturbance is detected, the coherency analysis is first used to determine the coherent groups, and the two groups are reduced to a two machine equivalent system. The out-of-step condition is determined, when the angle difference between the two equivalent machines (dCOA), increases as a function of time and the value of SCV is zero when the angles between the two sources are 180 degrees apart. The relation between the SCV and the phase angle difference of the equivalent machine of two equivalent voltage sources can be represented as given by Equation (4.1).

$$SCV = |E1| \cos \frac{dCOA}{2} \tag{4.1}$$

The rate of change of SCV provides the relationship with the slip frequency between the two equivalent systems as given in Equation (4.2) and is explored to detect the power swing.

$$\frac{d(SCV1)}{dt} = -\frac{E1}{2} \frac{d(dCOA)}{dt} \sin \frac{dCOA}{2} \tag{4.2}$$

The slip frequency for the system is not constant and varies with the time after disturbance is applied in the system. The reporting rates for the PMU is 120 samples/sec and each measurement sample is transmitted after an interval of 8.33 ms. The calculation of slip between two coherent groups in this fashion is prone to error due to the derivative term involved in the calculation, which tends to amplify the noise significantly. To overcome this problem, curve fitting is done to the noisy observations using a spline function [62]. Figure 4.34 shows the logic used for implementation of the SCV detection technique.

The SCV algorithm detects the power swing based on the absolute value of SCV1, rate of change of SCV1 (dSCV1) and the output of the rate of change of dSCV1 (discontinuity detector) [49]. During a power swing, the rate of change of SCV1 is observed to be significant and thus the detection is made when the absolute value of rate of change of SCV1 (| dSCV1/dt |) crosses the minimum threshold (d_SCV1_min) and the magnitude of the SCV1 remains within the range of maximum (SCV1_th_hi) and minimum(SCV1_th_low) threshold. When the absolute value of the rate of change of SCV1 exceeds a maximum threshold (d_SCV1_max) or the absolute value of the discontinuity detector exceeds a threshold value (dd_SCV1_thr), the output of the SCV detector is blocked.

For the WSCC 9 bus test system, the settings used for the swing detection are:
Maximum rate of change of SCV (d_SCV1_max) = 12 pu/s
Minimum rate of change of SCV (d_SCV1_min) = 4.5 pu/s
Higher threshold value of SCV (SCV1_th_hi)= 0.3 pu

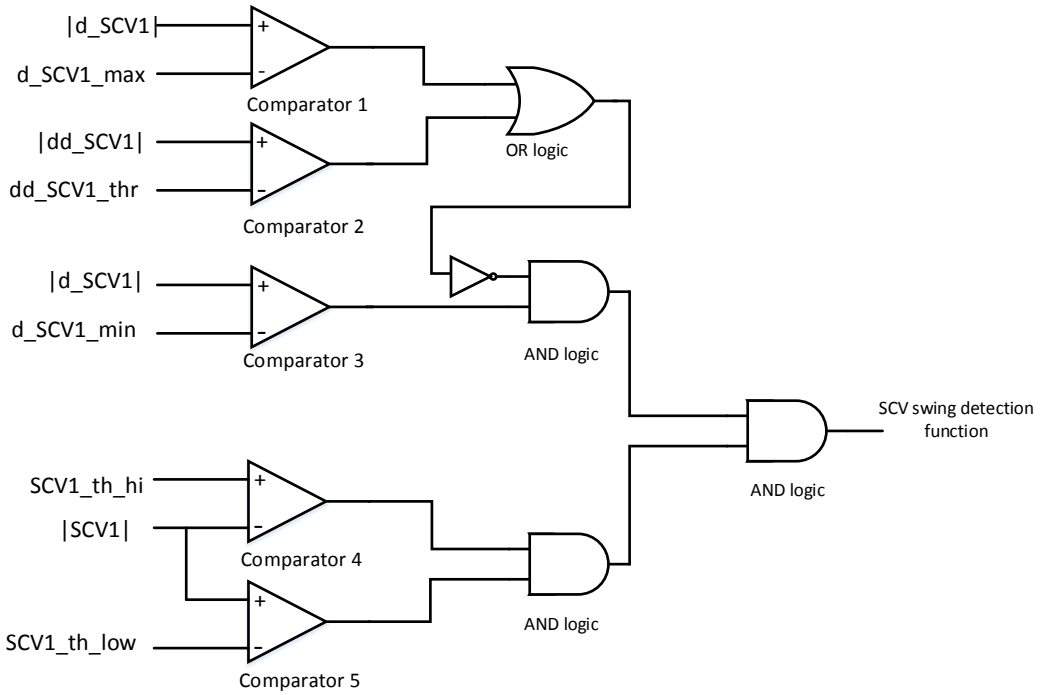

Figure 4.34: Swing center voltage detection algorithm

Lower threshold value of SCV (SCV1_th_low)= 0.1 pu
Threshold value of rate of change of dSCV1 (dd_SCV1_thr)= 50 pu/s^2

The results with the SCV method are presented for two stable and unstable condition scenarios and are compared with the proposed synchrophasor based method.

4.6.1 Case I: Fault on Bus 5

The performance of SCV method is analyzed for a fault on Bus 5. Three phase fault is applied at the bus for 6 cycles. The SCV1 calculation starts as soon as system separates into coherent groups at 2.2250 s, 82.90 ms after the fault was applied. Figure 4.35 shows the SCV1 for a stable case for fault duration of 6 cycles and the SCV1 value does reach zero value. Figure 4.36 shows the rate of change of SCV1 for the same 6 cycles fault scenario at Bus 5.

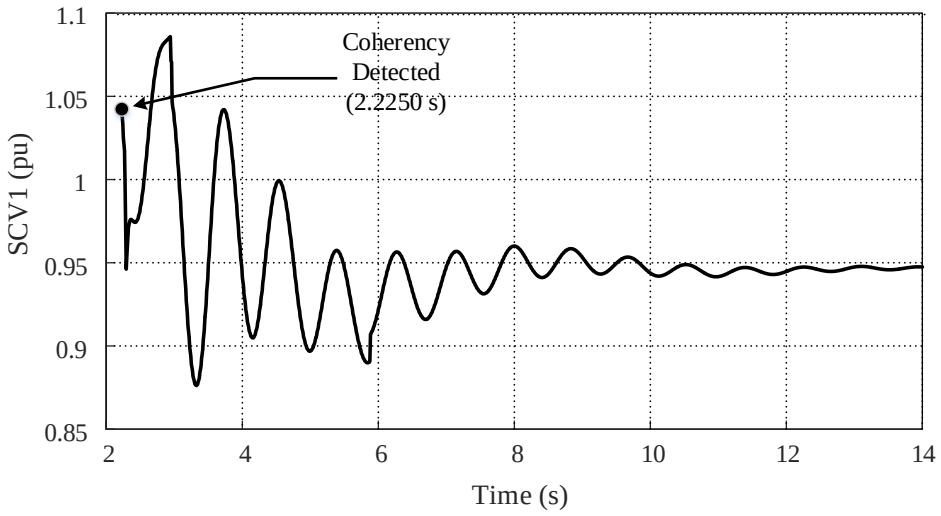

Figure 4.35: SCV1 for 5 cycles fault

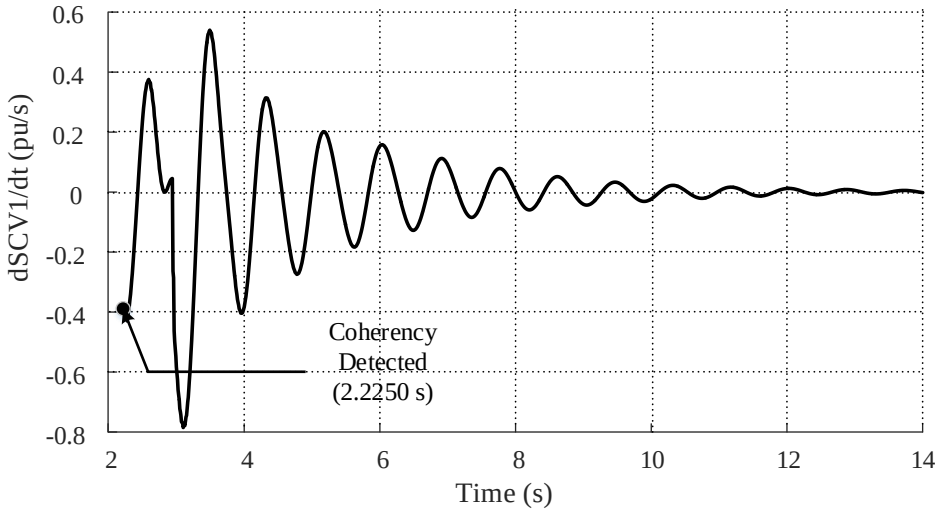

Figure 4.36: d(SCV1)/dt for 5 cycles fault

The duration of fault is increased to 13 cycles and values of SCV1 and rate of change of SCV1 are monitored. Fault is applied at 2.3090 s and the coherency is detected at 2.3920 s. As shown in the Figure 4.37 and Figure 4.38, unstable power swing is detected by the SCV swing detector at 2.9590 s, 0.65 s after the fault ia applied to the bus. For the same fault

scenario, proposed method was able to predict the OST condition in 0.2829 s after the fault.

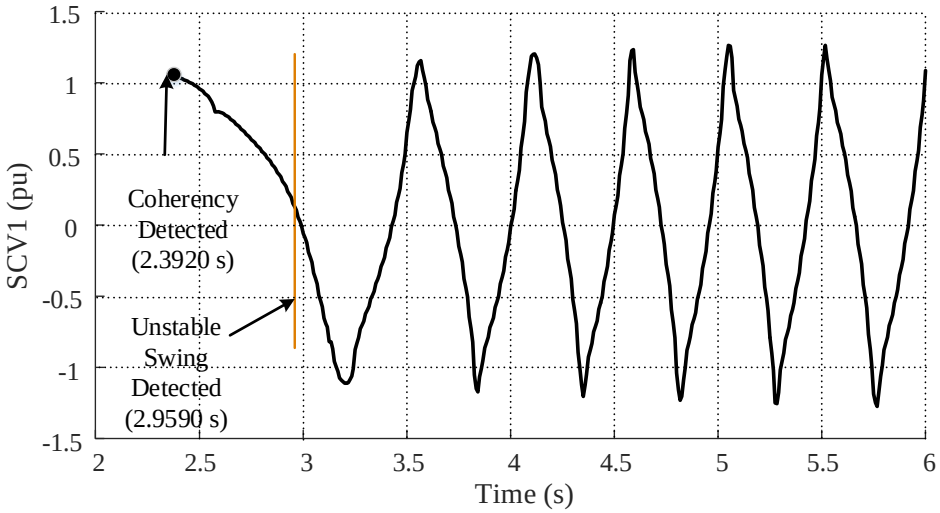

Figure 4.37: SCV1 for 13 cycles fault

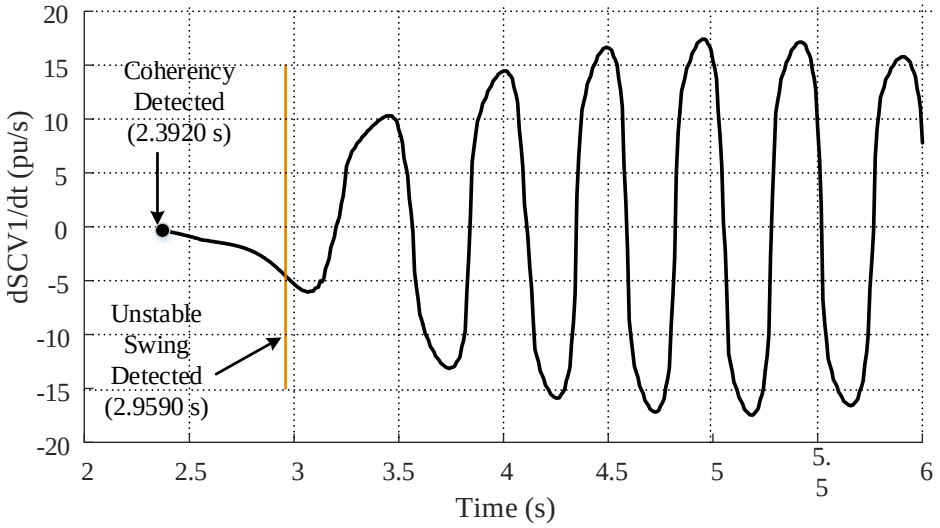

Figure 4.38: d(SCV1)/dt for 13 cycles fault

Figure 4.39 shows the SCV1 and rate of change of SCV1 during the unstable power swing. Unstable power swing is detected at an angular separation of 166.4323 degrees between equivalent machine. For the same fault case, proposed method is able to predict the OST condition at angular separation of 80.4965 degrees.

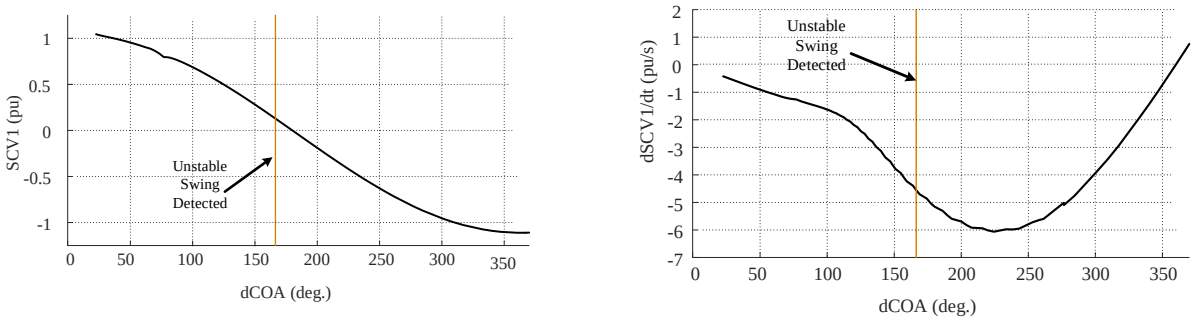

(a) SCV1 (b) d(SCV1)/dt

Figure 4.39: SCV and rate of change of SCV1 with respect to the dCOA

4.6.2 Case II: Fault at Bus 6

One more case study is presented to compare the proposed method with the performance of SCV method. Three phase fault is applied at the Bus 7 for cycles. A three phase fault is applied at 2.6409 s and the coherency is detected at 2.7160 s. The SCV1 swing detector in the relay initiates the logic immediately after system separates into coherent groups. Figure 4.35 shows the SVC1 for fault of 7 cycles where the SCV1 value does reach zero value. Figure 4.36 shows the rate of change of SCV1 for same fault case.

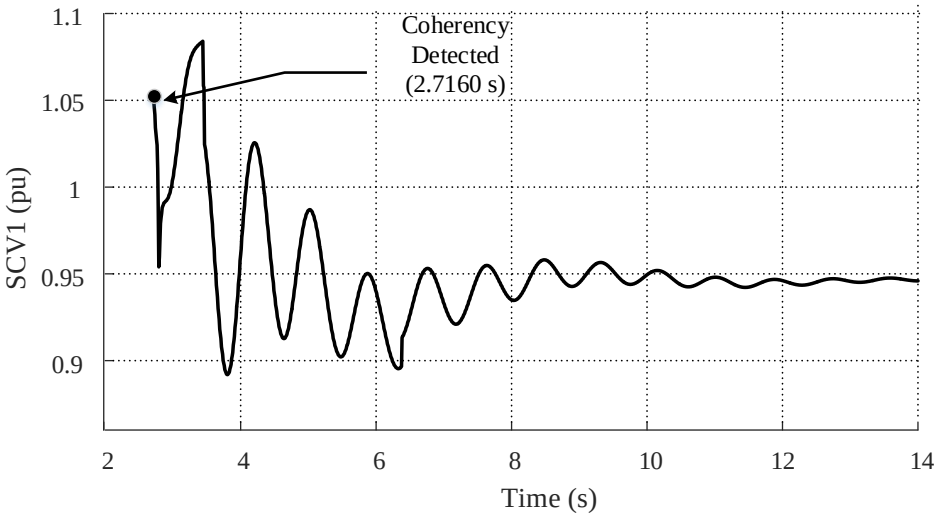

Figure 4.40: SCV for 7 cycles fault

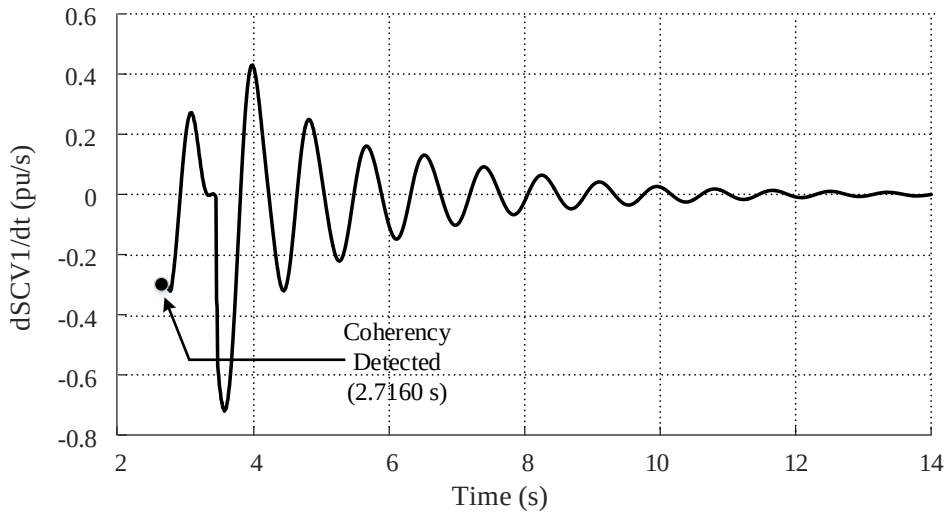

Figure 4.41: d(SCV)/dt for 7 cycles fault

A three phase fault is applied at 3.7079 s and fault duration is increased to 13 cycles. The SCV1 and rate of SCV1 is shown in Figure 4.42 and 4.43, respectively. Unstable power swing is detected by the SCV swing detector at 4.9820 s, 1.2740 s after the fault was applied to the bus. Proposed method was able to predict the OST condition for same fault scenario in 0.8080 s after the fault.

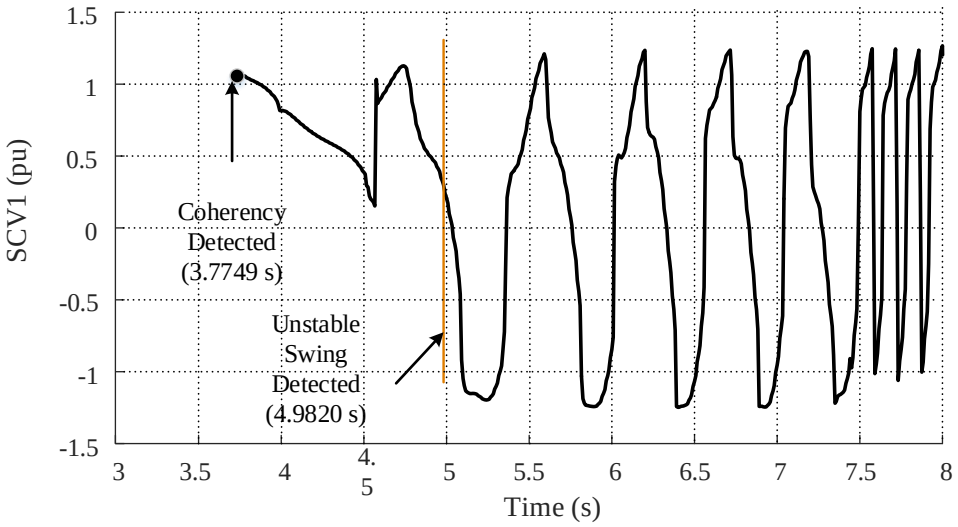

Figure 4.42: SCV for 16 cycles fault

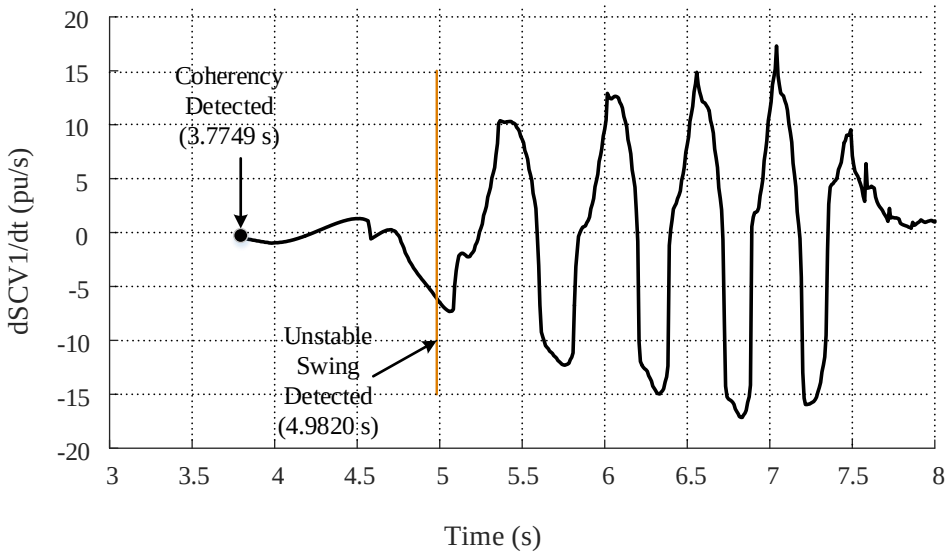

Figure 4.43: d(SCV)/dt for 16 cycles fault

Figure 4.44 shows the SCV1 and rate of change of SCV1 during the unstable power swing. Unstable power swing is detected at an angular separation of 150.1702 degrees between equivalent machine. For the same fault case, proposed method is able to predict the OST condition at angular separation of 84.1365 degrees. The results for the unstable cases are presented in the Table (4.6) and are measured after the the fault instance.

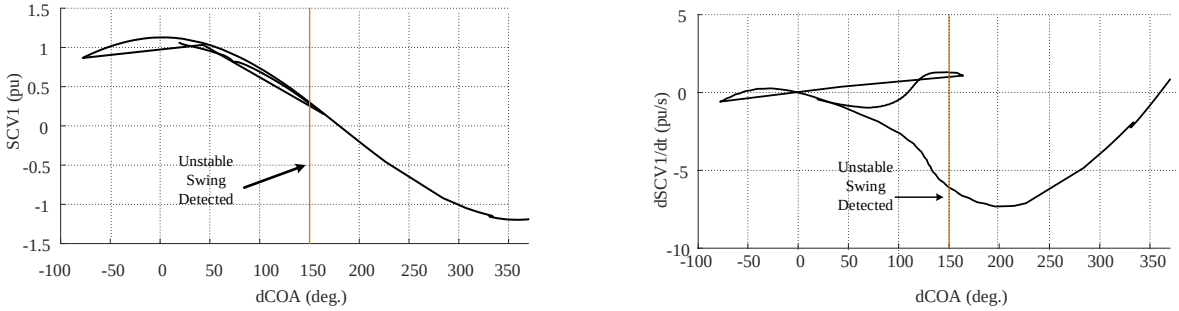

(a) SCV

(b) d(SCV)/dt

Figure 4.44: 16 cycles fault

Table 4.6: Summary of unstable swing using a SCV scheme

Fault Location	Fault duration (cycles)	Fault duration (s)	Coherency detection time (s)	Detection time (s)
Bus 4	12	0.200	0.0670	0.5840
Bus 5	13	0.2166	0.0830	0.6500
Bus 6	16	0.2666	0.0670	1.2741
Bus 7	9	0.1500	0.0590	0.7500
Bus 8	11	0.1833	0.0500	0.7839
Bus 9	11	0.1833	0.0410	0.6660

4.7 Summary

This chapter explained the application of synchrophasor-based OST prediction when applied to a multi-machine system. The technique was based on the assumption that the system separates into two groups of machines. The proposed method used a coherency analysis, with the system reduced to two equivalent coherent groups. After the coherency of machine groups was determined, the two coherent group equivalent procedure was carried out as discussed in Section 3.4.2.4. The angular separation between the equivalent groups was calculated and predicted in every instance after samples for the observation windows were available. The system state post-fault, whether stable or unstable, was assisted by three consecutive tripping or blocking criteria. Three consecutive checks were necessary to verify the accuracy of the estimated values and the predicted result. The test results discussed in this chapter show that the proposed technique using WAMS is able to accurately predict instability 8.5 to 24.5 cycles before the system actually enters an out-of-step condition. The angular separation at the instant of prediction is between 80.4965 and 137.7929 degrees.

This chapter also explained the swing locus in a complex system. The derivation of swing locus for the WSCC 9 bus system was helpful in determining the location of the power swing relay. The study confirmed that, during the transient condition, the swing passed through lines 5-7 and 6-9; the results are provided in Table 4.3. The proposed method was also

compared with the two blinder technique, with the time taken for instability detection using the technique found to be close to values obtained with the synchrophasor-based technique. Setting the blinders and implementation of this scheme, especially at the transmission line level, involves extensive and time-consuming network analysis and stability studies; however, the synchrophasor-based technique proposed in this thesis directly captures the effect of network topology changes, etc., with PMU measurements and therefore extensive offline simulations are not essential.

The proposed method was also compared with the SCV scheme. Test scenarios for two fault locations in the WSCC 9 bus system were presented and compared with the proposed method. The prediction time of the proposed method was much faster than the SCV method.

Chapter 5

Synchrophasor Based OST Prediction Using Actual PMUs

5.1 Introduction

Relays featuring PMUs are commercially available. Companies including General Electric, Schweitzer, and ABB are producing relays with synchrophasor measurement capabilities. In this chapter, the proposed method is tested using a GE N60 relay for the WSCC 9 bus test system to verify the capabilities of the proposed method. The proposed method was tested using the virtual PMU models in an RTDS in Chapter 4. The next step is to validate the work with commercial relays. Therefore, the GE N60 relay, which features PMUs, was used and tested with an RTDS [1]. A real-time simulator consists of digital processing cards in which a power system network can be modeled in detail. It performs electromagnetic transient power system simulations with very small steps, typically on the order of 2 to 50 microseconds. Complete digital simulation with all of the calculations required to determine the power systems state are computed in a time exactly equal to the simulation time step. Simulation of the system response over 1 second is computed in exactly 1 second, hence the term real-time digital simulator. This kind of simulator is very widely used by power utilities and equipment manufacturers for experimental verification of relays and hardware-in-the-loop testin [66].

The power system was modeled in RSCAD [2] which is a computer-based interface to

[1]RTDS is the registered trade mark of RTDS Technologies Inc., Winnipeg, Canada

[2]RSCAD is the registered trade mark of RTDS Technologies Inc., Winnipeg, Canada

frame the power system components before running a test in the simulator. The power system model developed in RSCAD is simulated in RTDS, and the signals from the RTDS fed to the CT and VT terminals of relay. The phasor information from the PMUs in the relay are sent to the phasor data concentrator via Ethernet communication link . The accumulated phasor information are used for offline analysis using the MATLAB program.

5.2 Description of Hardware and Software

The real time digital simulator and some of its component used in the course of research are explained in Section 4.2.1.1- 4.2.1.3. Another important component of RTDS used to interface the simulator and relay is Gigabit Transceiver Analog Output Card (GTAO) . This section explains the features and operation of GTAO card and GE N60 relay.

5.2.1 GTAO

The Gigabit Transceiver Analogue Output Card (GTAO) is one of the component card in RTDS used to interface analog signals from the RTDS to external devices. It consists of twelve, 16 bit analogue output channels with an output range of +/10 volts. The major benefits of 16 bit DACs in the card is to provide a wide dynamic range. Such a wide dynamic range may be required when using the GTAO to send measured current signals to an external protection device. Under fault conditions the current may be much larger than the steadystate current. The GTAO outputs are oversampled at a rate of 1 MHz and the cards output channels are updated synchronously. Each GTAO card connects to an RTDS processor card (GPC or PB5) via a fiber cable. Analog output signals connect to terminal blocks available on the GTAO card [55].

5.2.2 N60 relay

The GE N60 Network Stability and Synchrophasor Measurement System is a microprocessor based device intended for development of load shedding and special protection schemes.

It consist of modular design and can be configured to monitor upto 5 three phase power circuits. The relay provides for variety of metering functions, including active, reactive and apparent power on a per-phase and three-phase basis; true RMS value, phasors and symmetrical components of currents and voltages; and power factor and frequency. It has the collection of standard communications protocols and can be used independently over a range of communication ports like Ethernet and direct fast and secure digital inter-IED communication. The N60 also shares operational data from remotes N60s so that the system can generate intelligent decisions to maintain power system operation [15]. The N60 is available with 19-inch rack horizontal mount and consist of modules for power supply, CPU, CT/VT, digital input and output, transducer input and output, and inter-relay communications. It is packed with the protection functions like underfrequency, overfrequency and rate of change of frequency (df/dt), out-of-step tripping and power swing blocking, overcurrent, overvoltage and undervoltage protection. The key features of this relay includes the phasor measurement unit according to IEEE C37.118(2011) and IEC 61850-90-5 support. High reporting rate of 120 fps for P class is available in 4 PMUs, each with 46 configurable channels [15]. Implementation of proposed method is carried out with the PMUs in N60 relay.

5.3 Test Procedures

The test procedure includes three distinct steps: a) modeling a power system and simulating it, b) connecting the GTAO analog output to the N60, c) capturing the phasor data in PDC and analyzing the stability condition. Figure 5.1 shows a diagram of the process involved in implementing the proposed method.

5.3.1 Power System Modelling

The power system and control logic design is created in RSCAD. RSCAD provides custom library for power system and control components. The components are used to build test cases for WSCC 9 bus system. This system consists of 9 buses, 3 generators, 3 fix tap transformers and 6 transmission lines. Buses 5, 6 and 8 have constant active and

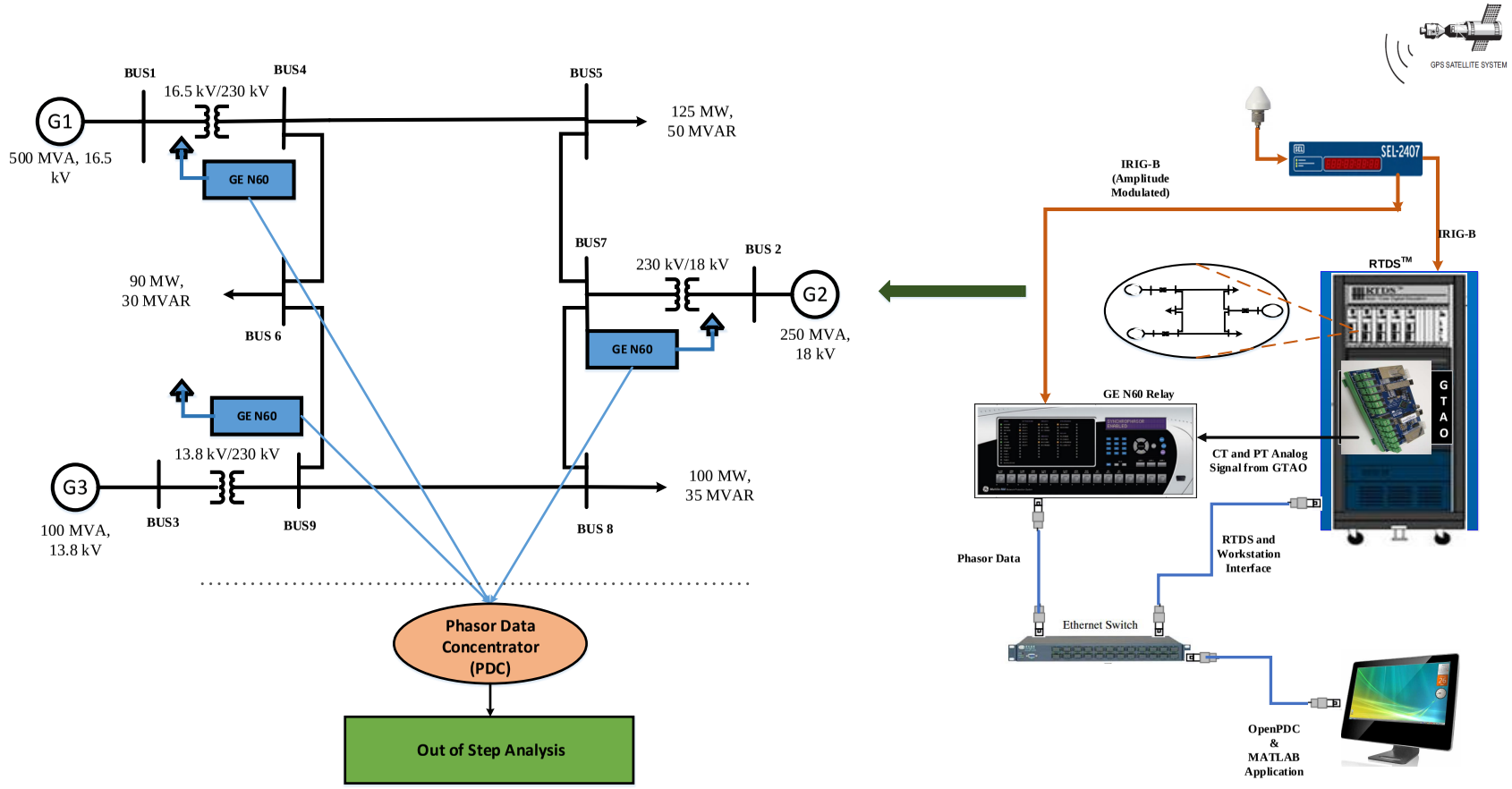

Figure 5.1: Test setup for the time series based swing curve prediction using the N60 relay

reactive loads totaling 315 MW and 115 MVAR [58]. All three generators in the system use two-axis flux decay dynamic models. For primary voltage regulation of the generators, IEEE Type I excitation system is used. The partial view of the system modeled in RTDS is shown in Figure 5.2 and the system data is provided in Appendix A. In the Figure 5.2, CT and CVT are connected near Bus 4, load is connected at Bus 5. The fault locations are shown. The fault control logic is designed so as to vary the fault duration using slider control LG_FTIME and fault location using 32 bits binary switch $FLTLOC$ as shown in Figure 5.3. The fault logic control is shown for one location in the figure.

5.3.2 Hardware Interface

The voltages and currents from the simulation are in a digital format and must be output of the RTDS through a GTAO card to produce the analog waveforms required by the relay. The RTDS hardware will produce a +/- 10 volt peak maximum signal; therefore the output hardware must be properly scaled to incorporate the deviation of voltage and current during disturbances. The output waveforms are normally connected to external amplifiers in order to bring its actual level before connecting to the inputs of relay. To avoid the complexity of additional amplifier in the connection between the RTDS and N60, the modified relay, with the low level interface CT/VT model provided by GE Multilin, Canada was used. These CT/VT model has maximum input voltage rating of 10V p-p (3.5355 Vrms) for both voltage and current channels.

The GTAO component is used to provide an analog interface to external equipment and uses the outputs from CTs and CVTs as the input signals. The current and voltage transformer model available in RSCAD are used to measure the current and voltage at the PMU locations. The current transformer (CT) ratio is selected to be 2000:5 and the capacitive voltage transformer (CVT) ratio is selected to be 2000:1. The GTAO component requires proper scaling of its D/A outputs. The GTAO is connected to N60 relay that can accept a low level interface signal. The following ratios were considered for the low level test interface in the GE N60 relay.

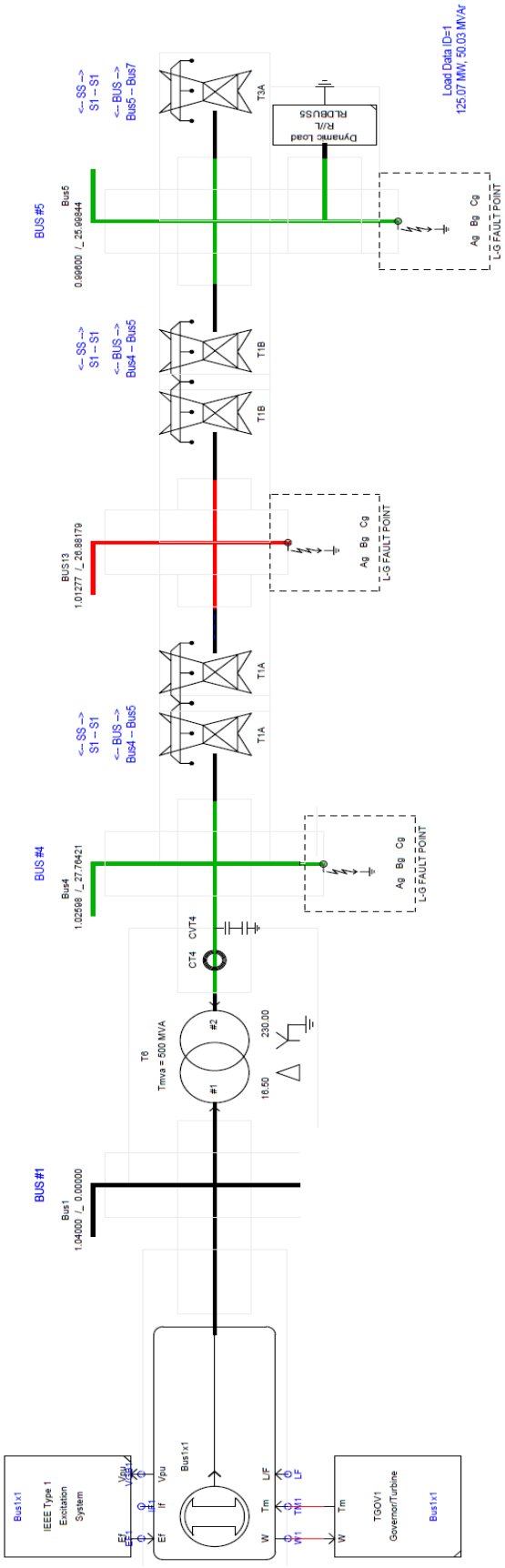

Figure 5.2: Portion of WSCC 9 bus system with Generator 1 and bus 1, 4 and 5

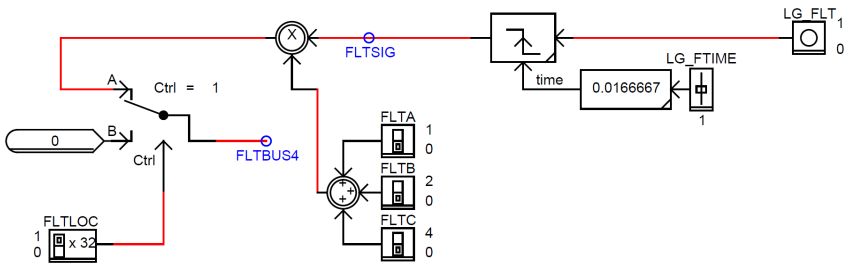

Figure 5.3: Fault control signal to control fault cycle and duration

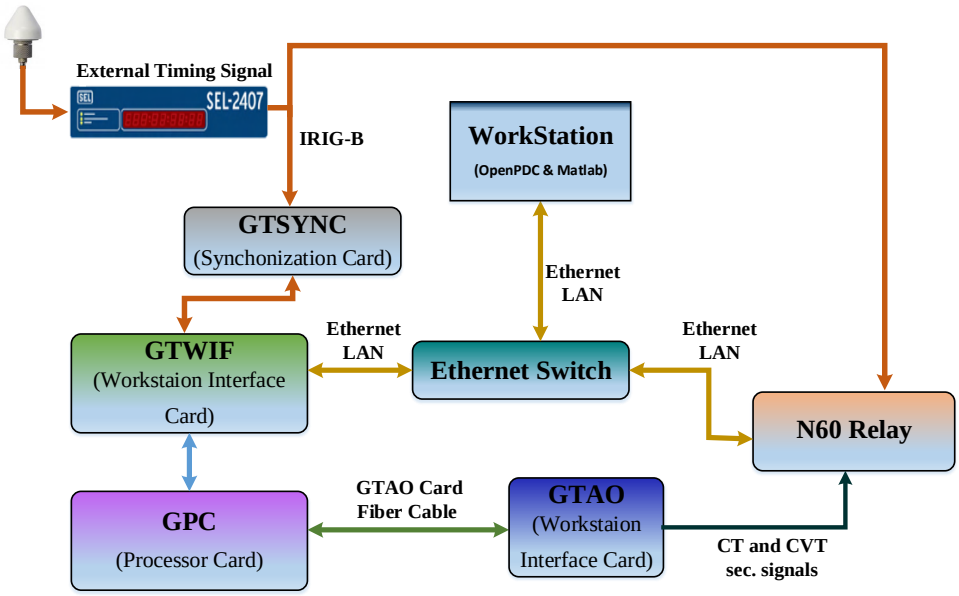

Figure 5.4: Block diagram RTDS and N60 interface for data acquisition

- Voltage output 67 $V \Rightarrow 1\ V$
- Current output 5 $A \Rightarrow 1\ V$

The scaling factor (SC) is calculated for GTAO as provided in reference [55] is

$$SCx = \frac{5}{scaled\ secondary\ value} \times Normal\ secondary\ quantity \tag{5.1}$$

Using the the Equation (5.1), the SC value for the voltage and current was calculated to be

335 and 25, respectively. The steady state voltage and current outputs from CTs/CVTs and GTAO are presented in Table 5.1 and Table 5.2, respectively.

Table 5.1: Voltage outputs from CVT and GTAO during steady condition

Location	Phase voltage (kV)	CVT ratio	CVTs secondary voltage(V)	GTAO Scaling	Scaling factor(SC)	GTAO output (V)
Bus 4	136.2275	2000:1	68.1249	67:1	335	1.0167
Bus 7	136.2525		68.1374			1.0169
Bus 9	137.1162		68.5693			1.0234

Table 5.2: Current outputs from CT and GTAO during steady condition

Location	Phase current (A)	CT ratio	CTs secondary Curent(A)	GTAO Scaling	Scaling factor(SC)	GTAO output (V)
Line 1-4	189.1340	2000:5	0.4725	5:1	25	0.0945
Line 2-7	397.8410		0.9940			0.1988
Line 3-9	209.0380		0.5223			0.1044

5.3.3 Data Acquisition and Analysis

The implementation of the synchrophasor in the N60 relay is shown in Figure 5.5 [15]. The P class synchrophasor has been selected since it is standardized for the protection purpose due to its short window filtering technique. The four PMUs within the relay is configured to read the sychrophasors from any of the six sources at the rate 120 sample per second. Two aggregators in the relay allow the user to aggregate selected PMUs as per IEC 37.118 to form a custom data set that is sent to PDC optimizing bandwidth. The highest reporting rate of 120 Hz for a 60 Hz system and the aggregator is configured to establish a TCP connection to a PDC allowing the relay for real-time data reporting. The timing signal is provided by SEL-2407 in amplitude modulated (AM) IRIG time code formats.

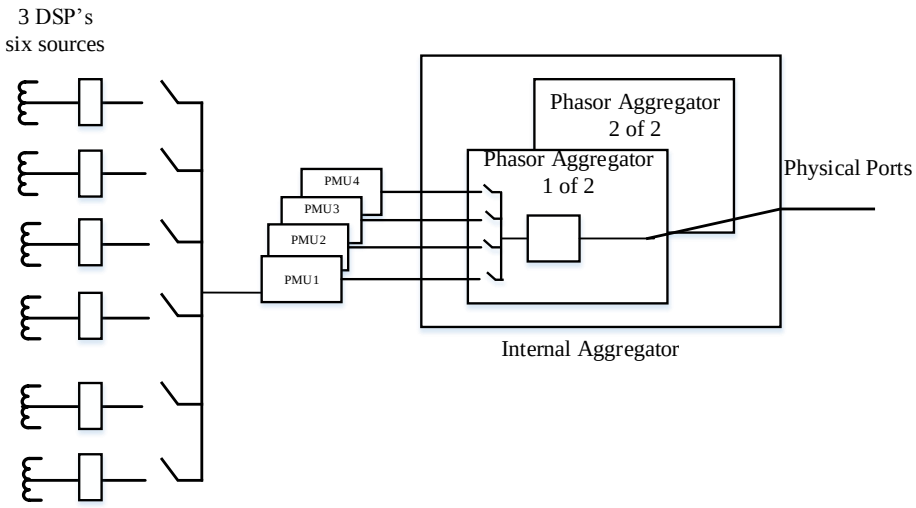

Figure 5.5: Synchrophasor implementation in N60

For every simulation, the synchronised PMU data of voltage and current is collected in the PDC. Offline analysis of the data to predict the stability of the system is carried out using Matlab. The econometric toolbox available in Matlab is used to model the data for finding the appropriate model and use the same model in forecasting the data.

5.4 Case studies: WSCC 9 Bus System

The proposed method is also tested for WSCC 9 bus system using N60 synchrophasor relay. This section presents the test results for 2 cases, each for stable and unstable scenario. A three phase fault is applied at bus 4 for the first case and at bus 8 for the second case. The fault durations are varied to get stable and unstable cases. For the fault at Bus 4, the fault is applied at 3.4339 s and is cleared after 5 cycles (0.0833 s). The voltage angle swing observed at different generator buses with respect to the reference generator bus are shown in Figure 5.6. The coherency is found at 3.4920 s where machine 2 and 3 separate out from the reference machine. This is the point where the calculations for finding center of angle (COA) of each coherent groups is carried out. The difference of COAs (dCOA) is predicted with the previously calculated samples of dCOA, enough to form the observation window after

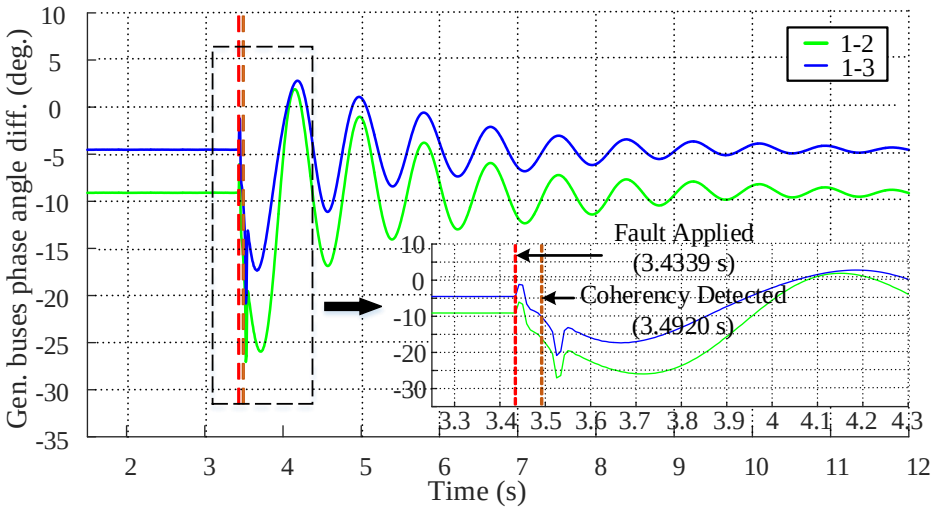

Figure 5.6: Generator bus voltage angles with respect to reference generator bus for the fault at bus 4 and fault cleared after 5 cycles

the coherency is declared. In Figure 5.7, instance of fault application, coherency detection and stable condition prediction are shown. The three consecutive prediction using each of

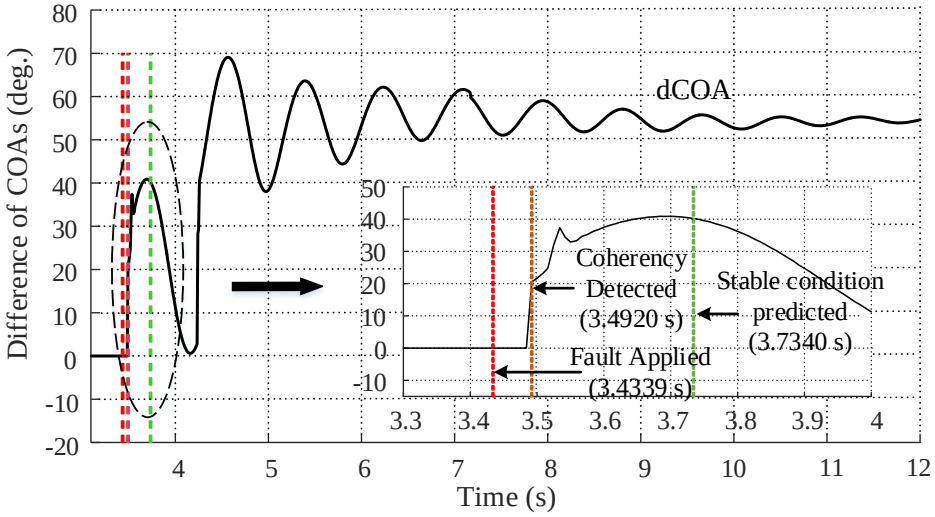

Figure 5.7: Difference of COAs for the fault at bus 4 and fault cleared after 5 cycles

20 samples observation window that meet the zero crossing to satisfy the stable condition criteria for the proposed method is shown in Figure 5.10. The stable condition was predicted

at 3.7340 s and the angular separation between the coherent groups at the instance is 40.2006 degrees.

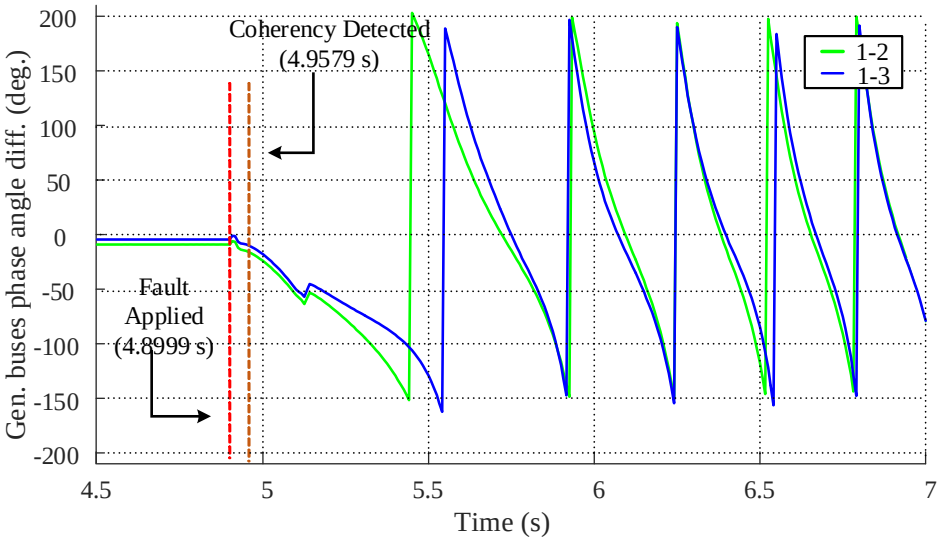

Figure 5.8: Generator bus voltage angles with respect to reference generator bus for fault at Bus 4 and fault cleared after 12 cycles

The fault duration is increased to 12 cycles (0.2 s) for the fault at Bus 4. The angular separation of the generator bus angles with respect to the reference generator bus angle is shown in Figure 5.8. All the other generator bus voltage angles deviate from the reference bus after the fault is applied at 2.3090 s. The center of angle for the two coherent groups are calculated as soon as the separation beyond 5 degrees is detected at 4.9579 s. At the same time, the difference of COAs is also calculated. This method waits for the first 20 samples to predict the future values of dCOA. The difference of COAs is predicted with the previously calculated samples of dCOA after the coherency is found. Figure 5.9 shows dCOA with the instance of fault application, coherency detection and stable condition prediction. Since the three consecutive prediction of difference of COAs has crossed the 180 degrees, the system becomes unstable. The last three observation windows and prediction window used to find the unstable condition is shown in Figure 5.11.

One more similar study is performed with the three phase fault applied at Bus 8 which

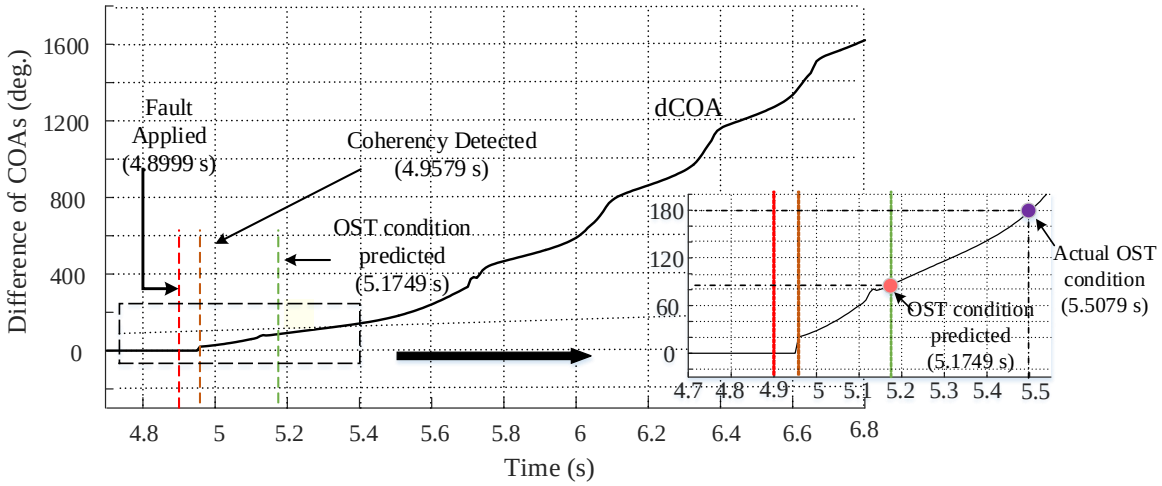

Figure 5.9: Difference of COAs for fault at Bus 4 and fault cleared after 12 cycles

is cleared after 6 cycles (0.1 s). The voltage angle swing, observed at different generator buses with respect to the reference generator bus, is shown in Figure 5.12. Machine 2 and 3 separate beyond 5 degrees from the reference machine at 0.04200 s after fault. Relay starts calculating center of angle of each group after the coherency is detected and machines begin forming 2 distinct groups. The relay waits for the 20 samples required to predicted the difference of COAs. Then the relay continues to perform prediction with arrival of each new sample. Once the 30 samples are available, relay use 30 samples to predict the future values. Figure 5.13 shows dCOA with the instance of fault application, coherency detection and stable condition prediction.

The three consecutive prediction using each of 30 samples observation window that meet the zero crossing to satisfy the stable condition criteria is shown in Figure 5.16. The stable condition was predicted at 4.1749 s and the angular separation between the coherent groups at the instance is 45.5995 degrees.

For the fault at same bus location, fault duration is increased to 11 cycles (0.1833 s). The plot of generator bus voltage angles for this fault is shown in Figure 5.14. The difference of COAs with the instance of fault application, coherency detection and stable condition prediction is shown in Figure 5.15 and the calculations are carried out as discussed earlier.

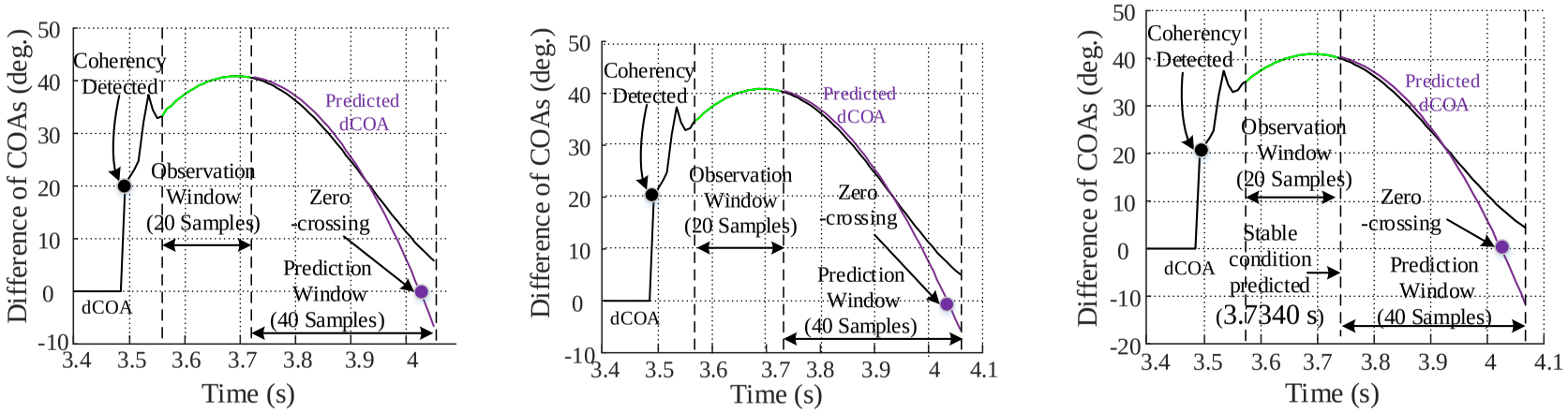

(a) First prediction

(b) Second prediction

(c) Third predicition

Figure 5.10: Three consecutive predictions before stable condition is declared for a 5 cycles fault at Bus 4

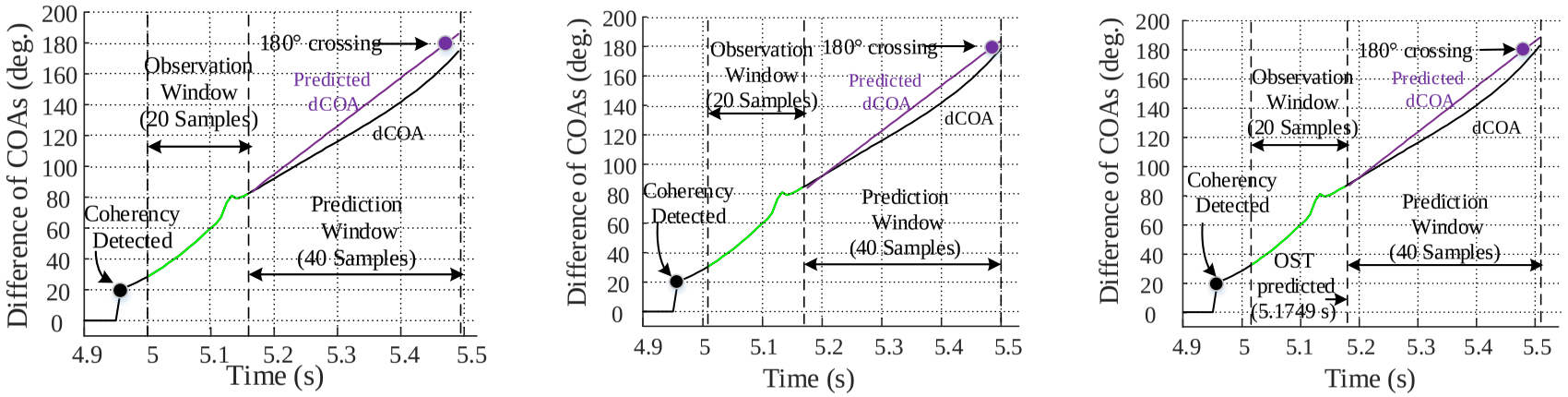

(a) First prediction

(b) Second prediction

(c) Third predicition

Figure 5.11: Three consecutive predictions before unstable condition is declared for 13 cycles fault at Bus 5

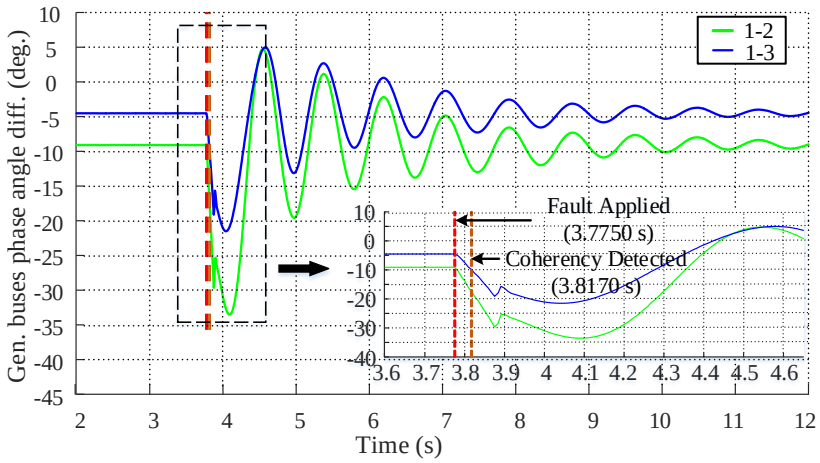

Figure 5.12: Generator bus voltage angles with respect to reference generator bus for fault at Bus 8 & fault cleared after 6 cycles

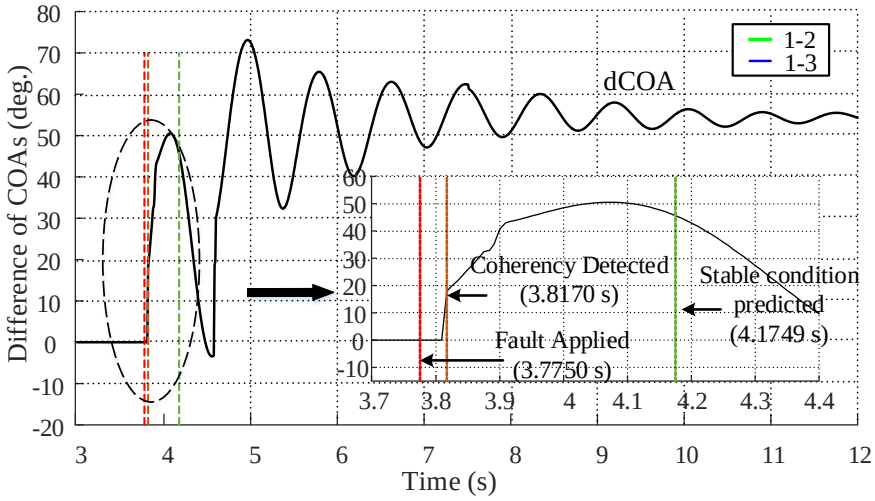

Figure 5.13: Difference of COAs for fault at Bus 8 & fault cleared after 6 cycles

Three successive predictions cross 180 degrees as shown in Figure 5.17, the system is detected to be unstable and the time of detection is 0.2580 s after the fault well ahead of actual out-of-step condition at 0.6000 s and the angular separation between the coherent groups at that instance is 83.7803 degrees.

Stability of system has been predicted for the fault at different locations using a similar

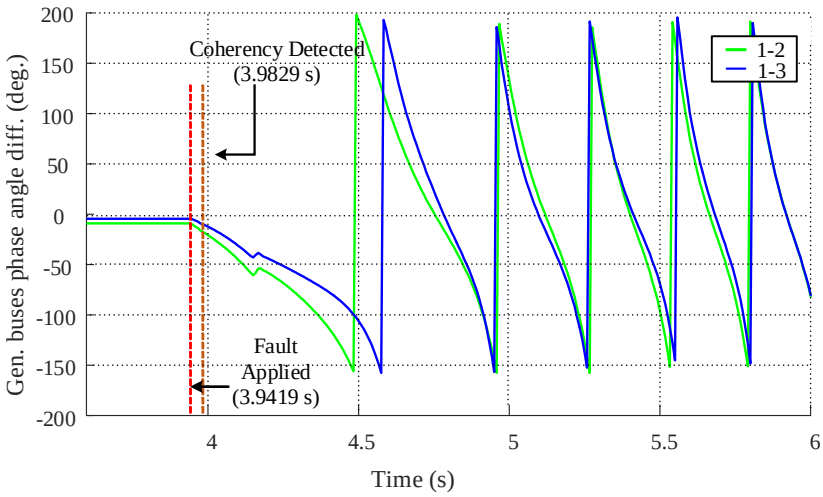

Figure 5.14: Generator bus voltage angles with respect to reference generator bus for fault at Bus 8 & fault cleared after 11 cycles

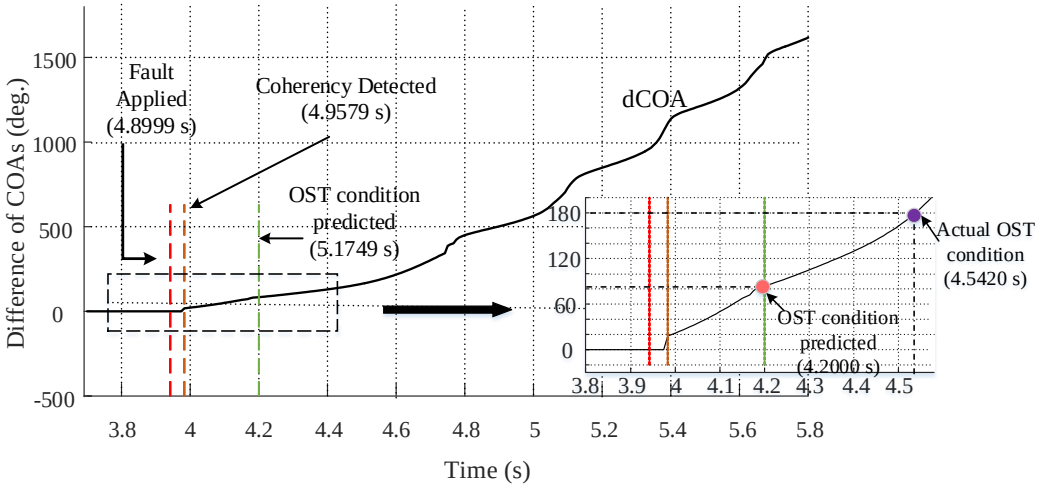

Figure 5.15: Difference of COAs for fault at Bus 8 & fault cleared after 11 cycles

procedure. The summary of those cases are shown in Table 5.3

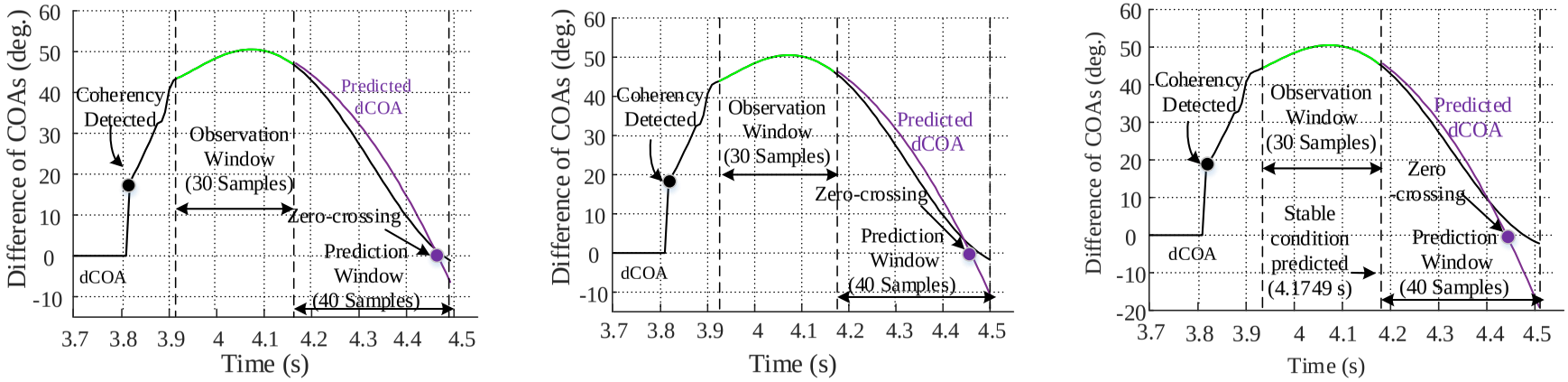

(a) First prediction

(b) Second prediction

(c) Third predicition

Figure 5.16: Three consecutive predictions before stable condition is declared for 6 cycles fault at Bus 8

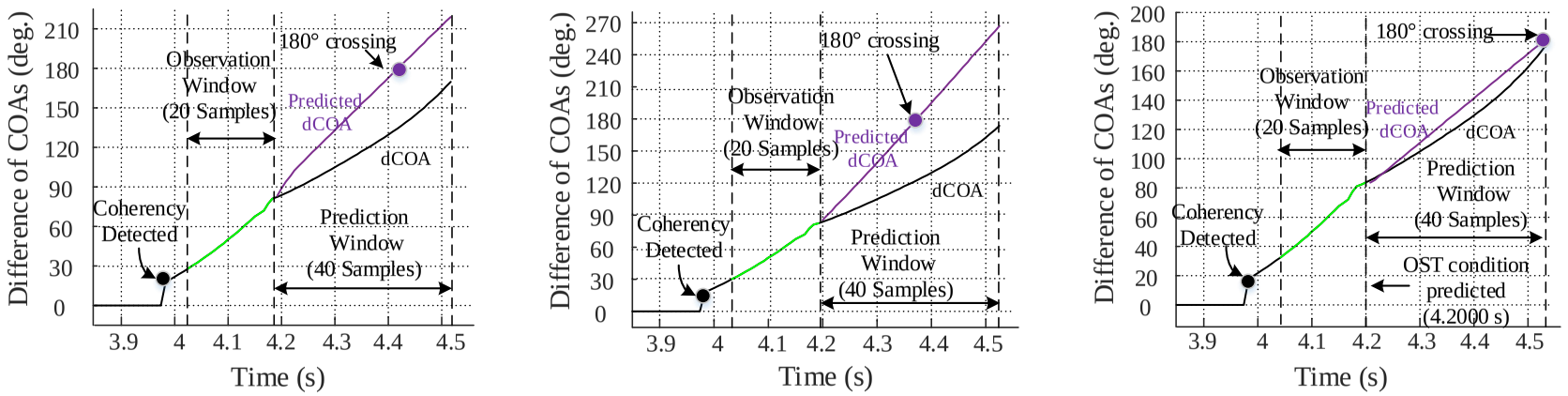

(a) First prediction

(b) Second prediction

(c) Third predicition

Figure 5.17: Three consecutive predictions before unstable condition is declared for 11 cycles fault at Bus 8

Table 5.3: Test results for instability prediction using swing curve

Fault Location	Fault dur. (*cycles*)	Coherency detected after fault (s)	Time of prediction (s)	Decision	dCOA (deg.)	Actual OST time (s)
Bus 4	5	0.0580	0.3000	Stable	40.2007	
	12	0.0579	0.2750	Unstable	85.8564	0.6080
Bus 5	6	0.0750	0.3920	Stable	35.9239	
	13	0.0749	0.6999	Unstable	131.9081	0.8829
Bus 7	4	0.0499	0.3830	Stable	37.6600	
	9	0.0510	0.5510	Unstable	127.9365	0.7340
Bus 9	6	0.0330	0.4000	Stable	43.8909	
	11	0.0339	0.4919	Unstable	123.3761	0.6910
Center of line 4-5	7	0.0660	0.4160	Stable	42.5614	
	12	0.0659	0.3749	Unstable	98.85453	0.7409
Center of line 4-6	8	0.0579	0.4410	Stable	42.0539	
	15	0.0579	0.2419	Unstable	64.2537	0.5919
Center of line 7-8	5	0.0500	0.3840	Stable	40.5215	
	10	0.0490	0.6250	Unstable	132.4642	0.7920

5.5 Summary

In this chapter, the proposed method was validated using actual PMUs in a GE N60 relay. The relay algorithm was validated using measurements from the optimal PMU location in a power system modelled in the RTDS and measured by the actual PMU in the N60 relay. Offline simulations were used to thoroughly validate the proposed method. Based on the experimental results, the prediction time using the actual PMU was found to be close to the prediction time using the virtual PMU in the RTDS. Prediction of stable and unstable cases for the WSCC 9 bus system, using the real PMU, is shown in Table 5.3.

Chapter 6

Conclusions

6.1 Summary

Power system protection can be categorized as local measurement-based or wide area-based protection. Local measurement-based protection methods use power system variables measured at specific points in the system. The operation of the relay is based on measurements at a given point. Wide area-based protection methods use the time-tagged synchronized measurements transferred by PMUs from different regions in the system. The availability of high-precision GPS clocks and a high-speed communication network along with PMUs have made real-time measurement possible. These real-time measurements represent the actual system conditions at a given time and are used for system level protection and remedial action schemes.

In this thesis, different types of out-of-step detection and prediction methods based on local measurements and wide area measurements were reviewed in the first chapter. The relaying functions implemented in local measurement based methods are the rate of change of impedance method [6, 15, 16, 18], swing center voltage method [6], rate of change of resistance method [19], EAC in time domain method [20], energy-based transient stability method [21, 22], third zone distance blocking scheme [23, 25], frequency deviation of voltage method [26], and power versus speed deviation method [27]. Accurate setting of blinders especially in large networks requires extensive *apriori* simulation studies and has been a problem for protection engineers using blinder based schemes. The settings are therefore made with certain assumptions of expected load conditions. The relays with these settings perform correctly for the assumed system conditions but may fail in the case of unforeseen

contingencies or boundary cases. The rate of change of impedance method and the R-Rdot method also require extensive simulation studies and have similar demerits to the blinder scheme. The SCV method uses the rate of change of voltage to detect a power swing. The SCV method usually detects the power swing at an angular separation of voltage close to 180 degrees. Operation of circuit breakers during the detection is delayed to reduce the stress that occurs at the 180 degree angular separation. Therefore, the instance when the angular separation is between 270 degrees to 360 degrees is favored for circuit breaker operation with this kind of method. EAC in time domain and energy-based transient stability methods are used for local generation protection and predicts OST conditions at higher values of angular separation. Third zone distance blocking scheme uses the relative speed of the equivalent SMIB system at the relay location of the entire system to determine the system stability. The frequency deviation of voltage method detects the unstable condition when the frequency measured at the point, where acceleration changes its sign from negative to positive, is greater than zero. Finding the OST condition using this method does not require the network parameters but poses practical issues while implementing the relaying application. The problem with this approach is inaccurate determination of frequency deviation especially during a fault due to the transient behavior of voltage angles. The power versus speed deviation method is an extension of the Voltage frequency deviation method and use generator speed deviation to detect instability. This method is less affected by switching transients, as the generator speed, due to the machine inertia, have smother change even during transient conditions but the rotor speed measurement has to be obtained from the physical measurement from turbine.

Wide area measurement based relaying functions utilized to determine the stability of the system are the EAC with PMU measurements [34], linear rotor angle prediction method [41], state plane method [36], polynomial rotor angle prediction method [42], finite difference based prediction method [43] and Post-disturbance voltage trajectory based OST prediction method [30, 31]. The EAC method involves the calculation of accelerating and decelerating areas using power-angle characteristics to find the instability condition. For large systems, EEAC [33] was proposed when the system separates into two oscillation groups. A relay

based on the EEAC approach using phasor measurements was implemented on the intertie between the states of Georgia and Florida in October 1993 and was operational until January 1995. The instability condition with the EEAC approach was also found at a large voltage angle of separation. It requires a step-by-step integration technique to calculate CCT. The linear rotor angle prediction method uses linear curve fitting of the generator rotor angle to identify the coherency among generators during a disturbance and the COAs of coherecnt groups to determine the stability. This method presents an adaptive relaying control but lacks the advance prediction. State plane analysis uses state plane plot of speed versus power angle utilizing WAMS measurements for larger power system configurations. CCA and CCT are used to predict the stability of the system, and complex calculations represent multi-machine system dynamic behavior with SMIB behavior after a disturbance using coherency analysis. The polynomial rotor angle prediction method uses the polynomial curve fitting method to determine the critical and non-critical groups and fundamental EAC to determine the stability of the equivalent SMIB derived for the identified groups. The performance of this method can be improved by using a larger number of samples to predict the stability of the system. The finite difference-based prediction method uses the rotor angle prediction using the finite difference method, and real-time data-mining-based clustering is used to identify the critical machines. The instability margin and time to instability are used to determine the stability using an SMIB equivalent of the separated system. Predictions can only be made for five samples ahead, which does not provide sufficient time for remedial action. Post-disturbance voltage trajectory-based OST prediction methods use the voltage magnitude at important buses to predict the stability of the system. The method in references [30, 31] uses pre-identified templates or boundary conditions to make predictions. The accuracy is highly dependent on the pre-calculated or pre-identified simulations. A new novel power versus integral of accelerating power method, which uses the electrical power and the integral of accelerating power of the generator to determine the stability of the system, was also investigated during the course of this research work. This method addresses the practical difficulties associated with deriving the rotor speed and acceleration in the frequency deviation of voltage method. This method uses the electrical power deviation instead of estimating the rotor acceleration and the integral of accelerating power instead

of directly estimating the rotor speed, and the measurements are available at the generator terminal. This method demonstrates potential for applications in out-of-step relaying and has benefits over the existing methods, including the frequency deviation of voltage method and the power versus speed deviation method. An SMIB system is used for the purpose of verifying the proposed local measurement-based method in Chapter 2. This method has also been included in the IEEE Power Systems Relaying Committee (PSRC) report by Working Group J5, entitled Application of Out-of-Step Protection Schemes for Generators.

The main focus of this thesis work was on a new technique based on synchrophasor measurement in WAMS to predict the stability of the system. The technique proposed is computationally simple. The main advantage of the proposed technique is that it uses an ARI time series model of swing curve for fast and accurate prediction of OST conditions. Faster prediction provides enough time for remedial action to prevent machine pole slipping, thereby preventing the system from becoming unstable. Implementation of the proposed relaying method is efficiently performed using PMU data and communicating the events and quantities (such as breaker status, voltage and currents, generator speeds, etc.) from different parts of the system to the relay. Considering the cost and amount of information to be processed for predicting the stability of the system, optimal PMU placement was determined. The optimal PMU location in the WSCC 9 bus system was studied for full observability of the system in Chapter 3. Measurements from the optimal PMU location are sufficient to assess the transient stability of the whole system.

The synchrophasor-based method was tested on a multi-machine power system configuration (WSCC 9 bus system). The PMU model in the RTDS uses the time-tagged voltage and current measurements from the optimal PMU locations. The voltage and current measurements from WAMS are utilized to find the swing angles. The prediction is based on representing the multi-machine dynamic behavior with a two-machine equivalent after the disturbance using coherency analysis. A time series analysis is done to predict the outcome of the evolving swing. Actual time series data of power swing having steady, continuous increasing, oscillating, or damping oscillation natures were represented using an ARI model instead of an AR model, which is only suitable for stationary data. Based on the simulation

results, the relay algorithm predicts both stable and unstable conditions accurately and, especially, well in advance of pole slipping occurring on generators or the two areas after severe disturbances.

The proposed method was also implemented with actual PMU measurements from a relay (General Electric (GE) N60 relay). The testing was carried out with an interface between the N60 relay and the RTDS. The WSCC 9 bus system was modelled in the simulator and the analog time signals from the optimal location in the network communicated to PMUs in the N60 relay. The synchronized phasor measurements from the actual PMU were used to evaluate and validate the proposed method. The simulations demonstrated the usefulness of these techniques for actual implementation. The results from the testing showed that the proposed scheme is accurate with respect to detecting instability in power system and the test results match quite well with results obtained from virtual PMU-based testing in the RTDS.

6.2 Thesis Contributions

Followings are the thesis contributions:

- *Power versus integral of accelerating power method:* A novel approach to detect the OST condition was investigated using real-time measurements of generator accelerating power. The state plane of the generator accelerating power and the integral of accelerating power were analyzed to detect instability conditions in power systems. In local measurement-based techniques, the speed and acceleration of the generator are calculated from the terminal voltage angles of the generator but are prone to errors due to the derivative terms. The derivative term introduces the error in the calculation and results in false power swing detection, with the error more dominant during the transient period. The proposed method overcomes the shortcomings of existing methods by using the integral of the accelerating power method, which eliminates the use of taking a derivative altogether.

- *Synchrophasor based transient stability prediction:* The major contribution of the research was to propose a synchrophasor-based method to predict the OST condition using an auto-regressive integrated time series model. The proposed method was tested with a multi-machine (WSCC 9 bus) system to predict the stability of the system. The fast and accurate swing prediction capabilities of the proposed scheme using a swing curve were demonstrated by performing numerous simulations. Predictions were made in advance of the generator groups reaching 180 degrees of angular separation. The proposed method quickly identifies the generators or generators separating into groups (within 100 ms) and applies a time series model to forecast the swing between the coherent groups. The ARI model used to predict the future sample swing could process the non-stationary time series data of the swing in the observation window and forecast future samples in the prediction window in order to determine whether the system is going to be stable or unstable.

- *Real-Time/EMT simulations based verification of proposed method:* EMT models are capable of accurately representing generator transient behavior. The RTDS simulator consists of custom hardware and software, specially designed to perform real-time EMT simulations. For all of the simulations carried out, the WSCC 9 bus system was modelled in the RTDS. The proposed method was compared with two industrial OST detection methods: the two blinder scheme method and the swing center voltage method. Test results show that the OST detection time required for the two blinder scheme is close to the prediction time of the proposed method whereas the SCV method takes longer to detect the OST condition.

- *Implementation of proposed method using an actual PMUs:* The proposed method was implemented using actual PMUs in a GE N60 relay. The performance of the proposed method was verified with actual PMUs in the relay interfaced with the RTDS; this approach is used by many manufacturing companies as a standard testing procedure. The prediction results obtained for the stability analysis of the WSCC 9 bus system using N60 PMUs were close to the results obtained from the stability analysis using virtual PMUs in the RTDS.

6.3 Future Work

- *Implementation of proposed techniques for large power system*: The implementation of the proposed algorithms was done for WSCC 9 bus test systems using the RTDS. With real-time digital simulation, the real-time behavior of the power system could be studied, which is helpful in offline testing of the proposed synchrophasor-based method. In real-time digital simulation, the power system is simulated with a fixed time step of 50 μs, and adequate processors are required to complete all calculations within that time step. Hence, the size of the power system that can be simulated depends on the processors available for the calculations. With the current processing capacity of the RTDS available in the power system research laboratory, an WSCC 9 bus system could be simulated. Interfacing the relay with the RTDS also requires a GTAO card within the RTDS to convert the digital current and voltage signals to analog signals. The channel capacity in the available GTAO card was not sufficient to validate the commercial relay for implementation in larger systems. Simulations of a large power system (such as an IEEE 39-bus test system) would require an upgrade to the RTDS facility with additional processing power and analog output cards.

- *Real time implementation of proposed techniques*: An offline simulation was performed for the proposed method using archived phasor information from the PDC. Real-time implementation of the proposed method using RTDS and the synchrophasor processor could be studied for closed loop testing. Currently, the phasor data concentrators are mostly used for collecting the stream of data per C37.118 and utilizing it for power flow monitoring, analyzing the wide area system events, and archiving system performance. A microprocessor-based processing device that receives the synchronized phasor stream from relays at optimal locations, time aligns these data, implements the time series prediction, and sends the trip or blocking signal based on the stability analysis performed in the processor can be studied in detail.

- *Intelligent islanding after instability detection*: The separation of the system into islands after an out-of-step condition is determined is necessary to avoid system collapse.

When a disturbance condition leads to instability between two coherent groups of generators, the power system is separated into islands containing sufficient generation and load. After separation into islands, each island has to establish load and generation balance for continuous operation at a safe system frequency. Islands having excess generation need to shed generation whereas islands having excess load need to shed load. Wide area measurements from PMUs can be used to identify desired boundaries of separation depending on which generators have formed a coherent group as well as what loads and generation within the islands to be formed would be controllable to the desired extent. This usually requires out-of-step blocking at undesirable points of separation and out-of-step tripping at desired locations to form the islands.

References

[1] "Oecd factbook 2011-2012," http://www.oecd-ilibrary.org (accessed on 21-Aug-2016), 2011.

[2] P. Kundur, *Power System Stability and Control*. The EPRI Power System Engineering Series, New York: TATA McGraw-Hill, 2004.

[3] S. H. Horowitz and A. G. Phadke, *Power System Relaying*, 3rd ed. John Wiley & Sons, New York, 2008.

[4] J. L. Blackburn and T. J. Domin, *Protective Relaying Principles and Applications*, 3rd ed. CRC Press, Taylor & Francis Group, 2007.

[5] Project Group Turkey, "Report on Blackout in Turkey on 31st March 2015 Final Version 1.0," https://www.entsoe.eu/publications/system-operations-reports/continental-europe/Pages/default.aspx (accessed on 25-Aug-2016), Tech. Rep., Sep 2015.

[6] "Power swing and out-of-step considerations on transmission lines," *IEEE PERC WG D6*, June 2005.

[7] D. Novosel, G. Bartok, G. Henneberg, P. Mysore, D. Tziouvaras, and S. Ward, "IEEE PSRC Report on Performance of Relaying During Wide-Area Stressed Conditions," *IEEE Transactions on Power Delivery*, vol. 25, no. 1, pp. 3 –16, jan. 2010.

[8] "Wide area protection and emergency control," *IEEE PSRC WG D6*, 2002.

[9] M. G. Adamiak, A. P. Apostolov, M. M. Begovic, C. F. Henville, K. E. Martin, G. L. Michel, A. G. Phadke, and J. S. Thorp, "Wide area protection—technology and infrastructures," *IEEE Transactions on Power Delivery*, vol. 21, no. 2, pp. 601–609, 2006.

[10] A. G. Phadke and J. S. Thorp, *Computer Relaying for Power Systems*, 2nd ed. John Wiley & Sons, New York, 2009.

[11] P. Kundur, J. Paserba, V. Ajjarapu, G. Andersson, A. Bose, C. Canizares, N. Hatziargyriou, D. Hill, A. Stankovic, C. Taylor, T. Van Cutsem, and V. Vittal, "Definition and classification of power system stability IEEE/CIGRE joint task force on stability terms and definitions," *IEEE Transactions on Power Systems*, vol. 19, no. 3, pp. 1387 – 1401, aug. 2004.

[12] W. A. Elmore, *Protective Relaying Theory and Applications*, 2nd ed. New York: Marcel Decker, Inc., 2004.

[13] V. Madani, D. Novosel, S. Horowitz, M. Adamiak, J. Amantegui, D. Karlsson, S. Imai, and A. Apostolov, "IEEE PSRC Report on Global Industry Experiences With System Integrity Protection Schemes (SIPS)," *IEEE Transactions on Power Delivery*, pp. pp. 2143–2155, 2010.

[14] *Network Protection and Automation Guide.* Areva, July,2002.

[15] *N60 Network Stability and Synchrophasor Measurement System UR Series Instruction Manual*, N60 revision: 6.0x ed., GE Multilin, 2011.

[16] P. Mooney and N. Fischer, "Application guidelines for power swing detection on transmission systems," in *Protective Relay Engineers, 2006. 59th Annual Conference for*, 0-0 2006, p. 10 pp.

[17] F. Plumptre, S. Brettschneider, A. Hiebert, M. Thompson, and M. Mynam, "Validation of out-of-step protection with a real time digital simulator," in *proceedings of the 33rd Annual Western Protective Relay Conference*, October, 2006.

[18] J. Blumschein, Y. Yelgin, and M. Kereit, "Proper detection and treatment of power swing to reduce the risk of blackouts," in *Electric Utility Deregulation and Restructuring and Power Technologies, 2008. DRPT 2008. Third International Conference on*, April 2008, pp. 2440–2446.

[19] C. Taylor, J. Haner, L. Hill, W. Mittelstadt, and R. Cresap, "A new out-of-step relay with rate of change of apparent resistance augmentation," *IEEE Transactions on Power Apparatus and Systems*, vol. PAS-102, no. 3, pp. 631 –639, march 1983.

[20] S. Paudyal, G. Ramakrishna, and M. Sachdev, "Out-of-step protection using the equal area criterion in time domain - smib and 3-machine case studies," in *TENCON 2008 - 2008 IEEE Region 10 Conference*, nov. 2008, pp. 1 –6.

[21] E. Farantatos, R. Huang, G. J. Cokkinides, and A. P. Meliopoulos, "A predictive out of step protection scheme based on pmu enabled dynamic state estimation," *IEEE PES General Meeting 2011*, 2011.

[22] E. Farantatos, R. Huang, G. J. Cokkinides, and A. P. Meliopoulos, "A predictive generator out-of-step protection and transient stability monitoring scheme enabled by a distributed dynamic state estimator," *IEEE Transactions on Power Delivery*, vol. 31, no. 4, pp. 1826–1835, Aug 2016.

[23] S. H. Horowitz and A. G. Phadke, "Third zone revisited," *IEEE Transactions on Power Delivery*, vol. 21, no. 1, pp. 23–29, Jan 2006.

[24] "Application of overreaching distance relays," *IEEE PSRC WG D4*, 2009.

[25] D. Kang and R. Gokaraju, "A new method for blocking third-zone distance relays during stable power swings," *IEEE Transactions on Power Delivery*, vol. 31, no. 4, pp. 1836–1843, Aug 2016.

[26] K. H. So, J. Y. Heo, C. H. Kim, R. K. Aggarwal, and K. B. Song, "Out-of-step detection algorithm using frequency deviation of voltage," *IET Generation, Transmission & Distribution*, vol. 1, no. 1, pp. 119–126, 2007.

[27] B. Shrestha, P. Sharma, and R. Gokaraju, "Out-of-step protection using the analysis of electrical power vs speed deviation in state plane," in *IEEE PES ISGT Europe 2013*, Oct 2013, pp. 1–5.

[28] "Draft-12, application of out-of-step protection schemes for generators," *IEEE PERC WG J5*, June 2016.

[29] E. S. Subcommittee, *IEEE Tutorial Course Power System Stabilization via Excitation Control*, Sponsored by Energy Development and Power Generation Committee, IEEE Power Engineering Society Life Long Learning Committee, 2007, 09TP250.

[30] A. Rajapakse, F. Gomez, K. Nanayakkara, P. Crossley, and V. Terzija, "Rotor angle instability prediction using post-disturbance voltage trajectories," in *IEEE PES General Meeting*, July 2010, pp. 1–1.

[31] D. R. Gurusinghe and A. D. Rajapakse, "Post-disturbance transient stability status prediction using synchrophasor measurements," *IEEE Transactions on Power Systems*, vol. 31, no. 5, pp. 3656–3664, Sept 2016.

[32] W. D. Stevenson, *Elements of Power System Analysis*. McGraw-Hill, 1982.

[33] Y. Xue, T. Van Custem, and M. Ribbens-Pavella, "Extended equal area criterion justifications, generalizations, applications," *IEEE Transactions on Power Systems*, vol. 4, no. 1, pp. 44–52, 1989.

[34] B. B. Monchusi, Y. Mitani, L. Changsong, and S. Dechanupaprittha, "Pmu based power system stability analysis," in *TENCON 2008 - 2008 IEEE Region 10 Conference*, Nov 2008, pp. 1–5.

[35] V. Centeno, A. Phadke, A. Edris, J. Benton, M. Gaudi, and G. Michel, "An adaptive out-of-step relay," *IEEE Transactions on Power Delivery*, vol. 12, no. 1, pp. 61 –71, 1997.

[36] B. Shrestha, "A fast method for out-of-step protection using state plane trajectories analysis," Master's thesis, University of Saskatchewan, 2011.

[37] B. Shrestha, R. Gokaraju, and M. Sachdev, "Out-of-step protection using state-plane trajectories analysis," *IEEE Transactions on Power Delivery*, vol. 28, no. 2, pp. 1083–1093, April 2013.

[38] W. Rebizant and K. Feser, "Fuzzy logic application to out-of-step protection of generators," in *Proc. IEEE Power Engineering Society Summer Meeting*, vol. 2, 2001, pp. 927–932.

[39] A. Abdelaziz, M. Irving, M. Mansour, A. El-Arabaty, and A. Nosseir, "Adaptive protection strategies for detecting power system out-of-step conditions using neural networks," *Generation, Transmission and Distribution, IEE Proceedings-*, vol. 145, no. 4, pp. 387 –394, jul 1998.

[40] A. D. Rajapakse, F. Gomez, K. Nanayakkara, P. A. Crossley, and V. V. Terzija, "Rotor angle instability prediction using post-disturbance voltage trajectories," *IEEE Transactions on Power Systems*, vol. 25, no. 2, pp. 947–956, 2010.

[41] D. Fan and V. Centeno, "Adaptive out-of-step protection schemes based on synchrophasors," in *2014 IEEE PES General Meeting — Conference Exposition*, July 2014, pp. 1–5.

[42] J. Hazra, R. K. Reddi, K. Das, D. P. Seetharam, and A. K. Sinha, "Power grid transient stability prediction using wide area synchrophasor measurements," in *2012 3rd IEEE PES Innovative Smart Grid Technologies Europe (ISGT Europe)*, Oct 2012, pp. 1–8.

[43] D. E. Echeverra, J. L. Rueda, J. C. Cepeda, D. G. Colom, and I. Erlich, "Comprehensive approach for prediction and assessment of power system transient stability in real-time," in *IEEE PES ISGT Europe 2013*, Oct 2013, pp. 1–5.

[44] L. L. Grigsby, Ed., *Electric Power Engineering Handbook*. CRC Press, Taylor & Francis Group, 2007.

[45] *Application Manual REL 531*2.3*, ABB.

[46] J. Berdy, *Application of Out-of-Step Blocking and Tripping Relays*, General Electric Company.

[47] "Ieee standard for ac high voltage generator circuit breakers rated on a symmetrical current basis," *IEEE Std C37.013-1993*, pp. 1–96, Oct 1993.

[48] J. M. Haner, T. D. Laughlin, and C. W. Taylor, "Experience with the r-rdot out-of-step relay," *IEEE Power Engineering Review*, no. 4, pp. 28–29, 1986.

[49] D. Hou, G. Benmouyal, and D. Tziouvaras, "Zero-setting power-swing blocking protection," *IEEE Conference Publications*, vol. 2005, no. CP508, pp. 249–254, 2005. [Online]. Available: http://link.aip.org/link/abstract/IEECPS/v2005/iCP508/p249/s1

[50] M. A. M. Ariff and B. C. Pal, "Adaptive protection and control in the power system for wide-area blackout prevention," *IEEE Transactions on Power Delivery*, vol. 31, no. 4, pp. 1815–1825, Aug 2016.

[51] P. Sharma, "Fast methods for transient stability prediction in large power systems and wind interconnected power systems," Master's thesis, University of Saskatchewan, 2013.

[52] A. G. Phadke and J. S. Thorp, *Synchronized phasor measurements and their applications*. Springer Science & Business Media, 2008.

[53] E. O. Schweitzer III and A. Guzman, "Synchrophasor processor detects out-of-step conditions," in *Smart Grid Communications (SmartGridComm), 2011 IEEE International Conference on*. IEEE, 2011, pp. 576–581.

[54] K. E. Martin, G. Benmouyal, M. G. Adamiak, M. Begovic, R. O. Burnett, K. R. Carr, A. Cobb, J. A. Kusters, S. H. Horowitz, G. R. Jensen, G. L. Michel, R. J. Murphy, A. G. Phadke, M. S. Sachdev, and J. S. Thorp, "IEEE Standard for Synchrophasors for Power Systems," *IEEE Transactions on Power Delivery*, vol. 13, no. 1, pp. 73–77, Jan 1998.

[55] *RTDS Manuals*, RTDS Technologies Inc., Winnipeg , Canada.

[56] S. Chakrabarti, E. Kyriakides, and D. G. Eliades, "Placement of synchronized measurements for power system observability," *IEEE Transactions on Power Delivery*, vol. 24, no. 1, pp. 12–19, Jan 2009.

[57] S. G. I. G. Program, "Factor affecting pmu installation costs," U.S. Department of Energy, Electricity Delivery & Enery Reliability, Tech. Rep., 2014.

[58] P. Anderson and A. Fouad, *Power System Control and Stability*, 1st ed. The Iowa State University Press, 1980, vol. 1.

[59] A. G. Phadke, "Wide area measurement applications for improved protection," dec 2010.

[60] "Ieee recommended practice for excitation system models for power system stability studies," *IEEE Std 421.5-2005 (Revision of IEEE Std 421.5-1992)*, pp. 1–93, April 2006.

[61] G. E. P. Box, G. M. Jenkins, and G. C. Reinsel, *Time Series Analysis Forecasting and Control*. John Wiley & Sons, Inc., 2008.

[62] *Econometrics Toolbox, MATLAB version 8.5.0.197613 (R2015a)*, The Mathworks, Inc., 2015.

[63] D. C. Montgomery, C. L. Jennings, and M. Kulahci, *Introduction to time series analysis and forecasting*. John Wiley & Sons, 2008.

[64] N. G. Bretas and A. G. Phadke, "Real time instability prediction through adaptive time series coefficients," in *Power Engineering Society 1999 Winter Meeting, IEEE*, vol. 1, Jan 1999, pp. 731–736 vol.1.

[65] D. X. Du, Z. Q. Bo, Z. X. Zhou, A. Perks, L. Denning, and B. Smith, "An advanced real time digital simulator based test system for protection relays," in *Proc. 41st Int. Universities Power Engineering Conf. UPEC '06*, vol. 3, 2006, pp. 851–855.

[66] P. Forsyth, T. Maguire, and R. Kuffel, "Real time digital simulation for control and protection system testing," in *Proc. IEEE 35th Annual Power Electronics Specialists Conf. PESC 04*, vol. 1, 2004, pp. 329–335.

[67] D. A. Tziouvaras and D. Hou, "Out-of-step protection fundamentals and advancements," in *Proc. 57th Annual Conf Protective Relay Engineers for*, 2004, pp. 282–307.

[68] G. Ziegler, *Numerical Distance Protection:Principles and Applications*, B. Siemens Aktiengesellschaft and Munchen, Eds. Publicis Corporate Publishing,Erlangen, 2008.

[69] B. Course Co-ordinated by Indian Institute of Technology, "Web course on power system protection," http://nptel.ac.in/courses/108101039/ (accessed on 21-Jul-2016), dec 2009, module 7, Lecture 25.

Appendix A

System data

A.1 SMIB Test System Parameters

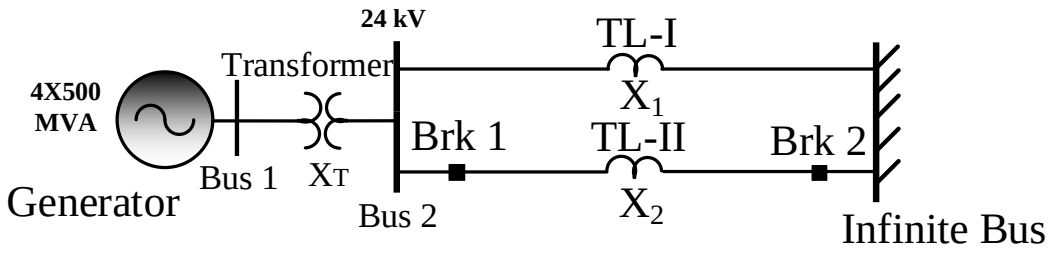

Base MVA=2220 MVA, Base kV=24 kV

Generator data:

2220 MVA, 24 kV, $r_a = 0.00125$ $p.u.$, $x_l = 0.163$ $p.u.$, $x_d = 1.81$ $p.u.$, $x_q = 1.76$ $p.u.$, $x'_d = 0.3$ $p.u.$, $x'_q = 0.65$ $p.u.$, $x''_d = 0.23$ $p.u.$, $x''_q = 0.25$ $p.u.$, $T'_{d0} = 8$ s, $T''_{d0} = 0.03$ s, $T'_{q0} = 1$ s, $T''_{q0} = 0.07$ s, $InertiaConstant(H) = 3.5$ s, $Frequency = 60$ Hz

Impedances:

$X_T = j0.15$ $p.u.$, $TL - I = j0.5$ $p.u.$, $TL - II = j0.93$ $p.u.$

Infinite Bus Voltage=0.9 $p.u.$

A.2 WSCC 9 Bus System Test System Parameters

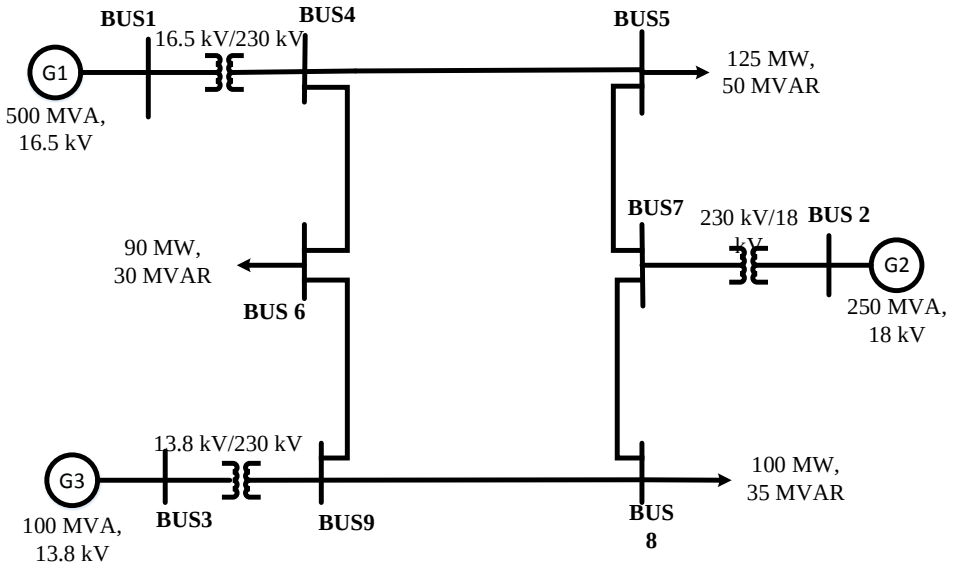

Table A.2: Transformer data(100 MVA base)

Transformer	$T1$	$T2$	$T3$
kV	16.5/230	18/230	13.8/230
X_T	0.0576	0.0625	0.0586

Table A.3: Line data(100 MVA base)

From Bus	To Bus	R	X	B/2
4	5	0.0100	0.0850	0.0880
4	6	0.0170	0.0920	0.0790
5	7	0.0320	0.1610	0.1530
6	9	0.0390	0.1700	0.1790
7	8	0.0085	0.0720	0.0745
8	9	0.0119	0.1008	0.1045

Table A.1: Generator data(100 MVA base)

Generator	$G1$	$G2$	$G3$
Rated MVA	500	250	100
kV	16.5	18	13.8
X_d	0.1460	0.8958	1.3125
X'_d	0.0608	0.1198	0.1813
X''_d	0.0400	0.0900	0.1500
X_q	0.0969	0.8644	1.2578
X'_q	0.0969	0.1969	0.2500
X''_q	0.0400	0.0900	0.1500
X_l	0.0300	0.0600	0.1200
T_do'	8.9600	6.0000	5.8900
T_qo'	0.3100	0.5350	0.6000
T_do''	0.0300	0.0300	0.0300
T_qo''	0.0500	0.0500	0.0500
H	23.6400	6.4000	3.0100

Table A.4: Load flow data (100 MVA base)

Bus	Type	Voltage (p.u.)	Load		Generator		Unit No.
			MW	MVar	MW	MVar	
1	PV	1.0400	0.0	0.0	71.60	27.10	Gen1
2	PV	1.0250	0.0	0.0	163.00	6.70	Gen2
3	PV	1.025	0.00	0.00	85.00	-10.90	Gen3
4	PQ	1.0260	0.00	0.00	0.0	0.0	
5	PQ	0.9997	125.00	50.00	0.0	0.0	
6	PQ	1.0123	90.00	30.00	0.0	0.0	
7	PQ	1.0268	0	0	0.0	0.0	
8	PQ	1.0173	100.00	35.00	0.0	0.0	
9	PQ	1.0327	0.0	0.0	0.0	0.0	

A.3 IEEE 12-Bus System Test System Parameters

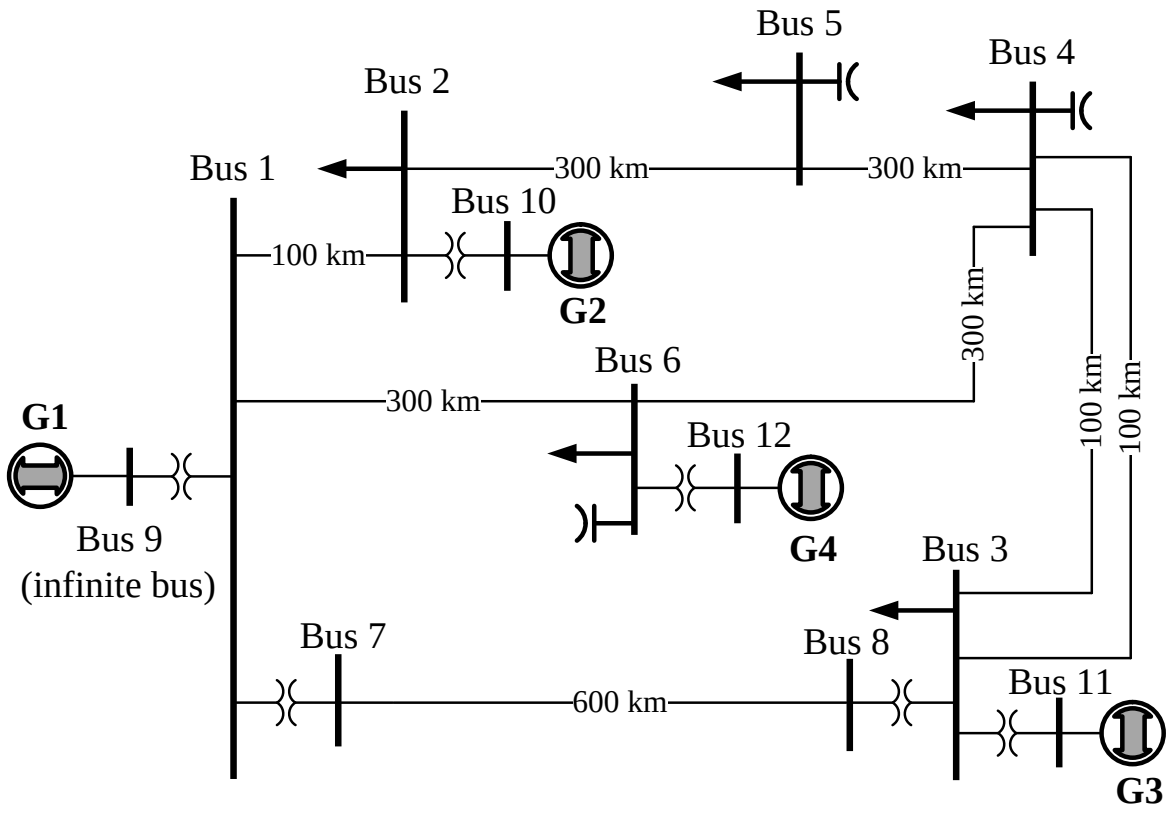

Table A.5: Bus Data

Bus No.	Nominal Voltage (kV)	Specified Voltage (p.u.)	Load (MVA)	Shunt (MVAr)	Generation (MW)
1	230				
2	230		280+j200		
3	230		320+j240		
4	230		320+j240	160	
5	230		100+j60	80	
6	230		440+j300	180	
7	345				
8	345				
9	22	1.05 (infinite bus)			
10	22	1.02			500
11	22	1.01			200
12	22	1.02			300

Table A.6: Transformer Data (100 MVA base)

From-To	Voltage (kV)	Leakage Reactance(pu)	Rating (MVA)
1-7	230-345	0.0100	1000
1-9	230-22	0.0100	1000
2-10	230-22	0.0100	1000
3-8	230-345	0.0100	1000
3-11	230-22	0.0100	1000
6-12	230-22	0.0200	500

Table A.7: Generator and Exciter Data

Bus	H	Leakage D	T'_{do}	X_d	X_q	X'_d	K_a	T_a
10(G2)	5.0	1.0	5.0	1.5	1.2	0.4	20	0.05
11(G3)	3.0	0.0	6.0	1.4	1.35	0.3	20	0.05
12(G4)	5.0	1.0	5.0	1.5	1.2	0.4	20	0.05

Table A.8: Branch Data (100 MVA Base)

Line	Voltage (kV)	Length (km)	R(pu)	X(pu)	B(pu)	Rating (MVA)
1-2	230	100	0.01144	0.09111	0.18261	250
1-6	230	300	0.03356	0.26656	0.55477	250
2-5	230	300	0.03356	0.26656	0.55477	250
3-4(1)	230	100	0.01144	0.09111	0.18261	250
3-4(2)	230	100	0.01144	0.09111	0.18261	250
4-5	230	300	0.03356	0.26656	0.55477	250
4-6	230	300	0.03356	0.26656	0.55477	250
7-8	345	600	0.01595	0.17214	3.28530	500

Appendix B

B.1 Guidelines for Blinder Settings

Most of the blinder settings are implemented using the following guidelines:

* RRO: Set the outer resistive blinder inside the maximum possible load with some safety margin.

* RRI: Set the inner resistive blinder out side the most overreaching protective zone that is to be blocked when the power swing occurs. Some safety margin should be applied between the blinder and the outer most relay characteristics.

* LRO: Same as RRO but in negative direction.

* LRI: Same as RRI but in negative direction.

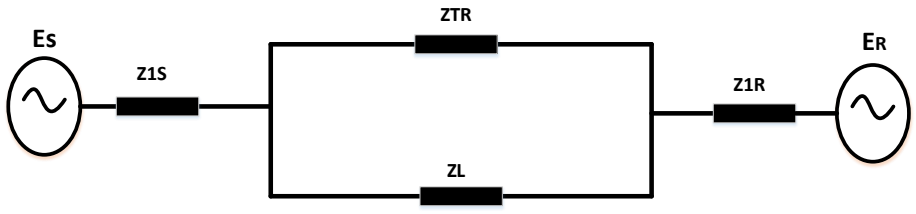

Figure B.1: Two machine equivalent

Based on the inner and outer blinders setting, power swing blocking time delay (PSBD) can be calculated using relation (B.1). PSBD is the time set to distinguish between power swing and fault. The distance relays equipped with this scheme is blocked for this time duration. If the swing is detected the blocking signal must be maintained until the impedance

exits the outer blinder or until the a fixed time delay [68]. The PSBD should represent a reasonable time delay to ensure secure decision without impacting the operation of PSB element.

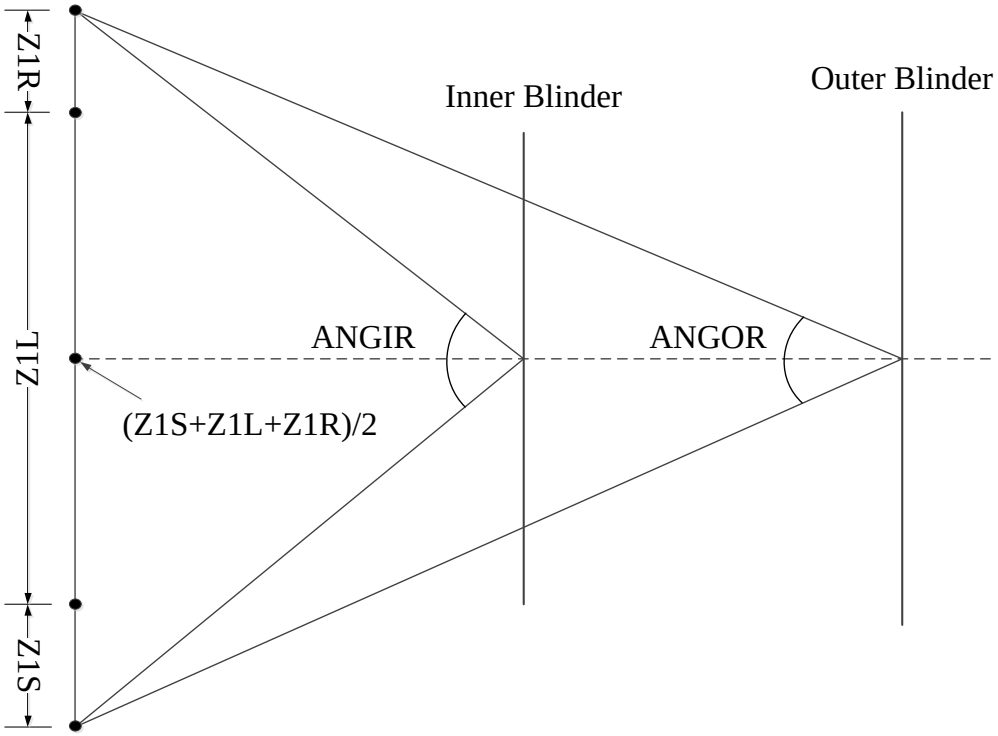

Figure B.2: Equivalent Source Angles During Power Swing

$$PSBD = \frac{(ANGIR - ANGOR) * F_{nom}}{360 * F_{slip}} \tag{B.1}$$

Where,

$ANGIR$: Machine angle at inner blinder

$ANGOR$: Machine angle at outer blinder

F_{nom}: System nominal frequency in Hz

F_{slip}: Power swing slip rate in Hz

$Z1L$: $ZTR||ZL$

Appendix C

Analysis of Power Swing in Multi-machine system

Reference [69] has explained the steps to analyze the power swing in multi-machine system.

C.1 Analysis of Tranmission Network

The two machine equivalent at the end of the transmission line can be used to analyze the swing in the nulti-machine system as shown in Figure C.1.

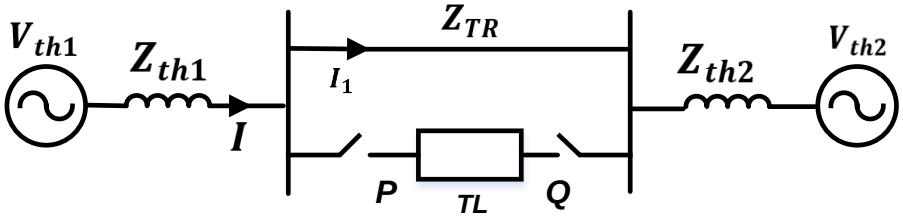

Figure C.1: Thevenin's equivalent of multi-machine system

Where V_{th1} and V_{th2} are the equivalent Thevenin's sources behind the terminal p and q, Z_{TR} is the transfer impedance between the node p and q and the transmission line is connected across the terminal node p and q.

Computation of Thevenin's equivalent parameter across P and Q with the line PQ being disconnected is carried out and Z_{bus} matrix is formed. The admittance matrix of the power

system is given by,

$$[I] = [Y_{bus}][V] \tag{C.1}$$

Considering the Y_{bus} is invertible, equivalent Z_{bus} model is given by,

$$[V] = [Z_{bus}][I] \; and \tag{C.2}$$

$$[\Delta V] = [Z_{bus}][\Delta I] \tag{C.3}$$

C.2 Two Source Equivalent Reduction

The current from the p end of the transmission line is I_{pq} and I_{qp} at the q end while connected as shown in the Figure C.2. The effect of transmission line can be evaluated by superimposing injected currents under assumption of linearity as $\Delta I_p = -I_{pq}$ and $\Delta I_q = I_{pq}$ when line pq is disconnected. Characterizing behavior at bus p and q and ignoring the remaining rows the Equation (C.3) can be written as,

$$\begin{bmatrix} \Delta V_p \\ \Delta V_q \end{bmatrix} = \begin{bmatrix} Z_{pp} & Z_{pq} \\ Z_{qp} & Z_{qq} \end{bmatrix} \begin{bmatrix} \Delta I_p \\ \Delta I_q \end{bmatrix} \tag{C.4}$$

Equivalently, Equation (C.4) can be written as,

$$\begin{bmatrix} \Delta I_p \\ \Delta I_q \end{bmatrix} = \begin{bmatrix} \hat{Y_{pp}} & \hat{Y_{pq}} \\ \hat{Y_{qp}} & \hat{Y_{qq}} \end{bmatrix} \begin{bmatrix} \Delta V_p \\ \Delta V_q \end{bmatrix} \tag{C.5}$$

Where $[Y]$ matrix is inverse of $[Z]$ matrix of size 2x2.

The equivalent circuit in Figure C.1 can be reduced as shown in Figure C.3 and equations can be written as,

$$\begin{bmatrix} \frac{V_{th1}}{Z_{th1}} \\ \frac{V_{th2}}{Z_{th2}} \end{bmatrix} = \begin{bmatrix} \frac{1}{Z_{th1}} + \frac{1}{Z_{TR}} & -\frac{1}{Z_{TR}} \\ -\frac{1}{Z_{TR}} & \frac{1}{Z_{th2}} + \frac{1}{Z_{TR}} \end{bmatrix} \begin{bmatrix} V_p \\ V_q \end{bmatrix} \tag{C.6}$$

The incremental model is given by,

$$\begin{bmatrix} \Delta I_p \\ \Delta I_q \end{bmatrix} = \begin{bmatrix} \frac{1}{Z_{th1}} + \frac{1}{Z_{TR}} & -\frac{1}{Z_{TR}} \\ -\frac{1}{Z_{TR}} & \frac{1}{Z_{th2}} + \frac{1}{Z_{TR}} \end{bmatrix} \begin{bmatrix} \Delta V_p \\ \Delta V_q \end{bmatrix} \tag{C.7}$$

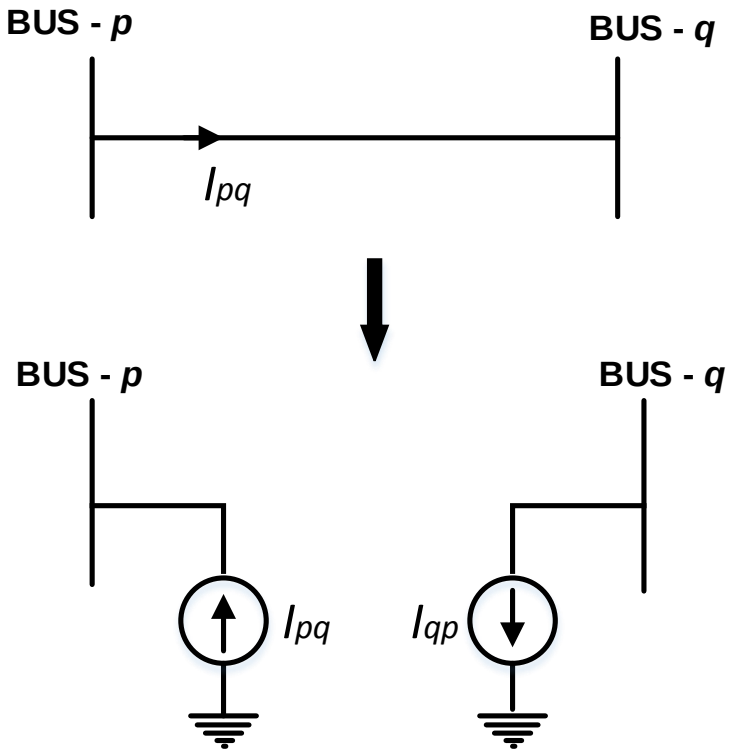

Figure C.2: Superimposing of injected current

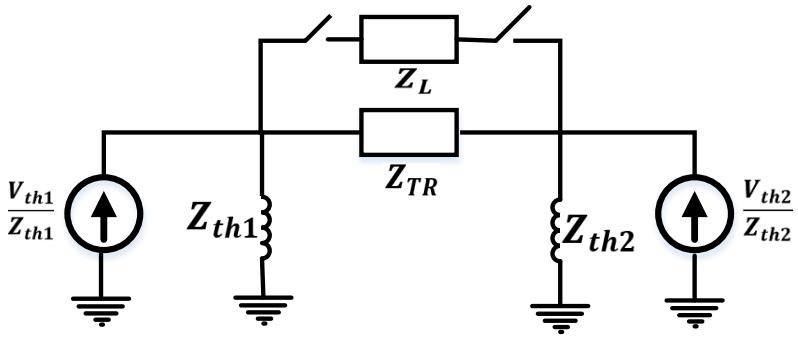

Figure C.3: Two source equivalent circuit

Therfore, equating Equation(C.5) and (C.7)

$$Z_{TR} = -\frac{1}{\hat{Y_{pq}}} \tag{C.8}$$

$$\frac{1}{Z_{th1}} = \hat{Y_{pp}} - \frac{1}{Z_{TR}} = \hat{Y_{pp}} + \hat{Y_{pq}} \tag{C.9}$$

$$\frac{1}{Z_{th2}} = \hat{Y_{qq}} - \frac{1}{Z_{TR}} = \hat{Y_{qq}} + \hat{Y_{pq}} \tag{C.10}$$

C.3 Determination of Power Swing Trajectory for Multi-machine System

After the two source equivalent reduction, the final equivalent circuit of multi-machine is shown in Figure C.4. The equivalent voltage source E_A leads E_B by angle δ.

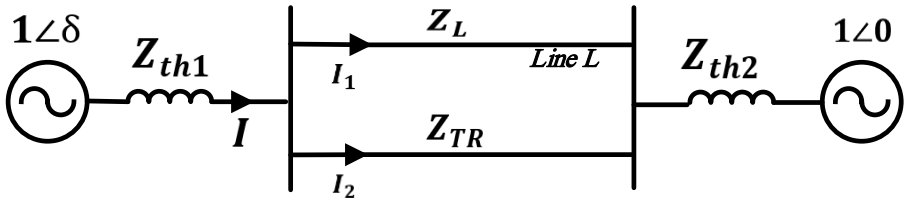

Figure C.4: Equivalent circuit of multi-machine system

The total impedance, $Z_T = Z_{th1} + Z_L||Z_{TR} + Z_{th2}$

Impedance seen by the relay at line L is

$$Z_{relay} = \frac{1\angle\delta - Z_{th1}I}{I_1}, \qquad where\ I_1 = \frac{Z_{TR}}{Z_L + Z_{TR}}I \tag{C.11}$$

Therefore,

$$Z_{relay} = \frac{1}{k}[-Z_{th1} + \frac{Z_T}{2} - j(cot(\frac{\delta}{2}))\frac{Z_T}{2}] \qquad where, k = \frac{Z_{TR}}{Z_L + Z_{TR}} \tag{C.12}$$

In order to determine whether the electrical center is formed on the line L, value of $\frac{1}{k}[-Z_{th1} + \frac{Z_T}{2}]$ is calculated and compared with the impedance of the line L. If the value calculated is less than Z_L then the electrical center falls within the line else lies outside the line.